

DEVELOPMENT OF Al-SBA-15-BASED CATALYSTS FOR
CONVERSION OF XYLOSE AND GLUCOSE TO FURANIC
COMPOUNDS



A Thesis Submitted in Partial Fulfillment of the Requirements for the
Degree of Doctor of Philosophy in Chemistry
Suranaree University of Technology
Academic Year 2022

การพัฒนาตัวเร่งปฏิกิริยาที่มี Al-SBA-15 เป็นหลัก สำหรับการเปลี่ยนไซโลส
และกลูโคสเป็นสารประกอบฟูแรน



นางสาวอิสราภรณ์ รักงาม

วิทยานิพนธ์นี้เป็นส่วนหนึ่งของการศึกษาตามหลักสูตรปริญญาวิทยาศาสตรดุษฎีบัณฑิต
สาขาวิชาเคมี
มหาวิทยาลัยเทคโนโลยีสุรนารี
ปีการศึกษา 2565

DEVELOPMENT OF Al-SBA-15-BASED CATALYSTS FOR CONVERSION
OF XYLOSE AND GLUCOSE TO FURANIC COMPOUNDS

Suranaree University of Technology has approved this submitted in partial fulfillment
of the requirements for the Degree of Doctor of Philosophy.

Thesis Examining Committee



(Asst. Prof. Dr. Suwit Suthirakun)
Chairperson



(Prof. Dr. Jatuporn Wittayakun)
Member (Thesis advisor)

Sirinuch Loiha

(Asst. Prof. Dr. Sirinuch Loiha)
Member



(Dr. Pongtanawat Khemthong)
Member



(Assoc. Prof. Dr. Sanchai Prayoonpokarach)
Member



(Assoc. Prof. Dr. Chatchai Jothityangkoon)
Vice Rector for Academic Affairs
and Quality Assurance



(Prof. Dr. Santi Maensiri)
Dean of Institute of Science

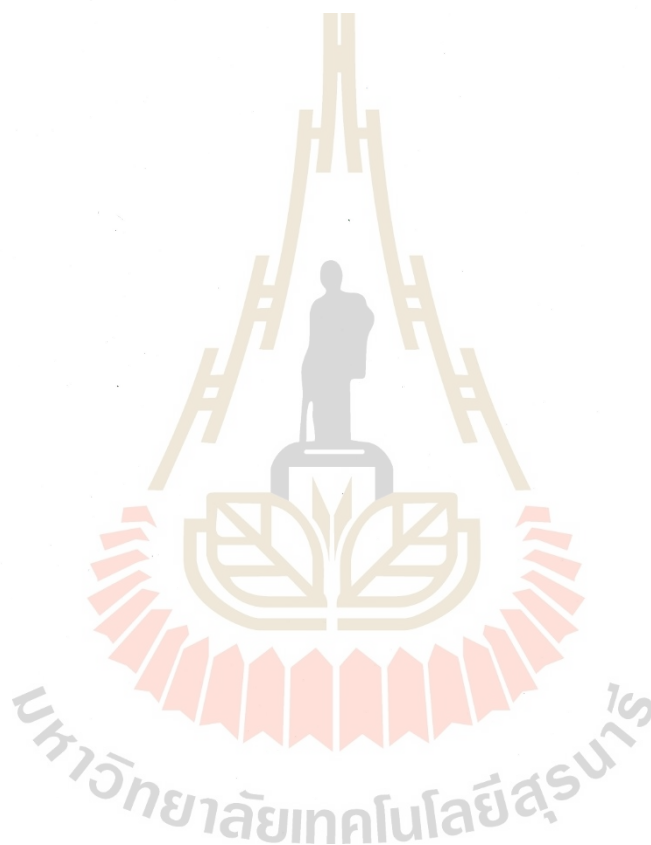
อิสราภรณ์ รังงาม : การพัฒนาตัวเร่งปฏิกิริยาที่มี Al-SBA-15 เป็นหลัก สำหรับการเปลี่ยน
ไซโลสและกลูโคสเป็นสารประกอบฟูแรน (DEVELOPMENT OF AL-SBA-15-BASED
CATALYSTS FOR CONVERSION OF XYLOSE AND GLUCOSE TO FURANIC
COMPOUNDS) อาจารย์ที่ปรึกษา : ศาสตราจารย์ ดร.จตุพร วิทยาคุณ, 108 หน้า

คำสำคัญ: ตัวเร่งปฏิกิริยากรด/ความเป็นกรด/อะลูมิเนียม/ปฏิกิริยาการกำจัดน้ำ/โลหะฟอสเฟต/
น้ำตาลไซโลส/น้ำตาลกลูโคส/เฟอร์ฟูรัล/5-ไฮดรอกซีเมทิลเฟอร์ฟูรัล

การเปลี่ยนน้ำตาลไซโลสและกลูโคสเป็นสารประกอบฟูแรนิก ได้แก่ เฟอร์ฟูรัล และ
5-ไฮดรอกซีเมทิลเฟอร์ฟูรัล (5-HMF) ตามลำดับ ได้รับความสนใจเป็นอย่างมาก กระบวนการ
ดังกล่าวเป็นขั้นตอนที่สำคัญสำหรับการผลิตสารเคมีมูลค่าเพิ่มหลายอย่างและเชื้อเพลิงชีวมวล
วิทยานิพนธ์นี้เกี่ยวข้องกับการพัฒนาตัวเร่งปฏิกิริยาวิวิธพันธุ์ที่มีความเป็นกรดสองชนิดสำหรับ
ปฏิกิริยาดังกล่าว สำหรับปฏิกิริยาการเปลี่ยนน้ำตาลไซโลสไปเป็นเฟอร์ฟูรัล ใช้ตัวเร่งปฏิกิริยาที่ใส่
อะลูมิเนียม (Al) เข้าไปในโครงสร้างของซิลิกาที่มีรูพรุนขนาดกลาง SBA-15 เรียกว่า Al-SBA-15 โดย
ใช้สารตั้งต้นของอะลูมิเนียมที่ต่างชนิดกัน ได้แก่ โซเดียมอะลูมิเนต (SA) อะลูมิเนียมซัลเฟต (AS) และ
อะลูมิเนียมไอโซพโรพอกไซด์ (AI) เป็นตัวเร่งปฏิกิริยาเทียบกับ SBA-15 สารตั้งต้นอะลูมิเนียมที่
แตกต่างกันส่งผลอย่างมากต่อคุณสมบัติพื้นผิวและความเป็นกรดของ Al-SBA-15 แม้จะมีอัตราส่วน
Si/Al ใกล้เคียงกัน แต่มีความเป็นกรดแตกต่างกัน ตัวเร่งปฏิกิริยา Al-SBA-15 ทั้งหมดมีตำแหน่งกรด
กรดแบบลิวอิส (L) และ บรอนสเตด (B) ซึ่งเป็นตำแหน่งกัมมันต์ที่สำคัญในปฏิกิริยานี้ จากการ
ทดสอบตัวเร่งปฏิกิริยาในระบบที่ใช้น้ำเป็นตัวทำละลาย พบว่า Al-SBA-15 ทั้งหมดให้ค่าการแปรผัน
ไซโลสและผลผลิตเฟอร์ฟูรัลที่ต่ำกว่า SBA-15 การแปรผันของไซโลสจะเพิ่มขึ้นตามความเป็นกรดรวม
ในขณะที่ผลผลิตเฟอร์ฟูรัลเพิ่มขึ้นตามอัตราส่วนของตำแหน่งกรด L/B ในงานนี้พบว่า Al-SBA-15
(SA) เป็นตัวเร่งปฏิกิริยาที่ดีที่สุด โดยให้ผลผลิตเฟอร์ฟูรัลสูงและผลพลอยได้น้อยกว่าตัวอื่น จากการ
ทดสอบปฏิกิริยาเพิ่มเติมพบว่า การเปลี่ยนแปลงของไซโลสเพิ่มขึ้นตามอุณหภูมิ เวลา และปริมาณ
ตัวเร่งปฏิกิริยาที่ใช้

สำหรับการเปลี่ยนน้ำตาลกลูโคสไปเป็น 5-HMF ได้ทำการเตรียมโลหะฟอสเฟตหลายชนิด
ได้แก่ โครเมียม (Cr) เซอร์โคเนียม (Zr) ไนโอเบียม (Nb) สตรอนเชียม (Sr) และดีบุก (Sn) ตรึงบน Al-
SBA-15 เรียกว่า MPO/Al-SBA-15 ด้วยวิธีทำให้เอิบชุ่มแบบง่าย ตัวเร่งปฏิกิริยา MPO/Al-SBA-15
ทั้งหมดมีทั้งตำแหน่งกรดแบบลิวอิสและบรอนสเตด ซึ่งพบว่า ชนิดของโลหะฟอสเฟตมีผลต่อสมบัติ
ความเป็นกรดของตัวเร่งปฏิกิริยา ในงานนี้ใช้ระบบตัวทำละลายแบบไบเฟสิกซึ่งประกอบด้วยไซเดียม
คลอไรด์ในน้ำและนอร์มัลบิวทานอลในการเร่งปฏิกิริยาเพื่อให้เกิดการแยกผลิตภัณฑ์แบบอินซิทู

พบว่า การแปรผันกลูโคสเพิ่มขึ้นตามความเป็นกรดรวม ในขณะที่ผลผลิต 5-HMF เพิ่มขึ้นตามอัตราส่วนของตำแหน่งกรด L/B และตัวเร่งปฏิกิริยา CrPO/Al-SBA-15 มีประสิทธิภาพการเร่งปฏิกิริยาสูงที่สุดเนื่องจากมีความเป็นกรดสูงสุด (0.65 mmol/g) และมีอัตราส่วน L/B (1.88) ที่เหมาะสม นอกจากนี้ยังได้ศึกษาผลกระทบของอัตราส่วนโดยโมลของ PO/ Cr ของตัวเร่งปฏิกิริยา (2.0 1.0 และ 0.5) CrPO/Al-SBA-15 ต่อคุณสมบัติและประสิทธิภาพการเร่งปฏิกิริยา พบว่า ตัวเร่งปฏิกิริยา CrPO/Al-SBA-15 ที่มีอัตราส่วนโดยโมลของ PO/Cr เท่ากับ 2 ซึ่งประกอบด้วย โครเมียม (III) ฟอสเฟตในโครงสร้างออกตะฮีดรัล ให้ผลผลิต 5-HMF และการแปรผันกลูโคสสูงที่สุด



สาขาวิชาเคมี

ปีการศึกษา 2565

ลายมือชื่อนักศึกษา อิสราภรณ์ รักงาม

ลายมือชื่ออาจารย์ที่ปรึกษา ศตพร หนาดคุณ

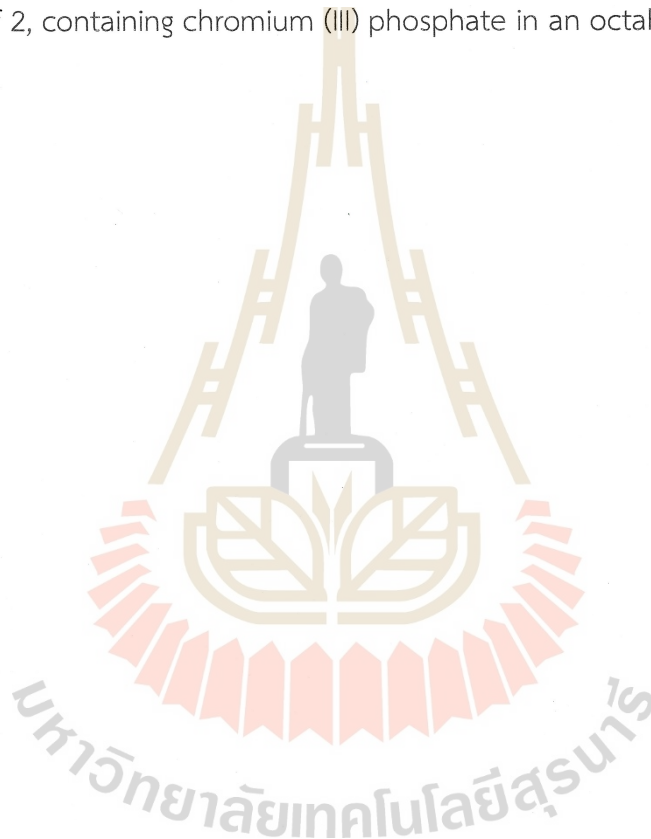
ISSARAPORN RAKNGAM : DEVELOPMENT OF AL-SBA-15-BASED CATALYSTS FOR CONVERSION OF XYLOSE AND GLUCOSE TO FURANIC COMPOUNDS. THESIS ADVISOR : PROF. JATUPORN WITTAYAKUN, Ph.D. 108 PP.

Keyword: ACID CATALYST/ACIDITY/SBA-15/ALUMINIUM/METAL PHOSPHATE/ DEHYDRATION/XYLOSE/GLUCOSE/ FURFURAL/5-HYDROXYMETHYLFURFURAL

Efficient conversion of xylose and glucose into furanic compounds including furfural and 5-hydroxymethylfurfural (5-HMF), respectively, has attracted great attention as a crucial step for the production of various value-added chemicals and biofuels. This thesis involves the development of heterogeneous bifunctional acid catalysts for such reactions. For xylose conversion to furfural, the incorporation of aluminium (Al) into the structure of mesoporous silica SBA-15, referred to as Al-SBA-15, synthesized from sodium aluminate (SA), aluminium sulfate (AS), and aluminium isopropoxide (AI) precursors were employed as catalysts compared with the pristine SBA-15. The difference in Al precursors strongly affected the textural and acidic properties of Al-SBA-15. Despite the similar Si/Al ratios, their total acidities are different. All Al-SBA-15 catalysts generated Lewis (L) and Brønsted (B) acids which are important active sites in this reaction. From the catalytic testing in an aqueous system, all Al-SBA-15 samples provided better xylose conversions and furfural yields than the pristine SBA-15. The xylose conversions increased with the total acidity while the furfural yield improved with the ratios of L/B acid sites. The Al-SBA-15 (SA) was considered as the best catalyst, giving high furfural yield and fewer by-products than the others. Further reaction investigation, the xylose conversion increased with the temperature, time, and catalyst loading.

For glucose conversion to 5-HMF, various metal phosphates of Chromium (Cr), Zirconium (Zr), Niobium (Nb), Strontium (Sr), and Tin (Sn) supported on mesoporous Al-SBA-15, referred to as MPO/Al-SBA-15, were prepared by a facile wet impregnation. All MPO/Al-SBA-15 catalysts possessed both Lewis and Brønsted acid sites. The types of metal phosphates had an influence on the acid properties of the catalysts. In this work, a biphasic solvent system consisting of NaCl-H₂O/*n*-butanol was employed in the

catalytic testing to provide an *in situ* product extraction. Glucose conversions increased with the total acidity of the catalysts. On the other hand, the 5-HMF yields depend on the ratio of L/B acid sites. The CrPO/Al-SBA-15 catalyst provided the highest performance, consistent with the highest acidity of 0.65 mmol/g and a suitable L/B ratio of 1.88. Furthermore, the effect of PO/Cr ratios (2.0, 1.0 and 0.5) of CrPO/Al-SBA-15 catalysts on catalytic properties and activity was also studied. The highest 5-HMF yield and glucose conversion were achieved over the CrPO/Al-SBA-15 with a PO/Cr molar ratio of 2, containing chromium (III) phosphate in an octahedral structure.



School of Chemistry
Academic Year 2022

Student's Signature อิสราภรณ์ รักงาม
Advisor's Signature จตุพร วัฒนกุล

ACKNOWLEDGEMENTS

I would like to extend my deep and heartfelt gratitude to my advisor Prof. Dr. Jatuporn Wittayakun, for his unwavering patience, motivation, and immense knowledge throughout the course of my graduate study. I am also immensely grateful to the members of my thesis committee including, Asst. Prof. Dr. Suwit Suthirakun, Assoc. Prof. Dr. Sanchai Prayoonpokarach, and Asst. Prof. Dr. Sirinuch Loiha, for their generous contributions of knowledge and expertise, which have greatly enriched this research.

Furthermore, I would like to express my sincere appreciation to Dr. Pongtanawat Khemthong from National Nanotechnology Center (NANOTEC), National Science and Technology Development Agency (NSTDA), Pathumthani, Thailand for providing invaluable advice and supporting my research project.

I am also grateful to Assoc. Prof. Karin Föttinger from the Institute of Materials Chemistry, Technische Universität Wien (TU Wien), Austria for granting me the opportunity and experience in research abroad. I would like to thank Jatuporn's group members for helping me and for their good friendship.

Special thanks to the financial support from the Thailand Research Fund (TRF) and the National Research Council of Thailand (NRCT) under the Royal Golden Jubilee Ph.D. program (Grant No. PHD/0221/2558).

Lastly, I want to express my deep appreciation to my parents and family for their endless love, support, and understanding during this challenging journey.

Issaraporn Rakngam

CONTENTS

	Page
ABSTRACT IN THAI	I
ABSTRACT IN ENGLISH	III
ACKNOWLEDGEMENTS	V
CONTENTS	VI
LIST OF TABLES	IX
LIST OF FIGURES	X
LIST OF ABBREVIATIONS	XV
CHAPTER	
I INTRODUCTION	1
1.1 Research objectives	3
1.2 Scope and limitation of the study	3
1.3 References	4
II LITERATURE REVIEWS	7
2.1 Xylose conversion to furfural	7
2.2 Glucose conversion to 5-HMF	9
2.3 Catalysts for sugar conversion to furanic compounds	10
2.3.1 Mesoporous siliceous SBA-15	10
2.3.2 Aluminium-containing mesoporous SBA-15	11
2.3.3 Metal phosphates and supported metal phosphates	12
2.4 Solvent system	15
2.4.1 Monophasic water	15
2.4.2 Biphasic system	16
2.5 References	17

CONTENTS (Continued)

	Page
III PROPERTIES OF MESOPOROUS AL-SBA-15 FROM ONE-POT HYDROTHERMAL SYNTHESIS WITH DIFFERENT ALUMINIUM PRECURSORS AND CATALYTIC PERFORMANCES IN XYLOSE CONVERSION TO FURFURAL	22
3.1 Abstract.....	22
3.2 Introduction	23
3.3 Experimental	24
3.3.1 Synthesis of Al-SBA-15 samples.....	24
3.3.2 Characterization of Al-SBA-15 samples	25
3.3.3 Catalytic testing on xylose conversion to furfural.....	26
3.4 Results and discussion	27
3.4.1 Characterization of the Al-SBA-15 samples with various Al precursors	27
3.4.2 Catalytic performance of Al-SBA-15 for xylose conversion to furfural.....	37
3.4.2.1 Effect of catalyst types and hydrothermal stability	37
3.4.2.2 Effect of reaction temperature, time, and catalyst loading.....	41
3.4.2.3 Catalyst recyclability of Al-SBA-15 (SA) catalyst.....	44
3.5 Conclusions	47
3.6 References	48
IV BIFUNCTIONAL METAL PHOSPHATE SUPPORTED ON AL-SBA-15 CATALYZED THE CONVERSION OF GLUCOSE TO HMF IN BIPHASIC SYSTEM	53
4.1 Abstract.....	53
4.2 Introduction	54
4.3 Experimental	56
4.3.1 Synthesis of MPO/Al-SBA-15 samples	56
4.3.2 Characterization of MPO/Al-SBA-15 samples.....	57

CONTENTS (Continued)

	Page
4.3.3 Catalytic testing on glucose conversion to 5-HMF.....	58
4.4 Results and discussion.....	59
4.4.1 Influence of various metal phosphates supported on Al-SBA-15	59
4.4.1.1 Characterization of MPO/Al-SBA-15 (M = Cr, Zr, Nb, Sr, and Sn).....	59
4.4.1.2 Catalytic screening of MPO/Al-SBA-15 for conversion of glucose to 5-HMF.....	67
4.4.2 Influence of PO/Cr ratios supported on Al-SBA-15 on the catalytic performance of glucose conversion to 5-HMF.....	70
4.4.2.1 Physicochemical and acid properties of the catalysts	70
4.4.2.2 Catalytic activity on glucose conversion to 5-HMF	80
4.4.2.3 Effect of reaction temperature, time, and glucose concentration	82
4.4.2.4 Catalyst reusability of CrPO(2)Al-SBA-15	84
4.4.3 Proposed catalytic reaction pathway in glucose conversion over Cr(III)PO ₄ /Al-SBA-15	85
4.5 Conclusions	89
4.6 References.....	90
V CONCLUSIONS	97
APPENDICES	
APPENDIX A ADDITIONAL CHARACTERIZATION RESULTS FOR Al-SBA-15 WITH VARIOUS ALUMINIUM PRECURSORS.....	99
APPENDIX B ADDITIONAL CHARACTERIZATION RESULTS FOR MPO/Al-SBA-15 WITH VARIOUS METALS	103
CURRICULUM VITAE.....	108

LIST OF TABLES

Table	Page
2.1 Physical properties of furfural and 5-HMF.....	7
3.1 Elemental compositions and XRD results of SBA-15 and Al-SBA-15	28
3.2 Peak area and ratios of L and B by pyridine adsorption and total acidity by NH ₃ -TPD for SBA-15 and Al-SBA-15 samples with different Al sources	32
3.3 XPS data of SBA-15 and Al-SBA-15 samples with three Al sources	33
3.4 Textural properties of SBA-15 and Al-SBA-15 from N ₂ sorption analysis	35
3.5 Comparison of catalytic performance for the conversion of xylose to furfural	46
4.1 Acidity and textural properties of Al-SBA-15 and MPO/Al-SBA-15	67
4.2 Acidity and textural properties of Cr/Al-SBA-15, PO/Al-SBA-15, and all CrPO/Al-SBA-15 with different PO/Cr molar ratios	78
4.3 Comparison of catalytic performance for the production of 5-HMF from glucose.....	88

LIST OF FIGURES

Figure	Page
2.1 Valuable chemicals produced by various reactions from furfural.....	8
2.2 The bifunctional acid-catalyzed conversion of xylose to furfural	8
2.3 Applications of 5-HMF	9
2.4 The bifunctional acid-catalyzed conversion of glucose to 5-HMF.....	10
2.5 Possible synthesis pathways for synthesis of mesoporous Al-SBA-15	11
2.6 Incorporation of aluminium (Al) into a mesoporous SBA-15 material	12
2.7 Structure of (a) α -ZrPO and (b) γ -ZrPO.....	13
2.8 Preparation of CrPO/Al-SBA-15 by wet impregnation method	15
3.1 Low-angle (A) and wide-angle (B) XRD patterns of SBA-15 and Al-SBA-15 samples synthesized from three Al sources (SA = sodium aluminate, AS = aluminium sulfate, and AI = aluminium isopropoxide).....	28
3.2 FTIR spectra of SBA-15 and Al-SBA-15 samples synthesized from three Al sources.....	29
3.3 NH ₃ -TPD profiles of SBA-15 and Al-SBA-15 samples synthesized from three Al sources.....	30
3.4 DRIFT spectra of pyridine adsorption at 150 °C for 3 h from SBA-15 and Al-SBA-15 samples synthesized from three Al sources.....	31
3.5 XPS spectra of (A) Si 2p for SBA-15 and Al-SBA-15 with three Al sources and (B) Al 2p for Al ₂ O ₃ and Al-SBA-15 with three Al sources.....	33
3.6 N ₂ sorption isotherms of SBA-15 and Al-SBA-15 from three Al sources; filled symbol = adsorption and hollow symbol = desorption	35
3.7 SEM and TEM images of (A) SBA-15, (B) Al-SBA-15 (SA), (C) Al-SBA-15 (AS), and (D) Al-SBA-15 (AI). 1= SEM, 2-3 = TEM	36

LIST OF FIGURES (Continued)

Figure	Page
3.8 (A) Catalytic performance in xylose conversion to furfural without a catalyst and with SBA-15 and Al-SBA-15 from three Al sources (SA= sodium aluminate, AS= aluminium sulfate, and Al = aluminium isopropoxide). Reaction conditions: 100 mL batch reactor, 0.9 g of xylose, and 0.1 g of catalyst, 30 mL of water under pressure of N ₂ of 15 bar. (B) XRD patterns of spent catalysts	39
3.9 Catalytic performance for xylose conversion to furfural; reaction temperature (A), reaction time (B), and catalyst loading (C).....	43
3.10 The recyclability of Al-SBA-15 (SA) catalyst. Reaction conditions: 100 mL batch reactor, 0.9 g of xylose, 0.1 g of catalyst, and 30 mL of water under pressure of N ₂ of 15 bar at 170 °C for 5 h.....	44
4.1 Low-angle (A) and wide-angle (B) XRD patterns of Al-SBA-15 and all MPO/Al-SBA-15 samples with different metal types (M = Cr, Zn, Nb, Sr, and Sn).....	60
4.2 N ₂ adsorption-desorption isotherms (A) and pore size distributions (B) of Al-SBA-15 and MPO/Al-SBA-15 with different metal types.....	61
4.3 XPS spectra of CrPO/Al-SBA-15 (A-B), ZrPO/Al-SBA-15 (C-D), NbPO/Al-SBA-15 (E-F), SrPO/Al-SBA-15 (G-H) and SnPO/Al-SBA-15 (I-G) samples.....	64
4.4 NH ₃ -TPD profiles (A) and pyridine-DRIFT spectra (B) of Al-SBA-15 and MPO/Al-SBA-15 samples (M = Cr, Zn, Nb, Sr, and Sn).....	66
4.5 Effect of monophasic (A) and biphasic (B) solvent on glucose conversion to 5-HMF over a mesoporous Al-SBA-15. Reaction condition: glucose 0.3 g in 30 mL of biphasic NaCl-H ₂ O/ <i>n</i> -butanol solvent, catalyst = 0.1 g, temperature = 150 °C, reaction time = 4 h.....	68

LIST OF FIGURES (Continued)

Figure	Page
4.6 (A) Catalytic screening of MPO/Al-SBA-15 on conversion of glucose to 5-HMF. (B) Effect of total acid amount on glucose conversion. (C) Effect of Lewis to Brønsted acid ratio (L/B) on 5-HMF yield. Reaction condition: glucose 0.3 g in 30 mL of biphasic NaCl-H ₂ O/ <i>n</i> -butanol solvent, catalyst = 0.1 g, temperature = 150 °C, reaction time = 4 h	70
4.7 Low-angle (A) and wide-angle (B) XRD patterns of PO/Al-SBA-15, Cr/Al-SBA-15, and CrPO/Al-SBA-15 with different PO/Cr molar ratios.....	71
4.8 (A) Cr K-edge XANES spectra of Cr/Al-SBA-15, CrPO/Al-SBA-15 with different PO/Cr ratios, CrPO ₄ , CrO ₃ , and Cr ₂ O ₃ . (B) P K-edge XANES spectra of PO/Al-SBA-15, CrPO/Al-SBA-15 with different PO/Cr ratios, Na ₄ P ₂ O ₇ , NH ₄ H ₂ PO ₄ , P powder	74
4.9 The <i>k</i> ² -weighted magnitude of the Fourier Transform for Cr K edge and P K edge in CrPO(2)/Al-SBA-15	75
4.10 XPS spectra of P 2p for PO/Al-SBA-15 and CrPO/Al-SBA-15 with PO/Cr ratio of 0.5, 1 and 2.....	76
4.11 FTIR spectra of Al-SBA-15, PO/Al-SBA-15, Cr/Al-SBA-15, and CrPO/Al-SBA-15 with different PO/Cr molar ratios.....	77
4.12 N ₂ adsorption-desorption isotherms (A) and pore size distributions (B) of PO/Al-SBA-15, Cr/Al-SBA-15, and all CrPO/Al-SBA-15 with different PO/Cr molar ratios.....	78
4.13 (A) NH ₃ -TPD profiles of PO/Al-SBA-15, Cr/Al-SBA-15, and CrPO/Al-SBA-15 with different PO/Cr molar ratios. (B) Pyridine-DRIFT spectra of PO/Al-SBA-15, Cr/Al-SBA-15, an CrPO/Al-SBA-15 with different PO/Cr molar ratios.....	80

LIST OF FIGURES (Continued)

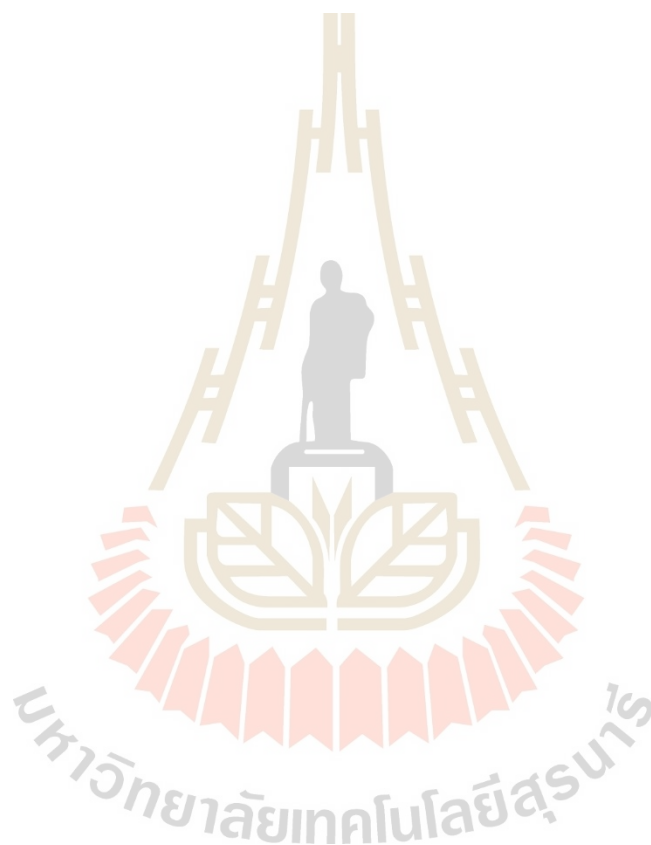
Figure	Page
4.14 Catalytic screening on conversion of glucose to 5-HMF. Reaction conditions: glucose 0.3 g in 30 mL of biphasic NaCl-H ₂ O/ <i>n</i> -butanol solvent, catalyst = 0.1 g, temperature = 170 °C, reaction time = 4 h	81
4.15 Effect of reaction temperatures and times. Reaction conditions: glucose 0.3 g in 30 mL of biphasic NaCl-H ₂ O/ <i>n</i> -butanol solvent, CrPO(2)/Al-SBA-15 catalyst = 0.1 g, reaction time of 4 h (A) and 2 h (B).....	83
4.16 Effect of glucose concentration on the conversion of glucose to 5-HMF. Reaction conditions: using a constant CrPO(2)/Al-SBA-15 catalyst loading = 0.1 g, temperature = 170 °C, and reaction time = 4 h.....	83
4.17 Reusability of CrPO(2)/Al-SBA-15 catalyst. Reaction conditions: catalyst 0.1 g, glucose 0.3 g in 30 mL of NaCl-H ₂ O/ <i>n</i> -butanol at 170 °C for 4 h.....	84
4.18 TEM images of (a) fresh and (b) spent CrPO(2)/Al-SBA-15 catalysts	86
4.19 XRD pattern of spent CrPO(2)/Al-SBA-15 catalyst.....	86

LIST OF ABBREVIATIONS

SBA-15	Santa Barbara Amorphous-15
Al-SBA-15	Aluminium-incorporated SBA-15
SA	Sodium aluminate
AS	Aluminium sulfate
Al	Aluminium isopropoxide
MPO	Metal phosphate
CrPO	Chromium phosphate
ZrPO	Zirconium phosphate
NbPO	Niobium phosphate
SrPO	Strontium phosphate
SnPO	Tin phosphate
5-HMF	5-Hydroxymethylfurfural
HPLC	High-performance liquid chromatography
XRD	X-ray diffraction
FTIR	Fourier transform infrared spectroscopy
DRIFT	Diffuse reflectance infrared Fourier transform spectroscopy
Py	Pyridine
XPS	X-ray photoelectron spectroscopy
NH ₃ -TPD	Temperature-programmed desorption of NH ₃
TCD	Thermal conductivity detector
BET	Brunauer-Emmett-Teller
BJH	Barrett-Joyner-Halenda
ICP-OES	Inductively coupled plasma-optical emission spectrometry
TEM	Transmission electron microscopy
SEM	Scanning electron microscopy
HPLC	High performance liquid chromatograph

LIST OF ABBREVIATIONS (Continued)

L	Lewis acid sites
B	Brønsted acid sites
XAS	X-ray absorption spectroscopy
XANES	X-ray absorption near edge structure spectroscopy
EXAFS	Extended X-ray absorption fine structure spectroscopy



CHAPTER I

INTRODUCTION

The conversion of renewable biomass materials to sustainable alternative production of value-added chemicals has recently attracted much attention (Mittal, Pilath, and Johnson, 2020; Zhou and Zhang, 2016). Among biomass derivatives, furanic compounds such as furfural and 5-hydroxymethylfurfural (5-HMF) are potential building block molecules that can be further converted to several high-value biobased chemicals and biofuels (Mittal et al., 2020). Furfural and 5-HMF can be produced from xylose and glucose, respectively, over bifunctional acid catalysts with Lewis and Brønsted acid sites via isomerization and dehydration steps.

This thesis focuses on the development of heterogeneous bifunctional acid catalysts with Lewis and Brønsted acid sites for the conversion of sugars to furanic compounds in a one-pot reaction process. The thesis is divided into two parts. The first part compares the catalytic properties and performances of mesoporous aluminosilicate Al-SBA-15 from three aluminium sources as catalysts for the conversion of xylose to furfural under an aqueous system. The second part combines the modification of various metal phosphates on mesoporous Al-SBA-15 (referred to as MPO/Al-SBA-15) catalysts and a biphasic solvent system to enhance the catalytic performance in glucose conversion to 5-HMF.

Because Al-SBA-15 processes moderated acidity with Lewis and Brønsted acids and uniform mesopores, it could enhance the catalytic application of large molecules (Ungureanu, Dragoi, Hulea, Cacciaguerra, Meloni, Solinas, and Dumitriu, 2012). Furthermore, the choice of aluminium precursors plays a crucial role in determining the properties of Al-SBA-15 materials due to variations in reactivity and solubility (Schwanke, Balzer, and Pergher, 2017). In the first part, Al-SBA-15 materials from three

different aluminium precursors were synthesized by a one-step hydrothermal with pH adjusting method. Since glucose conversion to 5-HMF is more difficult than xylose conversion to furfural in an aqueous system, the addition of more active acid sites is necessary to improve the 5-HMF yield.

Several kinds of metal phosphates, including CrPO (Xu, Yan, Bu, and Xia, 2016), ZrPO (Saravanan, Park, Jeon, and Bae, 2018), NbPO (Vieira, Paul, Iga, Cabral, Bueno, Bisio, and Gallo, 2021), SrPO (Daorattanachai, Khemthong, Viriya-empikul, Laosiripojana, and Faungnawakij, 2015), and SnPO (Hou, Zhen, Liu, Chen, Huang, Zhang, Li, and Ju, 2018) are active for this reaction because of their tunable Lewis and Brønsted acid sites and high thermal stability (Alam, De, Singh, Saha, and Abu-Omar, 2014; Zhang, Wei, Xiao, Li, Jin, Wei, and Wu, 2020). Metal phosphates exhibit unique acid properties containing Lewis acid sites from metal (M^{n+}) species and Brønsted acid sites from phosphate groups (Hou et al., 2017; Carniti et al., 2016), which are essential active sites for the conversion of glucose to 5-HMF (Zhu et al., 2017).

Another vital factor for the efficient conversion of 5-HMF is the nature of the solvent system. Typically, the yield of 5-HMF from glucose in an aqueous system is low due to the formation of by-products from side reactions such as rehydration and polymerization of intermediates and the decomposition of 5-HMF (Xue, Ma, Li, and Mu, 2016). Utilizing a biphasic system containing water and organic solvent could prevent the occurrence of side reactions because the produced 5-HMF is separated into the organic solvent phase *in situ* (Saha and Abu-Omar, 2014; Yu and Tsang, 2017). Therefore, the second part combines various metal phosphates on mesoporous Al-SBA-15 (MPO/Al-SBA-15) by a facile wet impregnation to produce bifunctional catalysts. They were tested in a biphasic solvent system to enhance the catalytic performance in glucose conversion to 5-HMF. The best MPO/Al-SBA-15 catalyst was further investigated on the effect of phosphate-to-chromium molar ratios on the structural property and catalytic activity.

1.1 Research objectives

The first part aims to understand the relation between the physicochemical properties of mesoporous Al-SBA-15 from different aluminum sources and the catalytic performance in xylose conversion to furfural. Al-SBA-15 samples were synthesized from sodium aluminate (SA), aluminium sulfate (AS), and aluminium isopropoxide (AI). Another objective of this part is to determine an optimum condition for the best catalyst and study the reusability of the best catalyst.

The objectives of the second part are to develop the bifunctional metal phosphates modified on Al-SBA-15 from different phosphates of Cr, Zr, Nb, Sr, and Sn by a facile impregnation method and to discuss the relationship between the catalyst properties and the catalytic performance of glucose conversion to 5-HMF in a biphasic NaCl-H₂O/*n*-butanol solvent. The last part aims to investigate the effect of phosphate-to-chromium molar ratios of the best catalyst on the structural properties related to the catalytic performance.

1.2 Scope and limitation of the study

In the first part of the research, mesoporous Al-SBA-15 materials with a Si/Al ratio of 20 were synthesized by a one-step hydrothermal with pH adjusting method modified from the procedure by Li et al. (2004) and Wu et al. (2004). The catalytic conversion of xylose to furfural was carried out in a batch reactor at 170 °C for 5 h under 15 bars of N₂ atmosphere and water as a solvent.

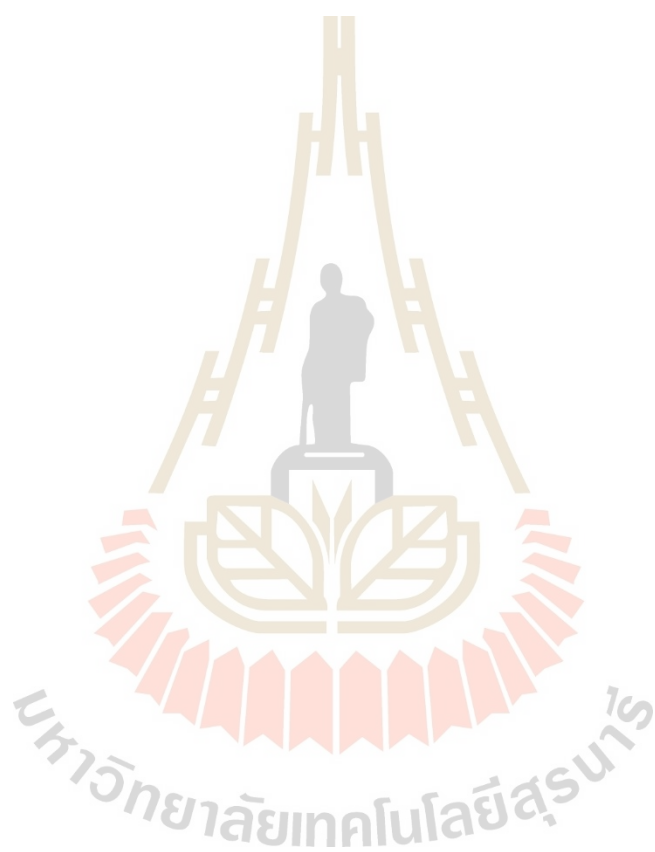
In the second part, mesoporous Al-SBA-15 as catalyst support was synthesized from sodium aluminate by the method from the first part. MPO/Al-SBA-15 from phosphates of Cr, Zr, Nb, Sr, and Sn were prepared by wet-impregnation method according to Yang et al. (2015) with metal loading of 10 wt.% with the phosphate-to-metal molar ratio of 2. The catalytic conversion of glucose to 5-HMF was carried out in a batch reactor at 150 °C for 4 h under 15 bars of N₂ atmosphere and a biphasic NaCl-H₂O/*n*-butanol solvent.

1.3 References

- Alam, M. I., De, S., Singh, B., Saha, B., and Abu-Omar, M. M. (2014). Titanium hydrogenphosphate: An efficient dual acidic catalyst for 5-hydroxymethylfurfural (HMF) production. *Applied Catalysis A: General*, 486, 42–48.
- Carniti, P., Gervasini, A., Bossola, F., and Dal Santo, V. (2016). Cooperative action of Brønsted and Lewis acid sites of niobium phosphate catalysts for cellobiose conversion in water. *Applied Catalysis B: Environmental*, 193, 93–102.
- Daorattanachai, P., Khemthong, P., Viriya-empikul, N., Laosiripojana, N., and Faungnawakij, K. (2015). Effect of calcination temperature on catalytic performance of alkaline earth phosphates in hydrolysis/dehydration of glucose and cellulose. *Chemical Engineering Journal*, 278, 92–98.
- Hou, Q., Zhen, M., Liu, L., Chen, Y., Huang, F., Zhang, S., Li, W., and Ju, M. (2018). Tin phosphate as a heterogeneous catalyst for efficient dehydration of glucose into 5-hydroxymethylfurfural in ionic liquid. *Applied Catalysis B: Environmental*, 224, 183–193.
- Li, Y., Zhang, W., Zhang, L., Yang, Q., Wei, Z., Feng, Z., and Li, C. (2004). Direct synthesis of Al-SBA-15 mesoporous materials via hydrolysis-controlled approach. *The Journal of Physical Chemistry B*, 108(28), 9739–9744.
- Mittal, A., Pilath, H. M., and Johnson, D. K. (2020). Direct conversion of biomass carbohydrates to platform chemicals: 5-Hydroxymethylfurfural (HMF) and furfural. *Energy & Fuels*, 34(3), 3284–3293.
- Saha, B., and Abu-Omar, M. M. (2014). Advances in 5-hydroxymethylfurfural production from biomass in biphasic solvents. *Green Chemistry*, 16(1), 24–38.
- Saravanan, K., Park, K. S., Jeon, S., and Bae, J. W. (2018). Aqueous phase synthesis of 5-hydroxymethylfurfural from glucose over large pore mesoporous zirconium phosphates: Effect of calcination temperature. *ACS Omega*, 3(1), 808–820.
- Schwanke, A. J., Balzer, R., and Pergher, S. (2017). Microporous and mesoporous materials from natural and inexpensive sources. *Handbook of Ecomaterials*, 5, 3379–3399.
- Ungureanu, A., Dragoi, B., Hulea, V., Cacciaguerra, T., Meloni, D., Solinas, V., and

- Dumitriu, E. (2012). Effect of aluminium incorporation by the “pH-adjusting” method on the structural, acidic and catalytic properties of mesoporous SBA-15. *Microporous and Mesoporous Materials*, 163, 51–64.
- Vieira, J. L., Paul, G., Iga, G. D., Cabral, N. M., Bueno, J. M. C., Bisio, C., and Gallo, J. M. R. (2021). Niobium phosphates as bifunctional catalysts for the conversion of biomass-derived monosaccharides. *Applied Catalysis A: General*, 617, 118099.
- Wu, S., Han, Y., Zou, Y., Song, J., Zhao, L., and Di, Y. (2004). Synthesis of heteroatom substituted SBA-15 by the “pH-adjusting” method. *Chemistry of Materials*, 16(17), 486–492.
- Xu, S., Yan, X., Bu, Q., and Xia, H. (2016). Highly efficient conversion of carbohydrates into 5-hydroxymethylfurfural using the bi-functional CrPO_4 catalyst. *RSC Advances*, 6(10), 8048–8052.
- Xue, Z., Ma, M. G., Li, Z., and Mu, T. (2016). Advances in the conversion of glucose and cellulose to 5-hydroxymethylfurfural over heterogeneous catalysts. *RSC Advances*, 6(101), 98874–98892.
- Yang, Y., Ochoa-Hernández, C., de la Peña O’Shea, V. A., Pizarro, P., Coronado, J. M., and Serrano, D. P. (2015). Transition metal phosphide nanoparticles supported on SBA-15 as highly selective hydrodeoxygenation catalysts for the production of advanced biofuels. *Journal of Nanoscience and Nanotechnology*, 15(9), 6642–6650.
- Yu, I. K. M., and Tsang, D. C. W. (2017). Conversion of biomass to hydroxymethylfurfural: A review of catalytic systems and underlying mechanisms. *Bioresource Technology*, 238, 716–732.
- Zhang, T., Wei, H., Xiao, H., Li, W., Jin, Y., Wei, W., and Wu, S. (2020). Advance in constructing acid catalyst-solvent combinations for efficient transformation of glucose into 5-Hydroxymethylfurfural. *Molecular Catalysis*, 498, 111254.
- Zhou, P., and Zhang, Z. (2016). One-pot catalytic conversion of carbohydrates into furfural and 5-hydroxymethylfurfural. *Catalysis Science & Technology*, 6, 3694–2712.
- Zhu, T., Song, H., Dai, X., and Song, H. (2017). Preparation of $\text{Ni}_2\text{P}/\text{Al-SBA-15}$ catalyst

and its performance for benzofuran hydrodeoxygenation. *Chinese Journal of Chemical Engineering*, 25(12), 1784–1790.

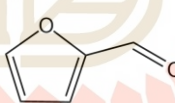


CHAPTER II

LITERATURE REVIEW

This chapter reviews the development of bifunctional acid catalysts with Lewis and Brønsted acid sites for the conversion of xylose to furfural and the conversion of glucose to 5-HMF. Due to the physical properties of furfural and 5-HMF (**Table 2.1**), their reactions were carried out in an aqueous system at the temperature range of 120 – 200 °C. The challenge of this work is the development of highly selective and water-tolerant solid acid catalysts.

Table 2.1 Physical properties of furfural and 5-HMF (Adapted from Mathew et al., 2018 with permission from Elsevier).

Properties	Furfural	5-HMF
Molecular formula	C ₅ H ₄ O ₂	C ₆ H ₆ O ₃
Structure		
Molecular weight (g/mol)	96.1	126.11
Boiling point (°C)	161.7	114-116
Melting point (°C)	-37	31.5
Density at 20 °C (g/cm ³)	1.16	1.29
Solubility in water (g/L)	83	7.0 × 10 ²
Vapor pressure (mmHg, 20 °C)	2	5.28 × 10 ⁻³

2.1 Xylose conversion to furfural

Furfural is a heteroaromatic furan ring with an aldehyde functional group. It has received attention as a starting reagent of various chemicals (**Figure 2.1**). It could be converted to products for a wide range of applications, including furfuryl alcohol, 2-

methyl furan, tetrahydrofuran, furfuryl amine, furoic acid, and furan (Mathew et al., 2018).

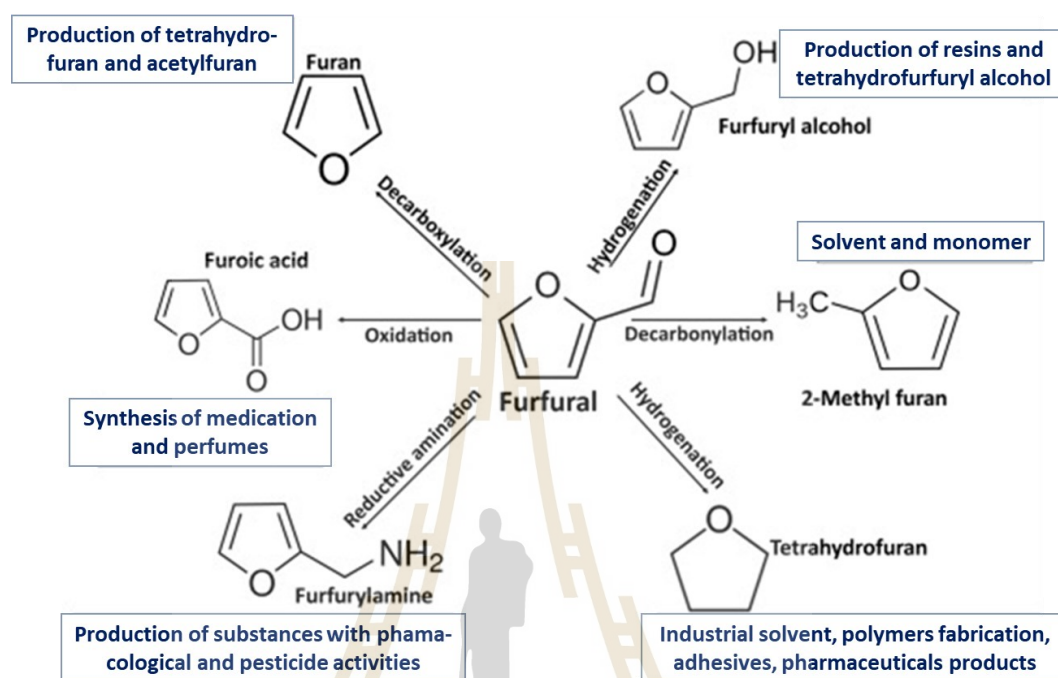


Figure 2.1 Valuable chemicals produced by various reactions from furfural (Reproduced from Mathew et al., 2018 with permission from Elsevier).

Furfural can be produced over acid catalysts from xylose contained in the hemicellulose portion of lignocellulosic biomass (Jia, Teng, Yu, Si, Li, Zhou, Cai, Qin, and Chen, 2019). The conversion of xylose to furfural over a bifunctional heterogeneous acid catalyst consists of two-step reactions, as shown in **Figure 2.2**. The first step is the isomerization of xylose to xylulose on Lewis acid sites. The second step is dehydration of xylulose to furfural on Brønsted acid sites (Pholjaroen, Li, Wang, Wang, and Zhang, 2013; Weingarten, Tompsett, Conner, and Huber, 2011).

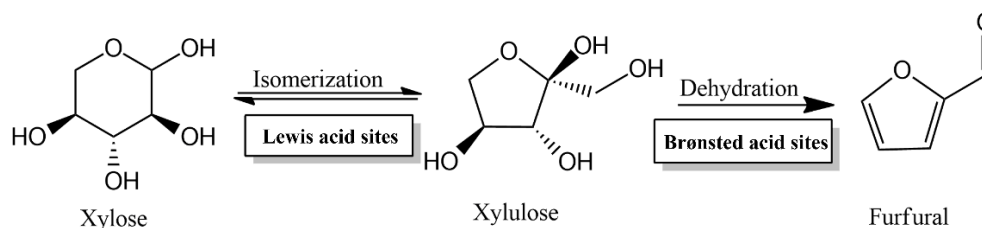


Figure 2.2 The bifunctional acid-catalyzed conversion of xylose to furfural (adapted from Pholjaroen et al. (2013) with permission from Elsevier).

2.2 Glucose conversion to 5-HMF

5-hydroxymethylfurfural (5-HMF) is a furan ring containing aldehyde and alcohol functional groups. It is an important platform chemical in biorefinery due to its high potential to produce various valuable derivatives (**Figure 2.3**) including, 2,5-furandicarboxylic acid, 2,5-dimethylfuran, 2,5-dimethyltetrahydrofuran, formic acid, levulinic acid, 2,5-bis(hydroxymethyl)furan, 2-methylfuran, and 2-hydroxymethylfuran (Mathew et al., 2018; Xia, Xu, Hu, An, and Li, 2018). These compounds are starting materials for the production of biopolymers and biofuels (Xia et al., 2018). 5-HMF can be produced from glucose, the most abundant monosaccharide in biomass (Song, Yue, Zhu, Wen, Chen, Liu, Ma, and Wang, 2021).

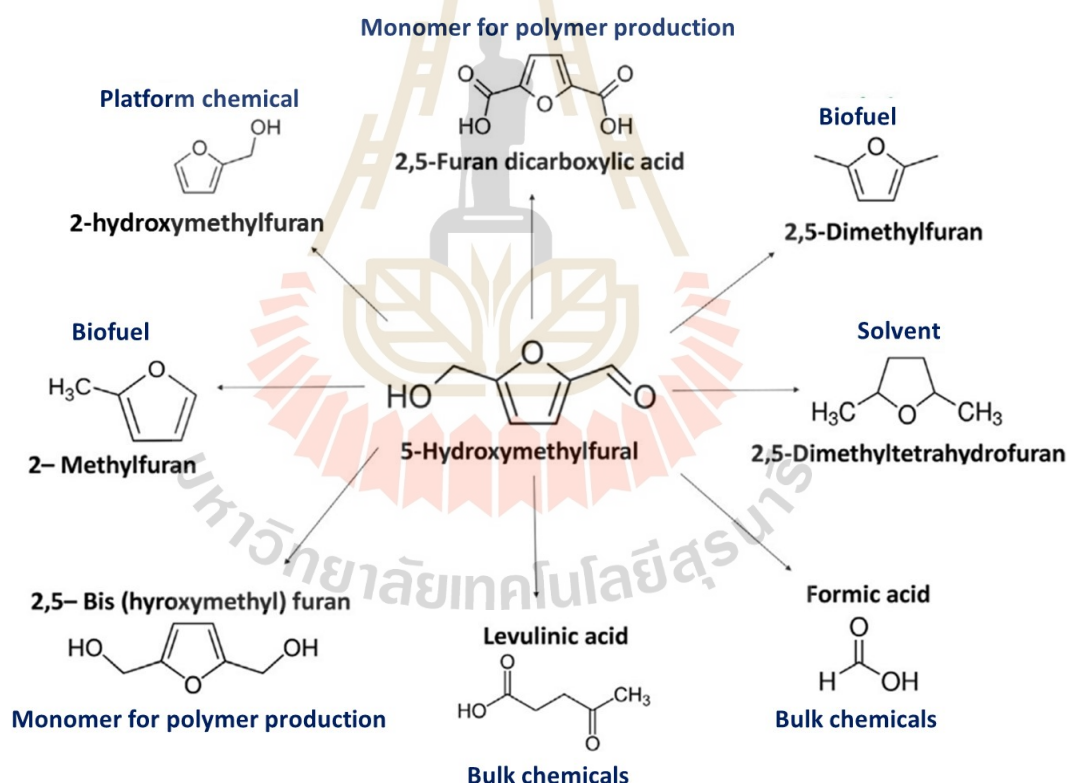


Figure 2.3 Applications of 5-HMF (Reproduced from Mathew et al., 2018 with permission from Elsevier).

Generally, the conversion of glucose to 5-HMF involves a two-step reaction process similar to xylose conversion to furfural (**Figure 2.4**). The first step is the isomerization of glucose to fructose on Lewis acid sites. The second step is the dehydration of fructose to 5-HMF on Brønsted acid sites (Swift et al., 2016).

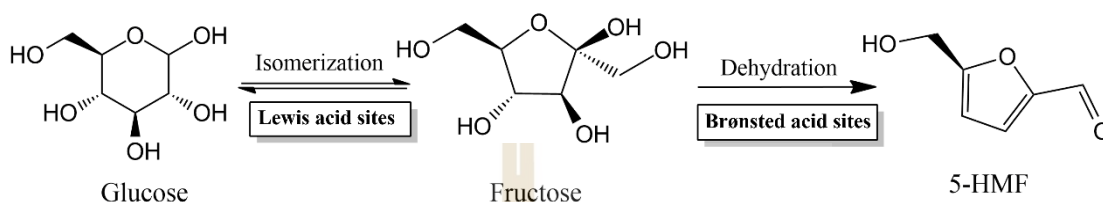


Figure 2.4 The bifunctional acid-catalyzed conversion of glucose to 5-HMF.

2.3 Catalysts for sugar conversion to furanic compounds

2.3.1 Mesoporous siliceous SBA-15

SBA-15 (Santa Barbara Amorphous No. 15) is an ordered mesoporous silica-based material first reported in 1998 (Zhao, Feng, Huo, Melosh, Glenn, Chmelka, Stucky, Zhao, Feng, Huo, Melosh, Fredrickson, Chmelka, and Stucky, 1998a; Zhao, Huo, Feng, Chmelka, and Stucky, 1998b). It was prepared in acidic media from tetraethyl orthosilicate (TEOS) as a silicon source and amphiphilic non-ionic triblock copolymer Pluronic P123 ($\text{EO}_{20}\text{PO}_{70}\text{EO}_{20}$, MW=5800) with polyethylene oxide (EO) and polypropylene oxide (PO) blocks as a template. SBA-15 could be synthesized via a $(\text{S}^0\text{H}^+)(\text{X}^-\text{I}^+)$ cooperative self-assembly mechanism as shown in **Figure 2.5** where (S^0H^+) is non-ionic surfactant hydrogen bonded to a hydronium ion, X^- is counter anion, and I^+ is protonated inorganic silica species (Meynen, Cool, and Vansant, 2009; Zhao et al., 1998b). This material has higher hydrothermal stability and thicker pore walls compared to MCM-41, another well-known mesoporous siliceous material. The purely siliceous SBA-15 only has silanol groups on its surface, resulting in low acid strength and low activity for reactions. Therefore, the modification of siliceous SBA-15 with aluminium (Al) species is necessary to enhance its acid property and catalytic performance.

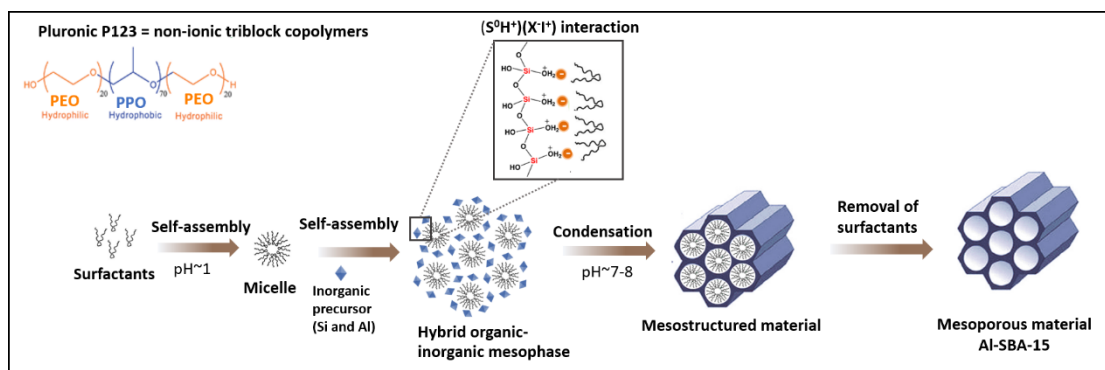


Figure 2.5 Possible pathways for synthesis of mesoporous Al-SBA-15 (Modified from Hoffmann, Cornelius, Morell, and Fröba, 2006 with permission from John Wiley and Sons).

2.3.2 Aluminium-containing mesoporous SBA-15 (Al-SBA-15)

The incorporation of aluminium (Al) into mesoporous silicas is one of the most modifications to improve the acid properties of siliceous materials. Al incorporated SBA-15 (Al-SBA-15) materials could be prepared either by post-synthesis with grafting (Li, Wu, Tu, Park, Ha, and Zhao, 2010; Lucas, Kokate, Nagpure, and Chilukuri, 2013; Yun, Bazardorj, and Ihm, 2009) or direct-synthesis method (Gallo, Bisio, Gatti, Marchese, and Pastore, 2010; Li, Zhang, Zhang, Yang, Wei, Feng, and Li, 2004; Muthu Kumaran, Garg, Soni, Kumar, Gupta, Sharma, Rama Rao, and Murali Dhar, 2008; Wu, Han, Zou, Song, Zhao, and Di, 2004). In particular, the substitution of Si⁴⁺ by Al³⁺, which has lower valence, creates negative charges in the framework that can be balanced by proton (H⁺). Hence, the Al-SBA-15 materials contain Brønsted acid sites from terminal silanol groups, so-called bridging hydroxyl groups, near an aluminium atom (Dragoi, Dumitriu, Guimon, and Auroux, 2009). Moreover, Lewis acid sites are derived from extra-framework Al species (Krishna and Selvam, 2017). Therefore, Al-SBA-15 with Lewis and Brønsted acid sites (as illustrated in **Figure 2.6**) can be used as a catalyst in acid-catalyzed reactions (Liu, Cai, Ni, Shi, Wang, and Lin, 2020; Lucas et al., 2013; Perez, Albuquerque, Borges, Hardacre, and Fraga, 2019; Pham, Nguyen, Le, Pham, Quan, Nguyen, Son, and Vu, 2019).

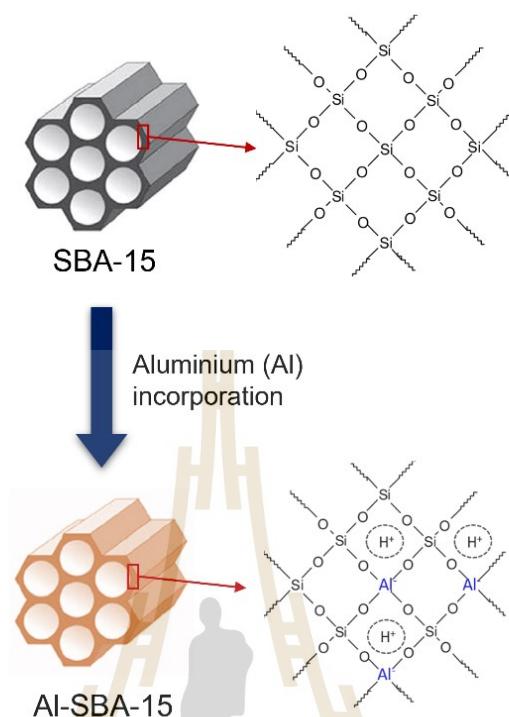


Figure 2.6 Incorporation of aluminium (Al) into a mesoporous SBA-15 material (Adapted from Krishna and Selvam, 2017 with permission from John Wiley and Sons).

2.3.3 Metal phosphates and supported metal phosphates

Metal phosphates have the potential as solid catalysts for the one-pot conversion of glucose to 5-HMF because they exhibit unique properties: containing both Lewis and Brønsted acids, tunable acidity, and thermal stability (Alam, De, Singh, Saha, and Abu-Omar, 2014; Zhang, Wei, Xiao, Li, Jin, Wei, and Wu, 2020). Lewis acid sites are from coordinatively unsaturated metal (M^{n+}) species and Brønsted acid sites are from hydroxyl groups of phosphates (Carniti, Gervasini, Bossola, and Dal Santo, 2016; Hou, Zhen, Liu, Chen, Huang, Zhang, Li, and Ju, 2018). Metal phosphates consist of metal (IV) in an octahedral configuration and phosphate tetrahedra (PO_4) with sharing oxygen atoms, resulting in a number of metal (IV) phosphate materials with different structures and morphology (Flem, 2012). For instance, the different structures of layered zirconium phosphate materials are illustrated in **Figure 2.7**.

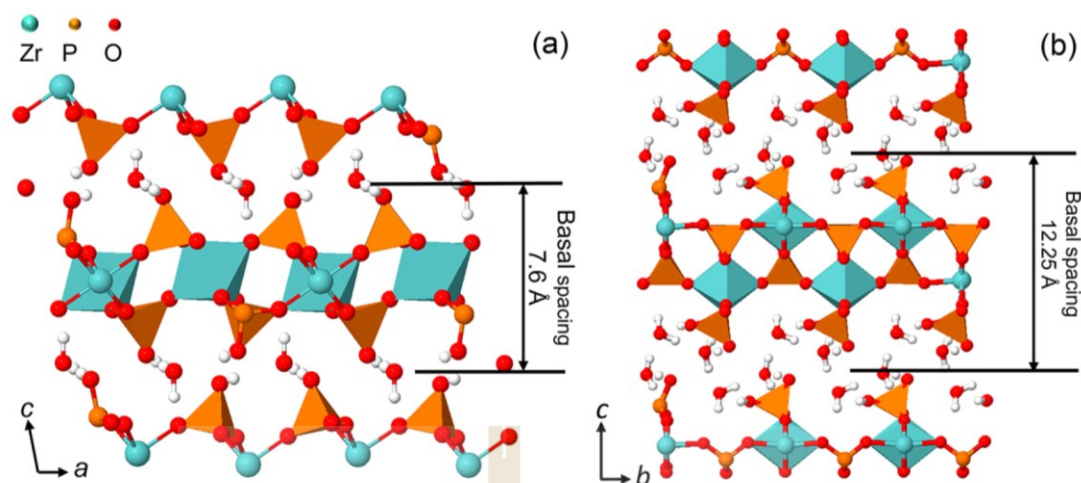


Figure 2.7 Structure of (a) α -ZrPO and (b) γ -ZrPO (Reproduced from Cheng, Dong Tony Wang, Jaenicke, and Chuah, 2018 with permission from American Chemical Society).

There are some examples of 5-HMF production from heterogeneous catalysis in the literature (Daorattanachai, Khemthong, Viriya-empikul, Laosiripojana, and Faungnawakij, 2015; Khemthong, Daorattanachai, Laosiripojana, and Faungnawakij, 2012; Ordonsky, Sushkevich, Schouten, Van Der Schaaf, and Nijhuis, 2013; Saravanan, Park, Jeon, and Bae, 2018). Ordonsky et al. (2013) reported that the glucose conversions increased with the amount of strong acid sites in the following order: AlPO < TiPO < ZrPO < NbPO. The selectivities to 5-HMF depended on the ratio of Brønsted to Lewis acid sites of the solid catalysts. Saravanan et al. (2018) used mesoporous ZrPO catalysts to convert glucose to 5-HMF in water. They found that glucose conversion decreased with increasing calcination temperature from 80 – 800 °C, attributing to the decrease in total acidity. They also found that the 5-HMF yields were directly proportional to the Brønsted to Lewis acid ratios. Daorattanachai et al. (2015) investigated the effect of calcination temperature in the preparation of CaPO and SrPO on the catalytic conversion of glucose in an aqueous system. They observed that the calcination temperature affected the structure and acid properties of the catalysts. The maximum 5-HMF yield of 21% was obtained from SrPO calcined at 900 °C.

Although those metal phosphates are active for glucose conversion to 5-HMF, they have small surface areas, which means small numbers of active sites. This

issue could be improved by dispersing metal phosphates on mesoporous materials such as SBA-15 (Samikannu, Konwar, Rajendran, Lee, Shchukarev, Virtanen, and Mikkola, 2020; Zhu, Wang, Zhao, Song, Sun, Wang, Cui, and Yi, 2017), KIT-6 (Najafi Sarpiri, Najafi Chermahini, Saraji, and Shahvar, 2021), and SiO₂ (Huang, Su, Long, Chen, and Yao, 2018). However, those materials have low acidity. Consequently, the deposition of metal phosphates on Al-containing mesoporous silica materials such as Al-MCM-41 and Al-SBA-15 is an attractive alternative approach. These materials have well-ordered hexagonal mesoporous structures, uniform pore size distribution, and moderate acidity with Lewis and Brønsted acid sites (Dragoi et al., 2009; Li et al., 2004; Ungureanu, Dragoi, Hulea, Cacciaguerra, Meloni, Solinas, and Dumitriu, 2012). Lucas and co-workers (2013) investigated the dehydration of fructose to 5-HMF over mesoporous Al-SBA-15 and H-zeolites (H-BEA, H-MOR, HZSM-5). They found that Al-SBA-15 provided the 5-HMF selectivity better than that of H-zeolite because it has a large pore size and weak acidity. Hence, the Al-SBA-15 is a proper support for metal phosphates.

In this work, a series of metal phosphates deposited on mesoporous Al-SBA-15 materials were prepared by a facile wet impregnation method. For instance, the preparation of CrPO/Al-SBA-15 is shown in **Figure 2.8**. The impregnation approach is the simplest catalyst preparation method in the industry. This method is simple and low-cost; the metal loading can be easily controlled.

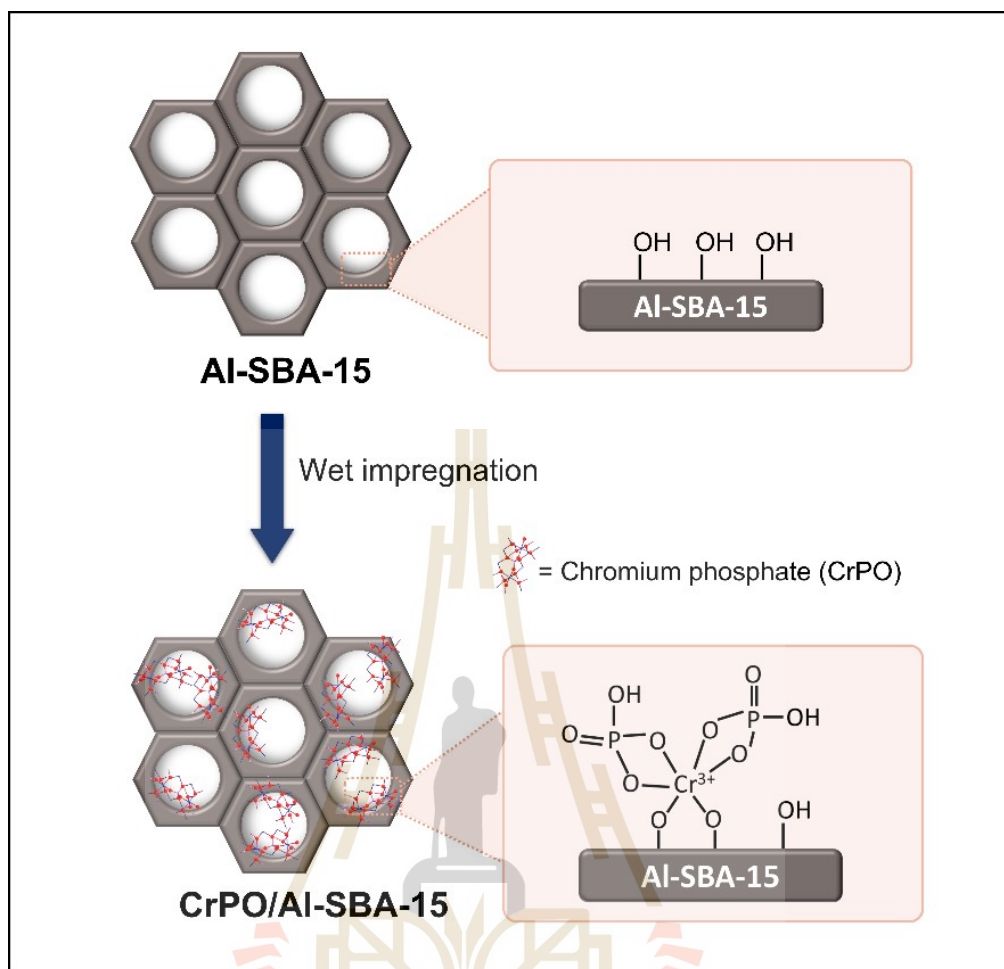


Figure 2.8 Preparation of CrPO/Al-SBA-15 by a wet impregnation method.

2.4 Solvent system

The solvent system is another significant factor for the efficient conversion of cellulosic sugars to furanic compounds. The solvent acts as a medium for dissolving the substrates and catalyst; serves multiple roles, such as stabilizing the substrates, intermediates, and products; and acts as a catalyst (Yu and Tsang, 2017). Therefore, the choice of solvent plays a vital role in improving catalytic activity.

2.4.1 Monophasic water

Water is an ideal solvent for green and sustainable chemical processes because it is cheap, non-toxic, and non-flammable (Xue, Ma, Li, and Mu, 2016). However, the yields of furfural and 5-HMF from xylose and glucose in a monophasic

aqueous system are usually low due to further side reactions according to rehydration and polymerization and the degradation of the furanic compounds (Xue et al., 2016). The xylose conversion to furfural in the monophasic water gave a moderate yield, while the glucose conversion to 5-HMF gave a meager product yield. To improve the 5-HMF yield from glucose, many researchers use biphasic solvent systems as reaction media in this reaction.

2.4.2 Biphasic solvent

Utilizing a biphasic system containing water and organic solvent could prevent the occurrence of side reactions as the produced 5-HMF is separated into the organic solvent phase in situ (Saha and Abu-Omar, 2014; Yu and Tsang, 2017). Rao and co-workers (Rao, Souzanchi, Yuan, Ray, and Xu, 2017) revealed that the highest 5-HMF yield of 61% was achieved over a SnPO catalyst at 175 °C for 1 h in a biphasic NaCl-H₂O/THF system. Zhang et al. (Zhang, Wang, Li, Liu, Xia, Hu, Lu, and Wang, 2015) obtained the maximum 5-HMF yield of 39% from glucose over a mesoporous NbPO at 140 °C for 1 h in a biphasic H₂O/MIBK system. Recently, some studies have demonstrated that metal phosphates of Cr and Zr are also active in producing 5-HMF. Xu et al. (Xu, Yan, Bu, and Xia, 2016) showed that a CrPO catalyst in a biphasic H₂O/THF solvent could provide the maximum 5-HMF yield of 63% at 140 °C for 30 min. Liu et al. (Liu, Ba, Jin, and Zhang, 2015) achieved a 5-HMF yield of 43% at 120 °C for 12 h over a Cr-incorporated mesoporous ZrPO catalyst with an ionic liquid [Bmim]Cl solvent. Nikolla et al. (Nikolla, Román-Leshkov, Moliner, and Davis, 2011) focused on adding inorganic salts to a biphasic H₂O/*n*-butanol system to convert glucose. They observed that the 5-HMF selectivity is in the following order: NaCl > MgCl₂ > KBr > KCl. This is because the highest partition coefficient, which reflects the extracting ability of organic solvents, was obtained with the addition of NaCl. 5-HMF formed in the aqueous phase of the NaCl-H₂O/*n*-butanol system is therefore extracted the most by *n*-butanol, leading to the maximum selectivity of 5-HMF.

2.5 References

- Alam, M. I., De, S., Singh, B., Saha, B., and Abu-Omar, M. M. (2014). Titanium hydrogenphosphate: An efficient dual acidic catalyst for 5-hydroxymethylfurfural (HMF) production. *Applied Catalysis A: General*, *486*, 42–48.
- Carniti, P., Gervasini, A., Bossola, F., and Dal Santo, V. (2016). Cooperative action of Brønsted and Lewis acid sites of niobium phosphate catalysts for cellobiose conversion in water. *Applied Catalysis B: Environmental*, *193*, 93–102.
- Cheng, Y., Dong Tony Wang, X., Jaenicke, S., and Chuah, G. K. (2018). Mechanochemistry-Based Synthesis of Highly Crystalline γ -Zirconium Phosphate for Selective Ion Exchange. *Inorganic Chemistry*, *57*(8), 4370–4378.
- Daorattanachai, P., Khemthong, P., Viriya-empikul, N., Laosiripojana, N., and Faungnawakij, K. (2015). Effect of calcination temperature on catalytic performance of alkaline earth phosphates in hydrolysis/dehydration of glucose and cellulose. *Chemical Engineering Journal*, *278*, 92–98.
- Dragoi, B., Dumitriu, E., Guimon, C., and Auroux, A. (2009). Acidic and adsorptive properties of SBA-15 modified by aluminum incorporation. *Microporous and Mesoporous Materials*, *121*(1–3), 7–17.
- Flem, G. Le. (2012). The phosphates of the world and the world of phosphates. (Belharouak, I. and Pol, V. G., Eds.). *Advances in Inorganic Phosphate Materials* (Vol. 233, 5). Canada: Wiley.
- Gallo, J. M. R., Bisio, C., Gatti, G., Marchese, L., and Pastore, H. O. (2010). Physicochemical characterization and surface acid properties of mesoporous [Al]-SBA-15 obtained by direct synthesis. *Langmuir*, *26*(8), 5791–5800.
- Hoffmann, F., Cornelius, M., Morell, J., and Fröba, M. (2006). Silica-based mesoporous organic-inorganic hybrid materials. *Angewandte Chemie - International Edition*, *45*(20), 3216–3251.
- Hou, Q., Zhen, M., Liu, L., Chen, Y., Huang, F., Zhang, S., Li, W., and Ju, M. (2018). Tin phosphate as a heterogeneous catalyst for efficient dehydration of glucose into 5-hydroxymethylfurfural in ionic liquid. *Applied Catalysis B: Environmental*, *224*, 183–193.

- Huang, F., Su, Y., Long, Z., Chen, G., and Yao, Y. (2018). Enhanced formation of 5 - hydroxymethylfurfural from glucose using a silica-supported phosphate and iron phosphate heterogeneous catalyst. *Industrial & Engineering Chemistry Research*, *57*, 10198–10205.
- Jia, Q., Teng, X., Yu, S., Si, Z., Li, G., Zhou, M., Cai, D., Qin, P., and Chen, B. (2019). Production of furfural from xylose and hemicelluloses using tin-loaded sulfonated diatomite as solid acid catalyst in biphasic system. *Bioresource Technology Reports*, *6*, 145–151.
- Khemthong, P., Daorattanachai, P., Laosiripojana, N., and Faungnawakij, K. (2012). Copper phosphate nanostructures catalyze dehydration of fructose to 5-hydroxymethylfurfural. *Catalysis Communications*, *29*, 96–100.
- Krishna, N. V., and Selvam, P. (2017). Acid-mediated synthesis of ordered mesoporous aluminosilicates: The challenge and the promise. *Chemistry - A European Journal*, *23*(7), 1604–1612.
- Li, Q., Wu, Z., Tu, B., Park, S. S., Ha, C. S., and Zhao, D. (2010). Highly hydrothermal stability of ordered mesoporous aluminosilicates Al-SBA-15 with high Si/Al ratio. *Microporous and Mesoporous Materials*, *135*(1–3), 95–104.
- Li, Y., Zhang, W., Zhang, L., Yang, Q., Wei, Z., Feng, Z., and Li, C. (2004). Direct synthesis of Al-SBA-15 mesoporous materials via hydrolysis-controlled approach. *The Journal of Physical Chemistry B*, *108*(28), 9739–9744.
- Liu, B., Ba, C., Jin, M., and Zhang, Z. (2015). Effective conversion of carbohydrates into biofuel precursor 5-hydroxymethylfurfural (HMF) over Cr-incorporated mesoporous zirconium phosphate. *Industrial Crops and Products*, *76*, 781–786.
- Liu, R., Cai, W., Ni, X., Shi, L., Wang, R., and Lin, S. (2020). Ultrastable and strongly acidic Al-SBA-15 with superior activity in LDPE catalytic cracking reaction. *Journal of Solid State Chemistry*, *286*, 121319.
- Lucas, N., Kokate, G., Nagpure, A., and Chilukuri, S. (2013). Dehydration of fructose to 5-hydroxymethyl furfural over ordered AlSBA-15 catalysts. *Microporous and Mesoporous Materials*, *181*, 38–46.
- Mathew, A. K., Abraham, A., Mallapureddy, K. K., and Sukumaran, R. K. (2018). Chapter 9 - Lignocellulosic biorefinery wastes, or resources ?. (Bhaskar, T., Pandey, A.,

- Mohan, S. V., Lee, D.-J., and Khanal, S. K., Eds.). *Waste Biorefinery*. (267–297). Elsevier B.V.
- Meynen, V., Cool, P., and Vansant, E. F. (2009). Verified syntheses of mesoporous materials. *Microporous and Mesoporous Materials*, 125(3), 170–223.
- Muthu Kumaran, G., Garg, S., Soni, K., Kumar, M., Gupta, J. K., Sharma, L. D., Rama Rao, K. S., and Murali Dhar, G. (2008). Synthesis and characterization of acidic properties of Al-SBA-15 materials with varying Si/Al ratios. *Microporous and Mesoporous Materials*, 114(1–3), 103–109.
- Najafi Sarpiri, J., Najafi Chermahini, A., Saraji, M., and Shahvar, A. (2021). Dehydration of carbohydrates into 5-hydroxymethylfurfural over vanadyl pyrophosphate catalysts. *Renewable Energy*, 164, 11–22.
- Nikolla, E., Román-Leshkov, Y., Moliner, M., and Davis, M. E. (2011). “One-pot” synthesis of 5-(hydroxymethyl)furfural from carbohydrates using tin-beta zeolite. *ACS Catalysis*, 1(4), 408–410.
- Ordonsky, V. V., Sushkevich, V. L., Schouten, J. C., Van Der Schaaf, J., and Nijhuis, T. A. (2013). Glucose dehydration to 5-hydroxymethylfurfural over phosphate catalysts. *Journal of Catalysis*, 300, 37–46.
- Perez, R. F., Albuquerque, E. M., Borges, L. E. P., Hardacre, C., and Fraga, M. A. (2019). Aqueous-phase tandem catalytic conversion of xylose to furfuryl alcohol over [Al]-SBA-15 molecular sieves. *Catalysis Science & Technology*, 9(19), 5350–5358.
- Pham, S. T., Nguyen, M. B., Le, G. H., Pham, T. T. T., Quan, T. T. T., Nguyen, T. D., Son, T. Le, and Vu, T. A. (2019). Cellulose conversion to 5 hydroxymethyl furfural (5-HMF) using Al-incorporated SBA-15 as highly efficient catalyst. *Journal of Chemistry*, 2019, 8.
- Pholjaroen, B., Li, N., Wang, Z., Wang, A., and Zhang, T. (2013). Dehydration of xylose to furfural over niobium phosphate catalyst in biphasic solvent system. *Journal of Energy Chemistry*, 22(6), 826–832.
- Rao, K. T. V., Souzanchi, S., Yuan, Z., Ray, M. B., and Xu, C. (2017). Simple and green route for preparation of tin phosphate catalysts by solid-state grinding for dehydration of glucose to 5-hydroxymethylfurfural (HMF). *RSC Advances*, 7(76), 48501–48511.

- Saha, B., and Abu-Omar, M. M. (2014). Advances in 5-hydroxymethylfurfural production from biomass in biphasic solvents. *Green Chemistry*, 16(1), 24–38.
- Samikannu, A., Konwar, L. J., Rajendran, K., Lee, C. C., Shchukarev, A., Virtanen, P., and Mikkola, J. P. (2020). Highly dispersed NbOPO₄/SBA-15 as a versatile acid catalyst upon production of renewable jet-fuel from bio-based furanics via hydroxyalkylation-alkylation (HAA) and hydrodeoxygenation (HDO) reactions. *Applied Catalysis B: Environmental*, 272, 118987.
- Saravanan, K., Park, K. S., Jeon, S., and Bae, J. W. (2018). Aqueous phase synthesis of 5-hydroxymethylfurfural from glucose over large pore mesoporous zirconium phosphates: Effect of calcination temperature. *ACS Omega*, 3(1), 808–820.
- Song, X., Yue, J., Zhu, Y., Wen, C., Chen, L., Liu, Q., Ma, L., and Wang, C. (2021). Efficient conversion of glucose to 5-hydroxymethylfurfural over a Sn-modified SAPO-34 zeolite catalyst. *Industrial & Engineering Chemistry Research*, 60(16), 5838–5851.
- Swift, T. D., Nguyen, H., Erdman, Z., Kruger, J. S., Nikolakis, V., and Vlachos, D. G. (2016). Tandem Lewis acid/Brønsted acid-catalyzed conversion of carbohydrates to 5-hydroxymethylfurfural using zeolite beta. *Journal of Catalysis*, 333, 149–161.
- Ungureanu, A., Dragoi, B., Hulea, V., Cacciaguerra, T., Meloni, D., Solinas, V., and Dumitriu, E. (2012). Effect of aluminium incorporation by the “pH-adjusting” method on the structural, acidic and catalytic properties of mesoporous SBA-15. *Microporous and Mesoporous Materials*, 163, 51–64.
- Weingarten, R., Tompsett, G. A., Conner, W. C., and Huber, G. W. (2011). Design of solid acid catalysts for aqueous-phase dehydration of carbohydrates: The role of Lewis and Brønsted acid sites. *Journal of Catalysis*, 279(1), 174–182.
- Wu, S., Han, Y., Zou, Y., Song, J., Zhao, L., and Di, Y. (2004). Synthesis of heteroatom substituted SBA-15 by the “pH-adjusting” method. *Chemistry of Materials*, 16(17), 486–492.
- Xia, H., Xu, S., Hu, H., An, J., and Li, C. (2018). Efficient conversion of 5-hydroxymethylfurfural to high-value chemicals by chemo- and bio-catalysis. *RSC Advances*, 8(54), 30875–30886.
- Xu, S., Yan, X., Bu, Q., and Xia, H. (2016). Highly efficient conversion of carbohydrates into 5-hydroxymethylfurfural using the bi-functional CrPO₄ catalyst. *RSC*

- Advances*, 6(10), 8048–8052.
- Xue, Z., Ma, M. G., Li, Z., and Mu, T. (2016). Advances in the conversion of glucose and cellulose to 5-hydroxymethylfurfural over heterogeneous catalysts. *RSC Advances*, 6(101), 98874–98892.
- Yu, I. K. M., and Tsang, D. C. W. (2017). Conversion of biomass to hydroxymethylfurfural: A review of catalytic systems and underlying mechanisms. *Bioresource Technology*, 238, 716–732.
- Yun, J. S., Bazardorj, S. E., and Ihm, S. K. (2009). Acidity control of Al-SBA-15 and its effect on the catalytic performance for steam reforming of dimethyl ether. *Journal of Chemical Engineering of Japan*, 42, 180–184.
- Zhang, T., Wei, H., Xiao, H., Li, W., Jin, Y., Wei, W., and Wu, S. (2020). Advance in constructing acid catalyst-solvent combinations for efficient transformation of glucose into 5-Hydroxymethylfurfural. *Molecular Catalysis*, 498, 111254.
- Zhang, Y., Wang, J., Li, X., Liu, X., Xia, Y., Hu, B., Lu, G., and Wang, Y. (2015). Direct conversion of biomass-derived carbohydrates to 5-hydroxymethylfurfural over water-tolerant niobium-based catalysts. *Fuel*, 139, 301–307.
- Zhao, D., Feng, J., Huo, Q., Melosh, N., Glenn, H., Chmelka, B. F., Stucky, G. D., Zhao, D., Feng, J., Huo, Q., Melosh, N., Fredrickson, G. H., Chmelka, B. F., and Stucky, G. D. (1998)a. Triblock Copolymer Syntheses of Mesoporous Silica with Periodic 50 to 300 Angstrom Pores. *Science*, 279(5350), 548–552.
- Zhao, D., Huo, Q., Feng, J., Chmelka, B. F., and Stucky, G. D. (1998)b. Nonionic triblock and star diblock copolymer and oligomeric surfactant syntheses of highly ordered, hydrothermally stable, mesoporous silica structures. *Journal of the American Chemical Society*, 120(24), 6024–6036.
- Zhu, L., Wang, J., Zhao, P., Song, F., Sun, X., Wang, L., Cui, H., and Yi, W. (2017). Preparation of the Nb-P/SBA-15 catalyst and its performance in the dehydration of fructose to 5-hydroxymethylfurfural. *Journal of Fuel Chemistry and Technology*, 45(6), 651–659.

CHAPTER III

PROPERTIES OF MESOPOROUS Al-SBA-15 FROM ONE-POT HYDROTHERMAL SYNTHESIS WITH DIFFERENT ALUMINIUM PRECURSORS AND CATALYTIC PERFORMANCES IN XYLOSE CONVERSION TO FURFURAL

3.1 Abstract

SBA-15 is a highly stable mesoporous silica with a uniform pore structure but a lack of active catalytic sites. The incorporation of aluminium (Al) into the SBA-15 structure introduces active sites, enhancing its catalytic properties. Here we report the synthesis of Al-incorporated SBA-15 (Al-SBA-15) by one-pot hydrothermal method from sodium aluminate (SA), aluminium sulfate (AS), and aluminium isopropoxide (AI). All Al-SBA-15 samples have mesoporous characteristics with the incorporation of Al in the structure, generating acidities. Despite the similar Si/Al ratios, their total acidities are different, ranging as follows: Al-SBA-15 (SA) < Al-SBA-15 (AS) < Al-SBA-15 (AI). In contrast, the ratio of Al in tetrahedral coordination (Al_{tet}) within the SBA-15 framework increases as follows: Al-SBA-15 (SA) > Al-SBA-15 (AS) > Al-SBA-15 (AI). From catalytic testing, all samples provide better xylose conversions and furfural yields than the pristine SBA-15. Xylose conversions increase with the total acidity, while furfural yields depend on the relative ratios of Lewis to Brønsted acid sites. Moreover, the lactic acid by-product increases with Al in octahedral coordination (Al_{oct}). The best catalyst is Al-SBA-15 (SA), giving high furfural yield and fewer by-products than the others. Further investigations of Al-SBA-15 (SA) revealed the optimum conditions: temperature of 170 °C, reaction time of 5 h, and catalyst loading of 0.10 g.

3.2 Introduction

Santa Barbara Amorphous No. 15 (SBA-15) is a mesoporous silica that has uniform pores with a two-dimensional hexagonal structure (Zhao, Huo, Feng, Chmelka, and Stucky, 1998). It has been widely employed as catalyst supports due to its high hydrothermal stability and thick pore walls (Zhao et al., 1998). Since the siliceous SBA-15 only has silanol groups on the surface, it has low acid strength and low catalytic activity. Therefore, the modification of siliceous SBA-15 with acid or heteroatom is necessary for catalytic roles.

The presence of aluminium (Al) in the structure of SBA-15, referred to as Al-SBA-15, could enhance the acidity for catalytic applications. The incorporation of aluminium into mesoporous silicas is one of the most modifications to improve the acid properties of materials. The obtained materials, Al-SBA-15 has both Lewis and Brønsted acidic sites which are essential active sites in acid-catalyzed reactions. Mesoporous aluminosilicate Al-SBA-15 materials could be prepared either by post-synthesis with grafting (Li, Wu, Tu, Park, Ha, and Zhao, 2010; Lucas, Kokate, Nagpure, and Chilukuri, 2013; Yun, Bazardorj, and Ihm, 2009) or direct-synthesis method (Gallo, Bisio, Gatti, Marchese, and Pastore, 2010; Li, Zhang, Zhang, Yang, Wei, Feng, and Li, 2004; Muthu Kumaran, Garg, Soni, Kumar, Gupta, Sharma, Rama Rao, and Murali Dhar, 2008; Wu, Han, Zou, Song, Zhao, and Di, 2004). The post-synthesis via the grafting method has some drawbacks, such as the requisite organic solvent, time-consuming process, and chemical diversity of Al species. Meanwhile, the direct synthesis via the pH-adjusting method is relatively simple, homogenizing the Al species incorporated in tetrahedral sites (Wu et al., 2004). The acidic properties of Al-SBA-15 can be adjusted by changing chemical compositions or varying Si/Al ratios, varying preparation conditions, and using different inorganic precursors. The choices of silicon and aluminium precursors have a significant effect on the formation of final materials since they are different in reactivity and solubility (Schwanke, Balzer, and Pergher, 2017).

Al-SBA-15 has been prepared from various Al sources, including aluminium sulfate ($\text{Al}_2(\text{SO}_4)_3$), aluminium nitrate ($\text{Al}(\text{NO}_3)_3$), aluminium hydroxide ($\text{Al}(\text{OH})_3$), and aluminium isopropoxide ($\text{Al}(\text{OC}_3\text{H}_7)_3$) to improve material properties (Vinu, Murugesan, Böhlmann, and Hartmann, 2004). The highest Al content in SBA-15 is obtained from

$\text{Al}(\text{OC}_3\text{H}_7)_3$. The effect of Al sources on the structure, acidity, and morphology of Al-SBA-15 was studied for the cracking reaction of low-density polyethylene (LDPE) (Liu, Cai, Ni, Shi, Wang, and Lin, 2020). The Al-SBA-15 using nitrate salt gives the highest catalytic activity due to the highest Brønsted acid strength. Hence, Al sources affect the acid strength of Al-SBA-15.

As biomass valorization has become a serious challenge to upgrade agricultural residues, there are no reports about Al-SBA-15 from different Al precursors involving in the acid-catalyzed transformation of xylose to furfural. Therefore, this work aims to study the effect of Al sources on the acidic properties and catalytic behavior of mesoporous aluminosilicate Al-SBA-15 catalysts prepared by the one-pot hydrothermal method.

3.3 Experimental

3.3.1 Synthesis of Al-SBA-15 samples

Al-SBA-15 samples were synthesized by a one-pot hydrothermal method modified from the literature (Li et al., 2004; Wu et al., 2004) from three aluminium sources including sodium aluminate (NaAlO_2 , 56% Al_2O_3 , Sigma-Aldrich), aluminium sulfate ($\text{Al}_2(\text{SO}_4)_3 \cdot 18\text{H}_2\text{O}$, 51-59%, Ajax Finechem), and aluminium isopropoxide ($\text{Al}(\text{OC}_3\text{H}_7)_3$, 98%, Sigma-Aldrich). Their final products were named Al-SBA-15 (SA), Al-SBA-15 (AS), and Al-SBA-15 (AI), respectively. The synthesis of Al-SBA-15 was carried out as follows: 5 g of copolymer Pluronic P123 (MW=5000, Sigma-Aldrich) as a template was dissolved in 80 mL of 0.1 M HCl solution at 40 °C. Then, 16 g of tetraethyl orthosilicate (98%, Sigma-Aldrich) as a silicon source was added into the clear solution and stirred for 2 h. Then, a powder of each aluminum source was added and stirred at 40 °C for 22 h to produce the gel with Si/Al = 20. After that, the pH of the mixture was adjusted to 7.5 by NH_3 solution (25%, Rankem). The gel was transferred to an autoclave and treated hydrothermally at 100 °C for 48 h. After being cooled down to room temperature, the solid product was filtered, washed with DI water, dried at 60 °C, and heated with a heating rate of 1 °C/min to 550 °C for 6 h. For comparison, siliceous SBA-15 was synthesized by the same procedure without adding any aluminum precursor and pH adjustment.

3.3.2 Characterization of Al-SBA-15 samples

Elemental compositions were determined by inductively coupled plasma-optical emission spectrometry (ICP-OES) on a PerkinElmer Optima 8000. The percentage of Al incorporation, analyzed by ICP, in the Al-SBA-15 structure is calculated using the following equation:

$$\text{Al incorporation (\%)} = \left[\frac{\text{Al}_p}{\text{Si}_p + \text{Al}_p} \right] \times \left[\frac{\text{Si}_i + \text{Al}_i}{\text{Al}_i} \right] \times 100 \quad (3.1)$$

Structural characteristics were analyzed by X-ray diffraction (XRD) on a Bruker-AXS D8 advance using Cu K α radiation in a 2θ range of 0.5-5° and 5-60° for low-angle and wide-angle scans, respectively. Functional groups were characterized by Fourier transform infrared (FTIR) spectroscopy using a Bruker Tensor 27 by KBr technique with a resolution of 4 cm⁻¹ and a scan number of 128.

Total acidity was measured by temperature-programmed desorption of NH₃ (NH₃-TPD) using a Chem Star instrument with a thermal conductivity detector. The samples were pretreated at 550 °C in He with a flow rate of 30 mL/min for 1 h and cooled down to 80 °C. Then, a mixed gas of 5%NH₃ in He was introduced with a flow rate of 30 mL/min for 1 h and flushed by He gas for 0.5 h to remove unadsorbed NH₃. The TPD process was performed in a temperature range of 50 - 600 °C with a heating rate of 10 °C/min under He flow with a rate of 30 mL/min.

Identification of acid sites using pyridine as a probe molecule was conducted by diffuse reflectance infrared Fourier transform (DRIFT) spectroscopy on a Thermo Scientific Nicolet iS50 FT-IR with a mercury cadmium telluride photo detector. The samples were pretreated at 150 °C for 1 h under N₂ with a flow rate of 60 mL/min. Pyridine was then introduced into the sample cell at 150 °C for 1 h. After that, N₂ gas with a flow rate of 60 mL/min was purged into the sample cell at 150 °C to remove non-adsorbed pyridine molecules, DRIFT spectra were recorded after 15, 30, 40, 60, 120, and 180 min. KBr powder was used as a reference.

N₂ adsorption-desorption isotherms were obtained using a BELSORP mini II physisorp analyzer. All samples were outgassed at 180 °C for 24 h. The specific surface area of all samples was calculated by the Brunauer-Emmett-Teller (BET) method.

Pore size and pore volume were analyzed by the Barrett–Joyner–Halenda (BJH) method. The morphologies of all samples were studied by scanning electron microscopy (SEM) on a Carl Zeiss AURIGA with a voltage of 3 kV.

Transmission electron microscopy (TEM) observations were performed on an FEI Tecnai G² 20 microscope operated at an accelerating voltage of 160 kV in bright field mode. For sample preparation, a small amount of each sample was dispersed in methanol, sonicated for a minute, and then dropped on a carbon-coated copper grid.

3.3.3 Catalytic testing on xylose conversion to furfural

The conversion of xylose to furfural was performed in a 100 mL batch reactor. In a typical procedure, xylose of 0.9 g and catalyst of 0.1 g were added to 30 mL of water. The reactor was purged, pressured with N₂ to 15 bar and heated at a desired temperature and time under stirring. A product mixture was separated and analyzed by high performance liquid chromatography (HPLC) on a Shimadzu using a Bio-rad Aminex HPX-87H ion exchange column at a temperature of 45 °C with a mobile phase of 0.5 mM H₂SO₄ at a flow rate of 0.6 mL/min. The products were analyzed by a UV detector at a wavelength of 210 nm, together with a refractive index detector. The xylose conversion and product yields were calculated by Equations (3.2) – (3.5):

$$\text{xylose conversion (mol\%)} = \frac{\text{mole of initial xylose} - \text{mole of final xylose}}{\text{mole of initial xylose}} \times 100 \quad (3.2)$$

$$\text{Furfural yield (mol\%)} = \frac{\text{mole of obtained furfural}}{\text{mole of initial xylose}} \times 100 \quad (3.3)$$

$$\text{Lactic acid yield (mol\%)} = \frac{3}{5} \times \frac{\text{mole of obtained lactic acid}}{\text{mole of initial xylose}} \times 100 \quad (3.4)$$

$$\text{Formic acid yield (mol\%)} = \frac{1}{5} \times \frac{\text{mole of obtained formic acid}}{\text{mole of initial xylose}} \times 100 \quad (3.5)$$

3.4 Results and discussion

3.4.1 Characterization of the Al-SBA-15 samples with various Al precursors

The Si/Al ratios of all Al-SBA-15 samples are listed in **Table 3.1**. All samples have similar Si/Al ratios, larger than the gel Si/Al ratio. This difference is normally observed from the direct synthesis (Bhange, Bhange, Pradhan, and Ramaswamy, 2011; Li et al., 2004; Lin, Shi, Ribeiro Carrott, Carrott, Rocha, Li, and Zou, 2011; Ungureanu, Dragoi, Hulea, Cacciaguerra, Meloni, Solinas, and Dumitriu, 2012; Vinu et al., 2004).

The low-angle XRD patterns of SBA-15 and Al-SBA-15 samples are shown in **Figure 3.1A**. SBA-15 shows peaks at 0.85, 1.46, and 1.69° corresponding to the (100), (110), and (200) reflections, respectively. These three diffraction peaks are characteristic of $P6mm$ hexagonal symmetry of SBA-15 materials (Luan, Hartmann, Zhao, Zhou, and Keven, 1999). The XRD patterns of all Al-SBA-15 also show three diffraction peaks indicating that they have the structural characteristic of SBA-15. However, the peaks appear at slightly lower angles than those from SBA-15. The (100) peaks of Al-SBA-15 (SA), Al-SBA-15 (AS), and Al-SBA-15 (AI) are at 0.81, 0.79, and 0.79°, respectively. From the literature (Calleja, Aguado, Carrero, and Moreno, 2007; Muthu Kumaran et al., 2008; van Grieken, Escola, Moreno, and Rodríguez, 2009), the shift was from the presence of Al in the SBA-15 structure. The substitution of Si^{4+} ion (ionic radius, 0.26 Å) by Al^{3+} ion (ionic radius, 0.39 Å) (Socci, Osatiashtiani, Kyriakou, and Bridgwater, 2019; van Grieken et al., 2009) leads to the expansion of the hexagonal unit cell (a_0). Therefore, the XRD results confirm that all samples contain Al in the SBA-15 structure. The intensity of diffraction peaks indicated the regularity of mesoporous array (Muthu Kumaran et al., 2008; Zhao, Wan, and Zhou, 2013). The incorporation of Al into SBA-15 reduced the hexagonal order of mesopores, which is in good agreement with the literature (Xing, Lv, Fu, Wang, Fan, Yang, and Yuan, 2017). In this work, the hexagonal order of mesopores decreased in a sequence of: SBA-15 > Al-SBA-15 (AI) > Al-SBA-15 (SA) > Al-SBA-15 (AS). Thus, the type of Al precursors affected both mesoporous structure and regularity of the mesoporous array of the obtained Al-SBA-15.

The wide-angle XRD patterns of all samples are shown in **Figure 3.1B**. Each sample shows a broad diffraction peak at 23°, indicating the amorphous phase of

SBA-5 (Bhange et al., 2011). The diffraction peaks associated with $\text{Al}(\text{OH})_3$ and Al_2O_3 phases could not be observed for any Al-SBA-15 samples, indicating the absence of $\text{Al}(\text{OH})_3$ and alumina phase or they are in amorphous forms (Bhange et al., 2011).

Table 3.1 Elemental compositions XRD results of SBA-15 and Al-SBA-15.

Sample	Si/Al ratio		XRD results	
	gel	product	$^1d_{(100)}$ (nm)	2a_0 (nm)
SBA-15	NA	NA	10.40	12.00
Al-SBA-15 (SA)	20	25.50	10.92	12.61
Al-SBA-15 (AS)	20	25.92	11.23	12.97
Al-SBA-15 (AI)	20	25.64	11.23	12.97

NA = not analyzed (no Al added)

1d -spacing of (100) was calculated from Bragg's law: $\lambda = 2d \sin \theta$

2 Unit cell was calculated as: $a_0 = 2d_{100} / \sqrt{3}$

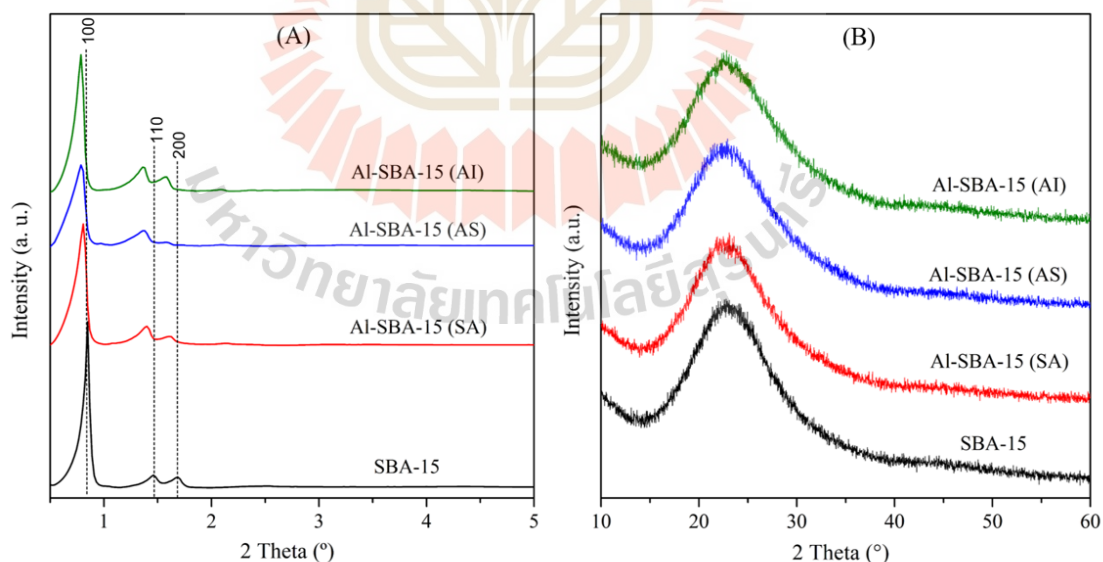


Figure 3.1 Low-angle (A) and wide-angle (B) XRD patterns of SBA-15 and Al-SBA-15 samples synthesized from three Al sources (SA = sodium aluminate, AS = aluminium sulfate, and AI = aluminium isopropoxide).

FTIR spectra of the Al-SBA-15 samples synthesized from three Al sources are compared to that of SBA-15 as shown in **Figure 3.2**. The FTIR of all samples are almost the same. The bands at 3458 and 1634 cm^{-1} are assigned to vibration of the -OH stretching (ν) and adsorbed water, respectively (Xing et al., 2017). All samples display four peaks at 1083, 960, 798, and 461 cm^{-1} which are attributed to Si-O-Si stretching, Si-OH stretching, T-O stretching (T = Si or Al), and Si-O-T bending (δ) modes of vibration, respectively (Betiha, Hassan, Al-Sabagh, Khder, and Ahmed, 2012; Xing et al., 2017). The intensity of the peak at 960 cm^{-1} for all Al-SBA-15 samples is lower than that of the pristine SBA-15. These results indicated that the isomorphous incorporation of Al in the Al-SBA-15 framework results in the reduction of silanol groups in comparison with the siliceous SBA-15. The results from FTIR and XRD are in good agreement, confirming the presence of Al in the structure of SBA-15.

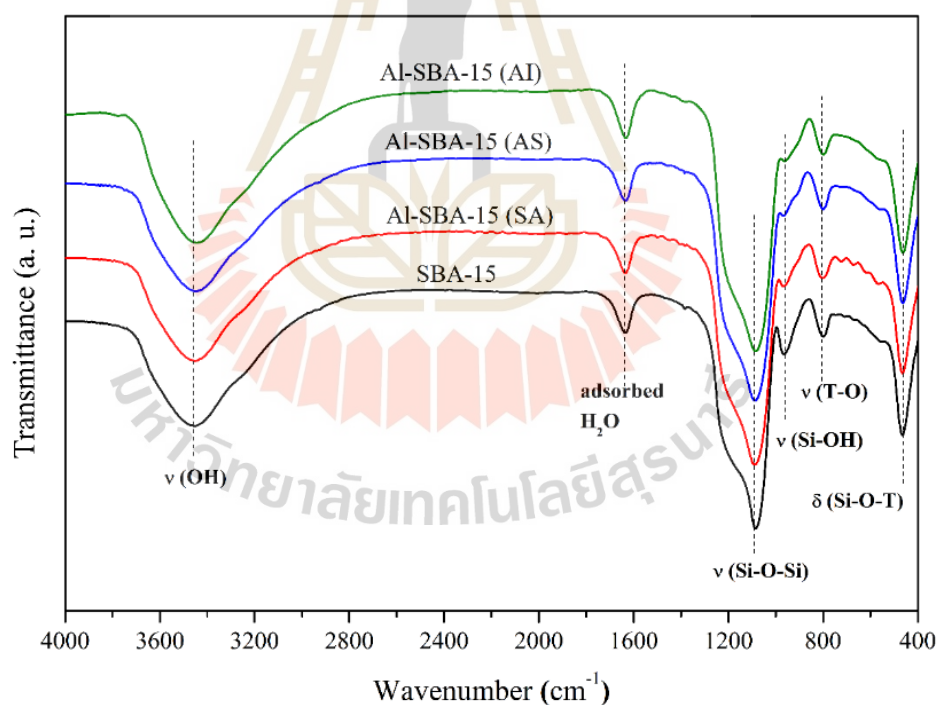


Figure 3.2 FTIR spectra of SBA-15 and Al-SBA-15 samples synthesized from three Al sources.

NH_3 -TPD profiles of SBA-15 and Al-SBA-15 from three Al sources are shown in **Figure 3.3**. The profile of SBA-15 shows no distinctive NH_3 desorption peak indicating

low acidity, due to the presence of only silanol groups. This observation is consistent with the literature (Li et al., 2004; Peng, Li, Liu, and Wang, 2017; Zhu, Wang, Xu, Xiao, and Li, 2013). On the other hand, the NH_3 -TPD profiles of all the Al-SBA-15 samples show a broad peak in a temperature ranging from 100 to 450 °C, suggesting the presence of acid sites in the studied samples with different acid strengths (Xing et al., 2017). Moreover, the obtained results confirm that the incorporation of Al species into the SBA-15 structure can increase the acidity of the SBA-15 (Koekkoek, Veen, Gerritsen, Giltay, Magusin, and Hensen, 2012; Xing et al., 2017). The profiles of Al-SBA-15 (AS) and Al-SBA-15 (AI) are similar, with the desorption in the temperature range of 120 - 400 °C with a peak of about 200 °C. The profile of Al-SBA-15 (SA) is different, having a broad plateau range with no distinct peak. Their total acidities are listed in **Table 3.2**. The order of total acidity is as follows: Al-SBA-15 (AI) > Al-SBA-15 (AS) > Al-SBA-15 (SA) > SBA-15. Besides the NH_3 -TPD technique, the samples were also analyzed by pyridine adsorption to distinguish the types of acid sites.

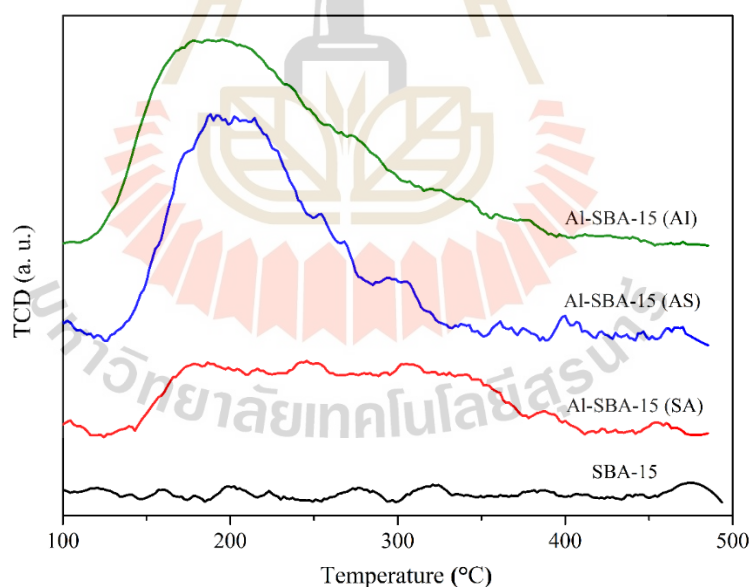


Figure 3.3 NH_3 -TPD profiles of SBA-15 and Al-SBA-15 samples synthesized from three Al sources.

DRIFT spectra for pyridine (Py) adsorption of the SBA-15 and all Al-SBA-15 samples are shown in **Figure 3.4**. The spectrum of pristine SBA-15 shows only one peak at 1446 cm^{-1} which is attributed to hydrogen bonding between Py and Si-OH (Py-

HO-Si) (Li et al., 2004). The spectra of all Al-SBA-15 from different Al sources show three adsorption peaks at 1546, 1491, and 1455 cm^{-1} which correspond to the bonding between Py and Brønsted acid sites (B), Lewis and Brønsted acid sites (L+B), and Lewis acid sites (L), respectively (Li et al., 2004). These results indicate that the incorporation of Al species into the SBA-15 created both L and B. The areas of L and B peaks as well as the L to B peak ratios of Al-SBA-15 with different Al precursors are summarized in **Table 3.2**. Relative quantities of L and B peak areas which directly correlate to a number of acid sites are in the following order: Al-SBA-15(AS) > Al-SBA-15(AI) > Al-SBA-15(SA). This trend is similar to that of the total acidity from NH_3 -TPD. This could imply highly-accessible non-framework Al species suggested by the FTIR and the NMR results from the literature (Calleja et al., 2007; Gallo et al., 2010; Li, Wang, Guo, Liu, Guo, Zhang, Wang, and Lu, 2007; Perez, Albuquerque, Borges, Hardacre, and Fraga, 2019). However, the L to B peak area ratios of all Al-SBA-15 samples were similar, suggesting that the distribution of acid sites would be proportional to the Si/Al ratio determined by ICP analysis.

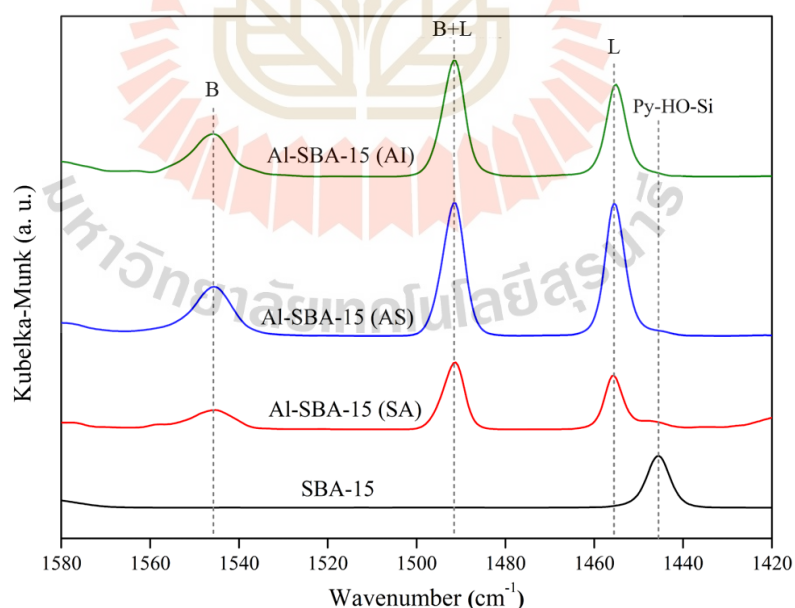


Figure 3.4 DRIFT spectra of pyridine adsorption at 150 °C for 3 h from SBA-15 and Al-SBA-15 samples synthesized from three Al sources.

Table 3.2 Peak area and ratios of L and B by pyridine adsorption and total acidity by NH_3 -TPD for SBA-15 and Al-SBA-15 samples with different Al sources.

Sample	Peak area			Total acidity by NH_3 -TPD (mmol/g)
	L	B	L/B	
SBA-15	-	-	-	0.038
Al-SBA-15 (SA)	0.1869	0.1297	1.4410	0.217
Al-SBA-15 (AS)	0.5221	0.3380	1.5447	0.409
Al-SBA-15 (Al)	0.3752	0.2801	1.3395	0.514

Figure 3.5 shows the XPS spectra of Al-SBA-15 samples. The binding energy values of Si 2p of the Al-containing samples are compared with the siliceous SBA-15 (**Figure 3.5A**), and those of Al 2p are compared with Al_2O_3 (**Figure 3.5B**). All binding energies are summarized in **Table 3.3**. Compared to SBA-15 in **Figure 3.5A**, the Si 2p binding energies of Al-SBA-15 shift to a lower value. The shift could be contributed to the presence of Si-O-Al species in the structure of Al-SBA-15. This observation is in good agreement with the work of Socci et al. (Socci et al., 2019). They reported that the shift to lower energies occurs with the increase of Al content. From this work, the order of the shift is Al-SBA-15 (SA) > Al-SBA-15 (Al) > Al-SBA-15 (AS). This could imply the degree of the incorporation of Al in the structure of SBA-15.

Al 2p spectra from all Al-SBA-15 samples are deconvoluted into two peaks at 74.8 and 73.1 eV (**Figure 3.5B**), corresponding to Al in octahedral and tetrahedral coordination (Al_{oct} and Al_{tet} , respectively) (Barr, Seal, Wozniak, and Klinowski, 1997). The Al_{tet} is referred to the Al incorporated in the structure of SBA-15 while Al_{oct} is attributed to extra-framework Al or Al_2O_3 species (Li et al., 2004). All samples have similar peak positions but the area ratios of $\text{Al}_{\text{tet}}/\text{Al}_{\text{oct}}$ are different (as listed in **Table 3.3**), depending on the Al precursor. Although the Si/Al ratios of these samples from ICP-OES are nearly similar (see **Table 3.1**), Al-SBA-15 (SA) has the highest $\text{Al}_{\text{tet}}/\text{Al}_{\text{oct}}$ ratio. The different coordination of Al could lead to the different catalytic activity of Al-SBA-15 for the conversion of xylose to furfural.

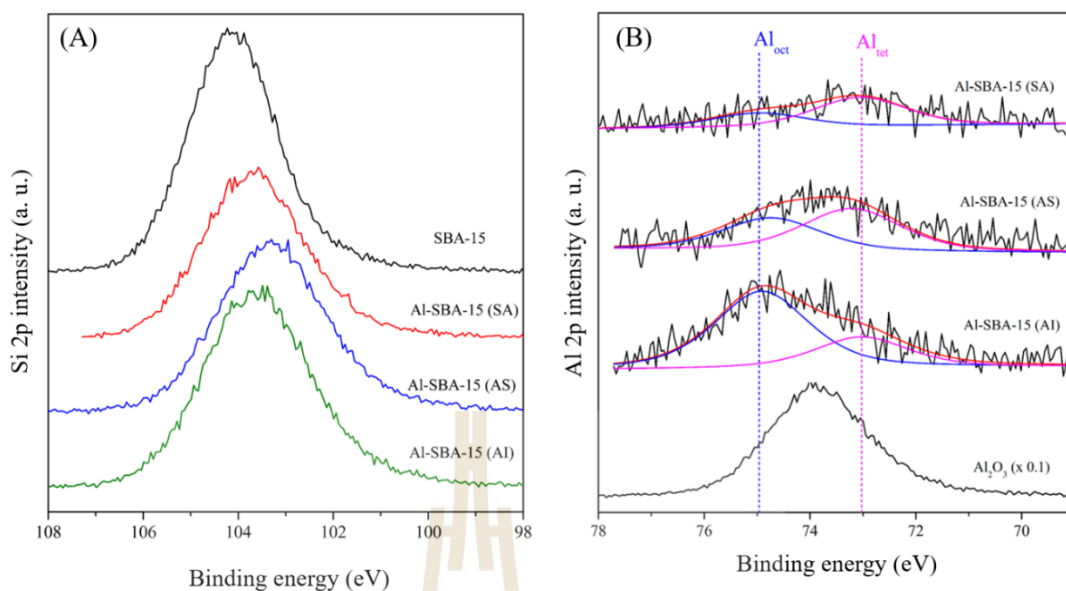


Figure 3.5 XPS spectra of (A) Si 2p for SBA-15 and Al-SBA-15 with three Al sources and (B) Al 2p for Al_2O_3 and Al-SBA-15 with three Al sources.

Table 3.3 XPS data of SBA-15 and Al-SBA-15 samples with three Al sources.

Sample	Binding energy (eV)			Ratio of $\text{Al}_{\text{tet}} : \text{Al}_{\text{oct}}$
	Si 2p	Al 2p		
		Al_{oct}	Al_{tet}	
SBA-15	104.2	-	-	-
Al-SBA-15 (SA)	103.6	74.9	73.0	67:33
Al-SBA-15 (AS)	103.3	74.8	73.1	57:45
Al-SBA-15 (AI)	103.5	74.9	72.9	29:71

The N_2 sorption isotherms of SBA-15 and Al-SBA-15 synthesized with different Al sources are shown in **Figure 3.6A**. All the samples show type IV(a) isotherm which is characteristic of mesoporous materials, according to IUPAC classification (Thommes, Kaneko, Neimark, Olivier, Rodriguez-Reinoso, Rouquerol, and Sing, 2015). The pristine SBA-15 shows a single step of desorption branch corresponding to the presence of open mesopores. The adsorbed volumes of N_2 on all Al-SBA-15 samples are higher than that on the pristine SBA-15. In brief, the adsorption starts from the formation of a monolayer followed by multilayers on mesoporous walls and

condensation inside the mesopores. Furthermore, the position and shape of hysteresis loops provide detailed information about the pores (Muthu Kumaran et al., 2008; Zhao et al., 2013). All samples show a hysteresis loop of type H1 indicating a narrow range of uniform mesopores with a diameter wider than 4 nm (Thommes et al., 2015). In addition, the formation of these loops for the Al-SBA-15 samples was at a higher relative pressure than the pristine SBA-15, implying that incorporating Al species into SBA-15 increases the pore size. These results agree with the previous literature report (Calleja et al., 2007; Krishna and Selvam, 2017; van Grieken et al., 2009; Xing et al., 2017). They explained that the pH adjustment led to disturbance of the double-walled hydrogen interactions $S^0H^+[X^-]H^{+0}$ during the formation of frameworks (where S^0 = surfactant, X^- = anions and $Al(OH)_4^-$, and I^0 = silica) (Krishna and Selvam, 2017). Moreover, the pH-adjusting method impacts the ordering of the mesoporous structures, which is consistent with the results of Ungureanu et al. (2012).

Al-SBA-15 (SA) exhibits a larger and oblique hysteresis loop. In the case of Al-SBA-15 (AS), the oblique hysteresis loop is larger than that of the Al-SBA-15 (SA) sample. While Al-SBA-15 (AI) presents a straight hysteresis loop similar to that of the pristine SBA-15, which corresponds to regular uniform mesopores as evidenced by pore size distributions in **Figure 3.6B**. BET specific surface area, pore size, and pore volume of all samples are summarized in **Table 3.4**. BET specific surface areas of all Al-SBA-15 samples were smaller than that of the pristine SBA-15, probably due to the presence of extra-framework Al species or amorphous alumina.

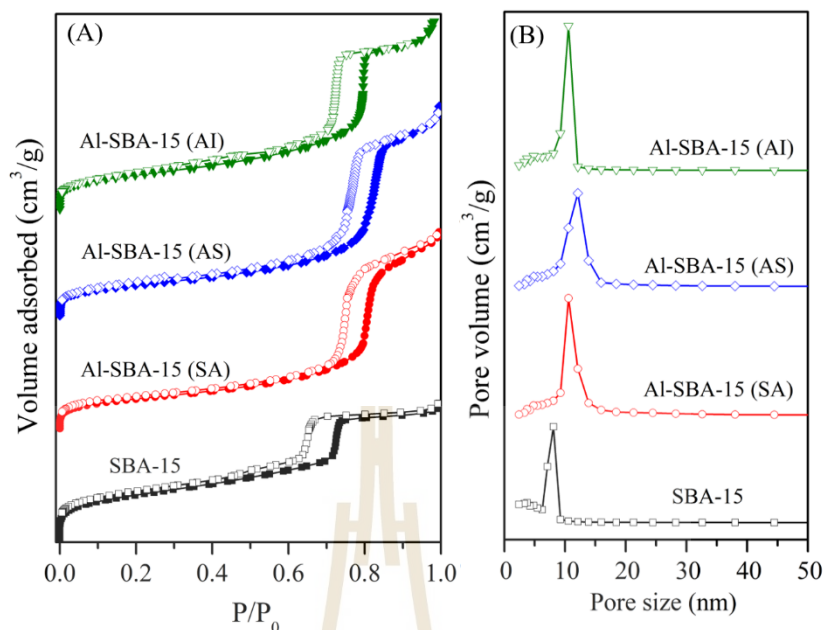


Figure 3.6 N₂ sorption isotherms of SBA-15 and Al-SBA-15 from three Al sources; filled symbol = adsorption and hollow symbol = desorption.

Table 3.4 Textural properties of SBA-15 and Al-SBA-15 from N₂ sorption analysis.

Sample	Specific surface area (m ² /g)	Pore size (nm)	Pore volume (cm ³ /g)
SBA-15	719	8.10	0.78
Al-SBA-15 (SA)	482	10.58	1.27
Al-SBA-15 (AS)	482	12.11	1.33
Al-SBA-15 (AI)	550	10.58	1.35

SEM images of the mesoporous SBA-15 and all Al-SBA-15 samples are shown in **Figure 3.7(A1-D1)**. The morphologies of all Al-SBA-15 samples are similar to that of the pristine SBA-15, except that there are amorphous particles on the surface. The particles could be the precipitate of silica during pH adjustment. This result indicated that the different Al precursors impact the morphology and particle size of the obtained Al-SBA-15 samples.

TEM images of the pristine SBA-15 and all Al-SBA-15 samples are shown in **Figure 3.7(A2-D3)**. The pristine SBA-15 shows well-ordered hexagonal arrays of mesopores (Osakoo, Henkel, Loiha, Roessner, and Wittayakun, 2014, 2015). TEM images of Al-SBA-15 (SA) and Al-SBA-15 (AI) samples prepared by the pH-adjusting one-step hydrothermal treatment show a similar structure as SBA-15. However, Al-SBA-15 (AS) sample exhibits an irregular hexagonal array, consistent with the XRD result which shows a broad peak of (100) reflection. In addition, the pore diameters of all Al-SBA-15 samples are larger than that of the pristine SBA-15, according to the N_2 sorption.

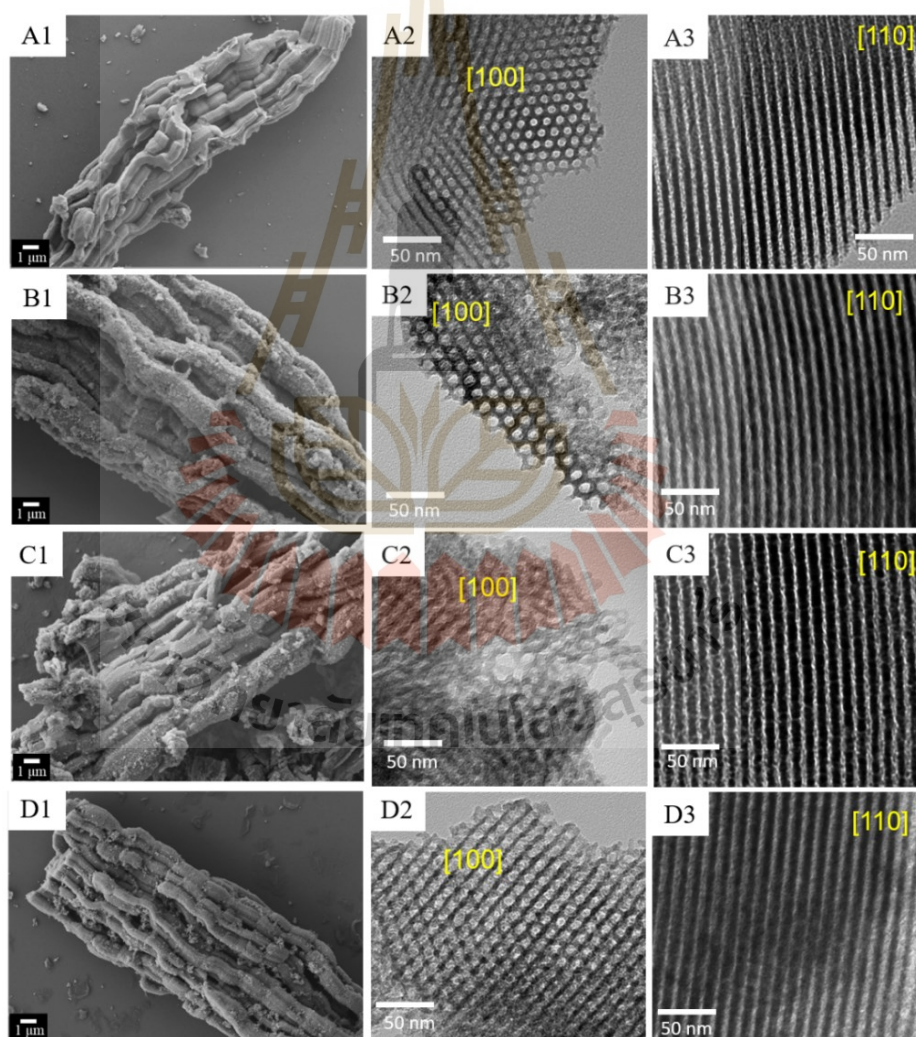


Figure 3.7 SEM and TEM images of (A) SBA-15, (B) Al-SBA-15 (SA), (C) Al-SBA-15 (AS), and (D) Al-SBA-15 (AI). 1= SEM, 2-3 = TEM.

According to all characterization results, the Al-SBA-15 samples from various Al precursors were successfully synthesized by the one-step hydrothermal treatment which is convenient, free from organic solvent and time-saving compared to the previous literature (Li et al., 2004; Wu et al., 2004). The introduction of Al from different sources into SBA-15 affects the textural and acidic properties of mesoporous Al-SBA-15 materials. Since the generated Al species determine mesostructured composites with different geometry and arrangement, the obtained samples could serve as effective catalysts to convert xylose to furfural.

3.4.2 Catalytic performance of Al-SBA-15 for xylose conversion to furfural

3.4.2.1 Effect of catalyst types and hydrothermal stability

The xylose conversion and product yields from the reaction at 170 °C for 5 h under the N₂ pressure of 15 bars are presented in **Figure 3.8A**. Without a catalyst, the xylose conversion was 52% and the products were furfural (43%) and formic yield (8%). Formic acid could be from the degradation of either xylose or furfural (Möller and Schröder, 2013). In addition, a small amount of unknown products is suggested from the mass balance. This could be humins from the condensation of furfural with reaction intermediates (You, Kim, and Park, 2014). Our results are consistent with the work by Termvidchakorn, Itthibenchapong, Songtawee, Chamnankid, Namuangruk, Faungnawakij, Charinpanitkul, Khunchit, Hansupaluk, Sano, and Hinode, (2017) who performed the reaction under the same testing but for 3 h. They reported the xylose conversion of $34.1 \pm 6.4\%$ and furfural selectivity of $57.6 \pm 7.1\%$. Qi and Xiuyang, (2006) investigated the non-catalyzed decomposition of xylose in a high-temperature water system at 180-220 °C under a pressure of 10 MPa. They observed an increase in both xylose conversion and furfural production with rising temperatures. In a high-temperature water system, water generates H₃O⁺ and OH⁻ ions by self-ionization, that act as acid-base catalysts and can facilitate the reaction in an aqueous solution (Akiya and Savage, 2002; Termvidchakorn et al., 2017). At high temperatures, the pH of water decreases (Plaza and Turner, 2015). Consequently, the increased H₃O⁺ is responsible for the conversion of xylose.

In the presence of SBA-15, the xylose conversion and furfural yield were slightly higher than in the system without the catalyst. The result could be attributed to the relatively low acidity of SBA-15, as evident from the NH_3 -TPD analysis. In the case of Al-SBA-15 catalysts, the xylose conversions and furfural yields were higher than those from the pristine SBA-15. The xylose conversions increased in this order: Al-SBA-15(SA) < Al-SBA-15(AS) < Al-SBA-15(Al), which correlated with the total acidity determined by NH_3 -TPD. Therefore, an increase in acidity is responsible for the higher conversion (Weingarten, Tompsett, Conner, and Huber, 2011).

Regarding the distribution of product yields, all Al-SBA-15 samples gave higher furfural yields than the pristine SBA-15. The furfural yield increased with the relative peak area ratios of LAS/BAS. Formic acid as a by-product was produced in the reactions and the yields were similar, despite the different catalysts. Moreover, lactic acid was also formed in the reaction systems with the Al-SBA-15 catalysts. The trend of lactic acid yields increases with the total acidity and xylose conversion. Thus, it is likely that xylose is preferably converted to lactic acid. According to the XPS data of Al 2p, the trend from the area ratio of $\text{Al}_{\text{tet}}/\text{Al}_{\text{oct}}$ is consistent with that of the yields of lactic acid. This finding suggests that the Al_{oct} sites have a significant role in the conversion of xylose to lactic acid.

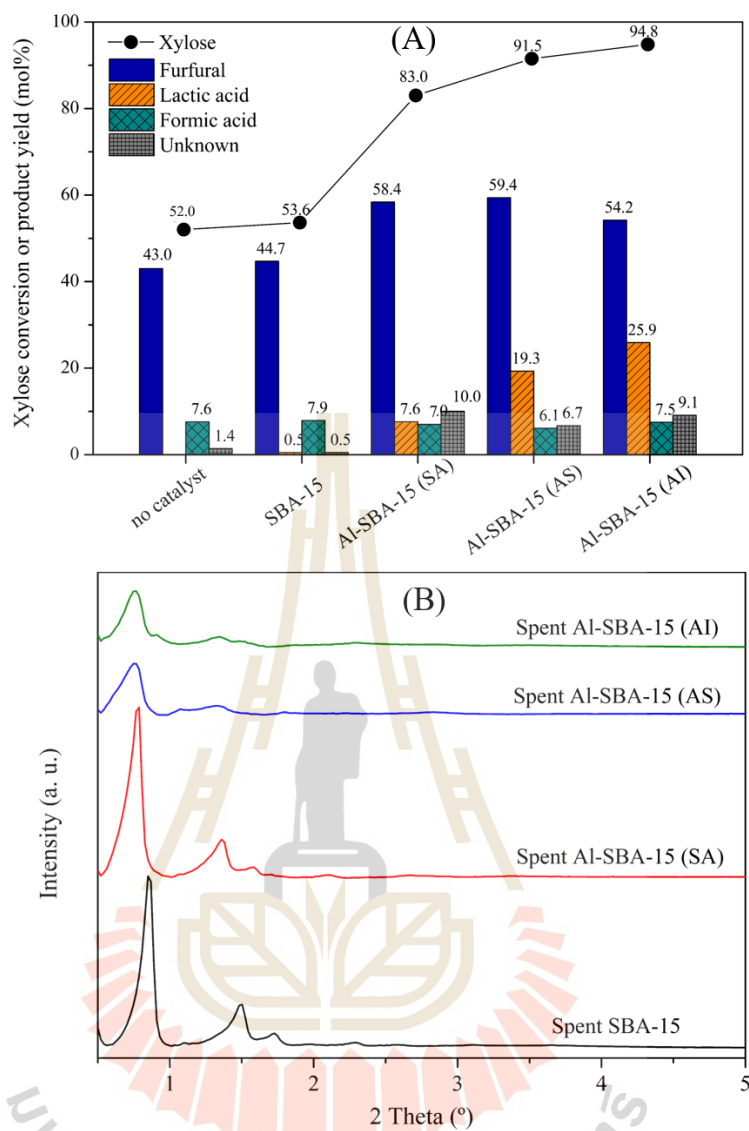
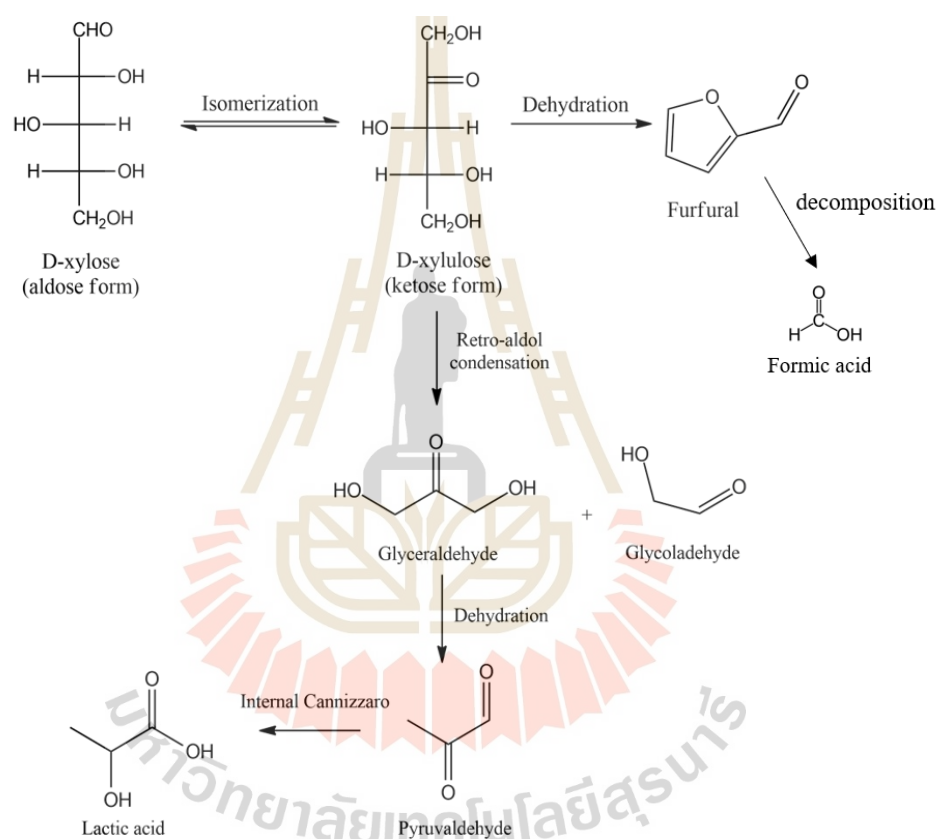


Figure 3.8 (A) Catalytic performance in xylose conversion to furfural without a catalyst and with SBA-15 and Al-SBA-15 from three Al sources (SA = sodium aluminate, AS = aluminium sulfate, and Al = aluminium isopropoxide). Reaction conditions: 100 mL batch reactor, 0.9 g of xylose, and 0.1 g of catalyst, 30 mL of water under pressure of N₂ of 15 bar at 170 °C for 5 h. (B) XRD patterns of spent catalysts.

Scheme 3.1 illustrates the proposed pathways of xylose conversion based on the findings of this study and the literature (Kammoun, Istasse, Ayebe, Rassaa, Bettaieb, and Richel, 2019; Möller and Schröder, 2013; Xu, Pan, Wu, Fan, Wu, Gao, Li, and Xiao, 2019). The formation of furfural occurs through the isomerization of xylose

to xylulose over Lewis acid sites, followed by the dehydration of xylulose facilitated by Brønsted acid sites (Xu et al., 2019). Lactic acid is produced from xylulose via retro-aldol condensation, dehydration, and internal Cannizzaro reaction on Lewis acid sites (Kammoun et al., 2019; Möller and Schröder, 2013). Moreover, the decomposition of furfural at high temperatures leads to the formation of formic acid (Möller and Schröder, 2013).



Scheme 3.1 Proposed reaction pathway of D-xylose conversion.

To investigate the catalyst stability after the reaction testing, the spent catalysts were washed, dried, and analyzed by low-angle XRD. **Figure 3.8B** displays the XRD patterns of spent SBA-15 and Al-SBA-15 (SA) catalysts, demonstrating that the characteristic peaks associated with the hexagonal mesoporous structure remained unchanged regarding peak position compared to the fresh catalyst. In contrast, the spent Al-SBA-15 (AS) and Al-SBA-15 (AI) catalysts exhibited weak diffraction peaks in

the low-angle region. This weak intensity can be attributed to the collapse of the hexagonal array of mesopore structures in these catalysts. According to these results, Al-SBA-15 (SA) was selected as a suitable solid acid catalyst for further reaction investigations.

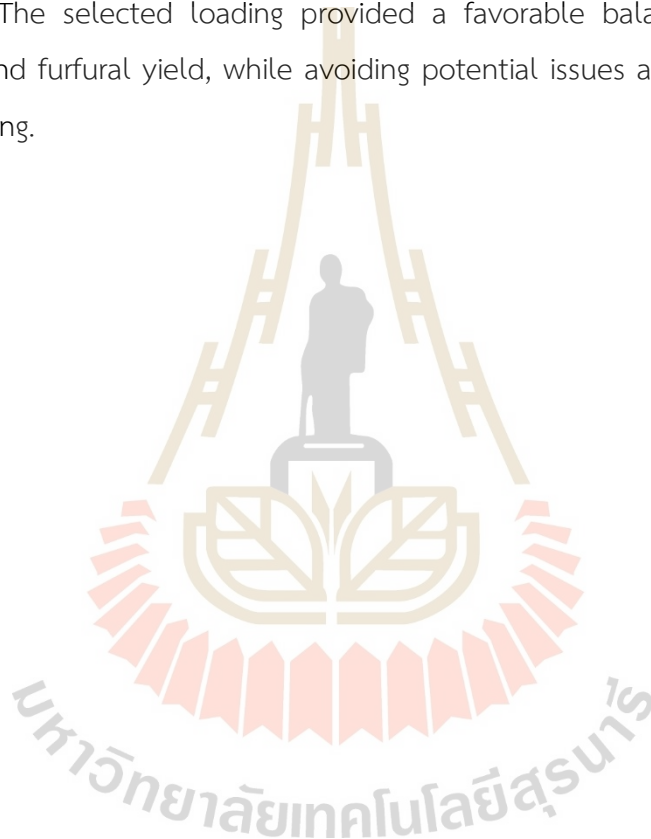
3.4.2.2 Effect of reaction temperature, time, and catalyst loading

In order to evaluate the performance of Al-SBA-15 (SA), the catalyst was tested for xylose conversion at different temperatures: 160, 170, and 180 °C for a reaction duration of 5 h with a catalyst loading of 0.10 g. The results of this investigation are presented in **Figure 3.9A**. It was observed that the xylose conversions increased with rising reaction temperatures, indicating that an increase in temperature typically increases the rate of the reaction. The highest yield of furfural was obtained at 170 °C. The yield of lactic acid and unknown products, suggested from the mass balance, also increased with the reaction temperature. This indicates that the formation of by-products is also an endothermic process. Possible reactions leading to the formation of by-products include fragmentation, condensation, and resinification (Wang, Liang, Shen, Qiu, Yang, and Qi, 2020; Xu, Pan, Wu, Song, Gao, Li, Das, and Xiao, 2018). The optimum temperature for xylose conversion to furfural using Al-SBA-15 (SA) as the catalyst in this study was 170 °C.

The reaction duration on Al-SBA-15 (SA) at 170 °C was studied for 3, 5, and 7 h, using a catalyst loading of 0.10 g. The results are shown in **Figure 3.9B**. It was observed that both the xylose conversion and the yields of all products increased with the reaction time. These results are consistent with the previous reports (Jia, Teng, Yu, Si, Li, Zhou, Cai, Qin, and Chen, 2019; Tran, Kongparakul, Karnjanakom, Reubroycharoen, Guan, Chanlek, and Samart, 2019). With the significant increase of by-products with time, 5 h was considered a suitable condition.

The influence of catalyst loading on xylose conversion to furfural over Al-SBA-15 (SA) at 170 °C for 5 h was investigated using three different amounts: 0.05, 0.10, and 0.20 g. The results are shown in **Figure 3.9C**. Although the catalyst loading of 0.10 g resulted in a lower xylose conversion compared to that of 0.20 g, it gave a high furfural yield of 58% which is considerably close to that of about 60% obtained

from the catalytic system with a catalyst loading of 0.20 g. Furthermore, the use of 0.10 g catalyst led to the production of furfural with the highest yield. Considering the obtained results, a catalyst loading of 0.10 g is suitable for the catalytic xylose conversion to furfural at 170 °C for 5 h. The excess loading of 0.20 g, could probably lead to more xylose adsorption on the catalyst and the excess acidity could accelerate the side reactions (Liu, Ma, Huang, Fu, and Chang, 2018). From the result, a catalyst loading of 0.10 g was optimal for the catalytic conversion of xylose to furfural at 170 °C for 5 h. The selected loading provided a favorable balance between xylose conversion and furfural yield, while avoiding potential issues associated with excess catalyst loading.



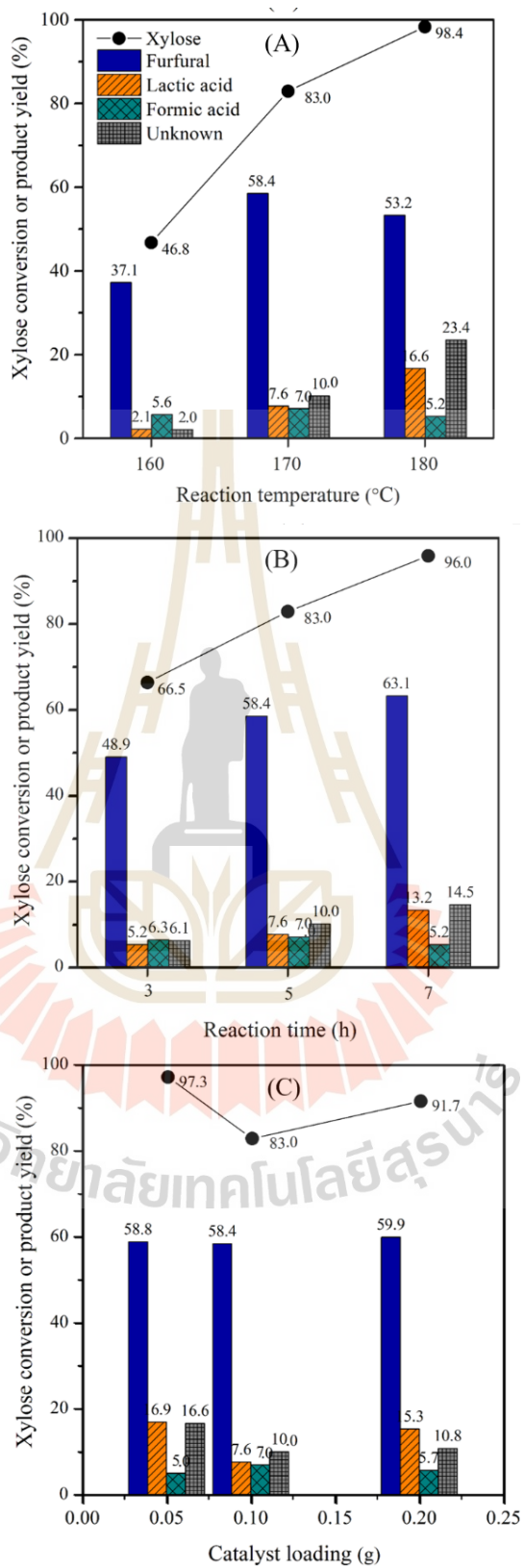


Figure 3.9 Catalytic performance for xylose conversion to furfural; reaction temperature (A), reaction time (B), and catalyst loading (C).

3.4.2.3 Catalyst recyclability of Al-SBA-15 (SA) catalyst

The recyclability of Al-SBA-15(SA) as a catalyst was investigated at 170 °C for 5 h, and the results are shown in **Figure 3.10**. In each reaction cycle, the catalyst was recovered by filtration, washing with water and acetone, drying at 100 °C before being used in the next reaction run. During the recycling process, it was observed that the catalytic activity of Al-SBA-15 (SA) decreased from the 1st to 3rd cycles. This decline in activity can be attributed to the deposition of solid humins on the active sites of the catalyst. After the 3rd cycle, the catalyst was regenerated by calcination at 550 °C for 4 h to remove residual organic compounds. The xylose conversion and furfural yield slightly increased after the regeneration step. This suggests that the regeneration process was effective in rejuvenating the catalyst by restoring its activity and removing the accumulated impurities.

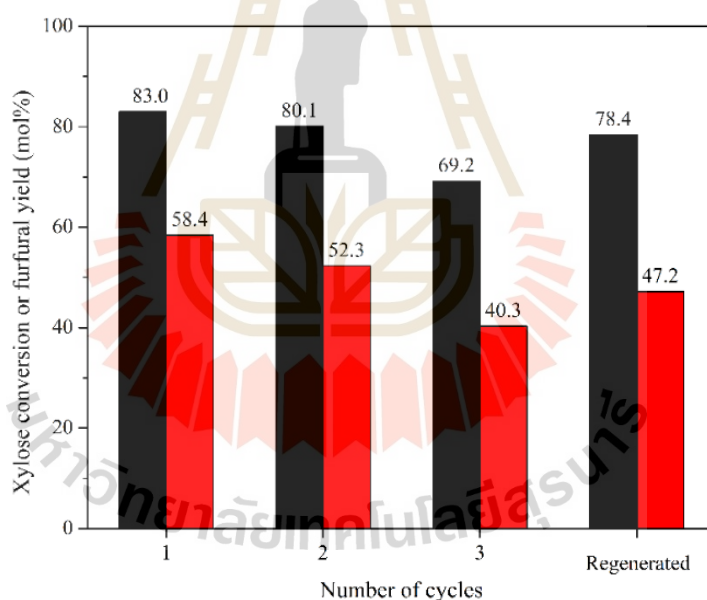


Figure 3.10 The recyclability of Al-SBA-15 (SA) catalyst. Reaction conditions: 100 mL batch reactor, 0.9 g of xylose, 0.1 g of catalyst, and 30 mL of water under pressure of N₂ of 15 bar at 170 °C for 5 h.

The catalytic performance of Al-SBA-15 (SA) in this work is compared to the works of other researchers in **Table 3.4**. In a short reaction time, Al-SBA-15 (SA) prepared by pH adjustment with the one-step hydrothermal treatment provided higher

xylose conversion and furfural yield than those of H-ZSM-5 synthesized by multi-steps (Gao, Liu, Pang, Yu, Du, Zhang, and Wang, 2014) and ZrPO prepared by using a precious metal precursor (Zhu, Kanamori, Brun, Péliesson, Moitra, Fajula, Hulea, Galarnéau, Takeda, and Nakanishi, 2016). In a long reaction time, the Al-SBA-15 (SA) still gave a higher catalytic activity than other catalysts (Antunes, Lima, Fernandes, Pillinger, Ribeiro, and Valente, 2012).



Table 3.5 Comparison of catalytic performance for the conversion of xylose to furfural.

Catalyst	Reaction condition					Acidity (mmol/g)	Xylose conversion (%)	Furfural yield (%)	Reference
	Solvent	Temp. (°C)	Time (h)	Pressure (bar)	Xylose/catalyst (g/g)				
H-MCM-22	H ₂ O	170	8	-	0.03/0.02	0.168	97	53	(Antunes et al., 2012)
ITQ-2	H ₂ O	170	16	-	0.03/0.02	0.198	73	51	
H-ZSM-5	H ₂ O	190	3	-	2.5/1.0	NA	75	30	(Gao et al., 2014)
ZrPO	H ₂ O	170	4	-	0.45/0.03	0.830	59	35	(Zhu et al., 2016)
SBA-15	H ₂ O	170	5	15	0.9/0.1	0.038	54	45	This work
Al-SBA-15 (SA)	H ₂ O	170	5	15	0.9/0.1	0.217	84	58	This work
Al-SBA-15 (SA)	H ₂ O	170	7	15	0.9/0.1	0.217	96	63	This work
Al-SBA-15 (AS)	H ₂ O	170	5	15	0.9/0.1	0.409	92	59	This work
Al-SBA-15 (AI)	H ₂ O	170	5	15	0.9/0.1	0.514	95	54	This work

3.5 Conclusions

Three different types of Al-SBA-15 catalysts were successfully synthesized by a one-pot hydrothermal with pH adjusting method from sodium aluminate (SA), aluminium sulphate (AS), and aluminium isopropoxide (AI). The choice of aluminium sources significantly impacted the structural properties, surface acidity, and morphologies of Al-SBA-15. The Al-SBA-15 samples exhibited higher acidity compared to pristine SBA-15, with the acidity increasing in the order of Al-SBA-15 (SA) < Al-SBA-15 (AS) < Al-SBA-15 (AI). In the catalytic testing, the xylose conversion increased with the total acidity of the catalyst. The furfural yields increase with the relative ratios of Lewis to Brønsted acid sites, while the by-product lactic acid increases with increasing amounts of Al in octahedral coordination. The preservation of their mesoporous structure confirmed the thermal stability of the catalysts after catalytic testing. Based on the results, Al-SBA-15 (SA) was identified as the most suitable catalyst, exhibiting high xylose conversion and furfural selectivity. The optimum reaction conditions were determined as a temperature of 170 °C, a reaction time of 5 h, and a catalyst loading of 0.10 g. Therefore, the one-pot hydrothermal synthesis of Al-SBA-15 (SA) demonstrated promising potential as a catalyst for the production of value-added chemicals in the conversion of xylose to furfural.

3.6 References

- Akiya, N., and Savage, P. E. (2002). Roles of water for chemical reactions in high-temperature water. *Chemical Reviews*, 102(8), 2725–2750.
- Antunes, M. M., Lima, S., Fernandes, A., Pillinger, M., Ribeiro, M. F., and Valente, A. A. (2012). Aqueous-phase dehydration of xylose to furfural in the presence of MCM-22 and ITQ-2 solid acid catalysts. *Applied Catalysis A: General*, 417–418, 243–252.
- Barr, T. L., Seal, S., Wozniak, K., and Klinowski, J. (1997). ESCA studies of the coordination state of aluminium in oxide environments. *Journal of the Chemical Society - Faraday Transactions*, 93(1), 181–186.
- Betiha, M. A., Hassan, H. M. A., Al-Sabagh, A. M., Khder, A. E. R. S., and Ahmed, E. A. (2012). Direct synthesis and the morphological control of highly ordered mesoporous ALSBA-15 using urea-tetrachloroaluminate as a novel aluminum source. *Journal of Materials Chemistry*, 22(34), 17551–17559.
- Bhange, P., Bhange, D. S., Pradhan, S., and Ramaswamy, V. (2011). Direct synthesis of well-ordered mesoporous Al-SBA-15 and its correlation with the catalytic activity. *Applied Catalysis A: General*, 400(1–2), 176–184.
- Calleja, G., Aguado, J., Carrero, A., and Moreno, J. (2007). Preparation, characterization and testing of Cr/ALSBA-15 ethylene polymerization catalysts. *Applied Catalysis A: General*, 316(1), 22–31.
- Gallo, J. M. R., Bisio, C., Gatti, G., Marchese, L., and Pastore, H. O. (2010). Physicochemical characterization and surface acid properties of mesoporous [Al]-SBA-15 obtained by direct synthesis. *Langmuir*, 26(8), 5791–5800.
- Gao, H., Liu, H., Pang, B., Yu, G., Du, J., Zhang, Y., and Wang, H. (2014). Bioresource Technology Production of furfural from waste aqueous hemicellulose solution of hardwood over ZSM-5 zeolite. *Bioresource Technology*, 172, 453–456.
- Jia, Q., Teng, X., Yu, S., Si, Z., Li, G., Zhou, M., Cai, D., Qin, P., and Chen, B. (2019). Production of furfural from xylose and hemicelluloses using tin-loaded sulfonated diatomite as solid acid catalyst in biphasic system. *Bioresource Technology Reports*, 6, 145–151.
- Kammoun, M., Istasse, T., Ayeb, H., Rassaa, N., Bettaieb, T., and Richel, A. (2019). Hydrothermal dehydration of monosaccharides promoted by seawater:

- Fundamentals on the catalytic role of inorganic salts. *Frontiers in Chemistry*, 7, 132.
- Koekkoek, A. J. J., Veen, J. A. R. Van, Gertsen, P. B., Giltay, P., Magusin, P. C. M. M., and Hensen, E. J. M. (2012). Brønsted acidity of Al/SBA-15. *Microporous and Mesoporous Materials*, 151, 34–43.
- Krishna, N. V., and Selvam, P. (2017). Acid-mediated synthesis of ordered mesoporous aluminosilicates: The challenge and the promise. *Chemistry - A European Journal*, 23(7), 1604–1612.
- Li, C., Wang, Y., Guo, Y., Liu, X., Guo, Y., Zhang, Z., Wang, Y., and Lu, G. (2007). Synthesis of highly ordered, extremely hydrothermal stable SBA-15/Al-SBA-15 under the assistance of sodium chloride. *Chemistry of Materials*, 19(2), 173–178.
- Li, Q., Wu, Z., Tu, B., Park, S. S., Ha, C. S., and Zhao, D. (2010). Highly hydrothermal stability of ordered mesoporous aluminosilicates Al-SBA-15 with high Si/Al ratio. *Microporous and Mesoporous Materials*, 135(1–3), 95–104.
- Li, Y., Zhang, W., Zhang, L., Yang, Q., Wei, Z., Feng, Z., and Li, C. (2004). Direct synthesis of Al-SBA-15 mesoporous materials via hydrolysis-controlled approach. *The Journal of Physical Chemistry B*, 108(28), 9739–9744.
- Lin, S., Shi, L., Ribeiro Carrott, M. M. L., Carrott, P. J. M., Rocha, J., Li, M. R., and Zou, X. D. (2011). Direct synthesis without addition of acid of Al-SBA-15 with controllable porosity and high hydrothermal stability. *Microporous and Mesoporous Materials*, 142(2–3), 526–534.
- Liu, R., Cai, W., Ni, X., Shi, L., Wang, R., and Lin, S. (2020). Ultrastable and strongly acidic Al-SBA-15 with superior activity in LDPE catalytic cracking reaction. *Journal of Solid State Chemistry*, 286, 121319.
- Liu, Y., Ma, C., Huang, C., Fu, Y., and Chang, J. (2018). Efficient conversion of xylose into furfural using sulfonic acid-functionalized metal-organic frameworks in a biphasic system. *Industrial and Engineering Chemistry Research*, 57(49), 16628–16634.
- Luan, Z., Hartmann, M., Zhao, D., Zhou, W., and Keven, L. (1999). Alumination and ion exchange of mesoporous SBA-15 molecular sieves. *Chemistry of Materials*, 11(6), 1621–1627.
- Lucas, N., Kokate, G., Nagpure, A., and Chilukuri, S. (2013). Dehydration of fructose to

- 5-hydroxymethyl furfural over ordered ALSBA-15 catalysts. *Microporous and Mesoporous Materials*, 181, 38–46.
- Möller, M., and Schröder, U. (2013). Hydrothermal production of furfural from xylose and xylan as model compounds for hemicelluloses. *RSC Advances*, 3(44), 22253–22260.
- Muthu Kumaran, G., Garg, S., Soni, K., Kumar, M., Gupta, J. K., Sharma, L. D., Rama Rao, K. S., and Murali Dhar, G. (2008). Synthesis and characterization of acidic properties of Al-SBA-15 materials with varying Si/Al ratios. *Microporous and Mesoporous Materials*, 114(1–3), 103–109.
- Osakoo, N., Henkel, R., Loiha, S., Roessner, F., and Wittayakun, J. (2014). Effect of support morphology and Pd promoter on Co/SBA-15 for Fischer-Tropsch Synthesis. *Catalysis Communications*, 56(3), 168–173.
- Osakoo, N., Henkel, R., Loiha, S., Roessner, F., and Wittayakun, J. (2015). Comparison of PdCo/SBA-15 prepared by co-impregnation and sequential impregnation for Fischer-Tropsch synthesis. *Catalysis Communications*, 66(3), 73–78.
- Peng, K., Li, X., Liu, X., and Wang, Y. (2017). Hydrothermally stable Nb-SBA-15 catalysts applied in carbohydrate conversion to 5-hydroxymethyl furfural. *Molecular Catalysis*, 441, 72–80.
- Perez, R. F., Albuquerque, E. M., Borges, L. E. P., Hardacre, C., and Fraga, M. A. (2019). Aqueous-phase tandem catalytic conversion of xylose to furfuryl alcohol over [Al]-SBA-15 molecular sieves. *Catalysis Science & Technology*, 9(19), 5350–5358.
- Plaza, M., and Turner, C. (2015). Pressurized hot water extraction of bioactives. *TrAC - Trends in Analytical Chemistry*, 71, 39–54.
- Qi, J., and Xiuyang, L. (2006). Kinetics of non-catalyzed decomposition of xylose in high temperature liquid water. *Chinese Journal of Chemical Engineering*, 22(5), 472–475.
- Schwanke, A. J., Balzer, R., and Pergher, S. (2017). Microporous and mesoporous materials from natural and inexpensive sources. *Handbook of Ecomaterials*, 5, 3379–3399.
- Socci, J., Osatiastiani, A., Kyriakou, G., and Bridgwater, T. (2019). The catalytic cracking of sterically challenging plastic feedstocks over high acid density Al-SBA-15

- catalysts. *Applied Catalysis A: General*, 570, 218–227.
- Termvidchakorn, C., Itthibenchapong, V., Songtawee, S., Chamnankid, B., Namuangruk, S., Faungnawakij, K., Charinpanitkul, T., Khunchit, R., Hansupaluk, N., Sano, N., and Hinode, H. (2017). Dehydration of D-xylose to furfural using acid-functionalized MWCNTs catalysts. *Advances in Natural Sciences: Nanoscience and Nanotechnology*, 8(3), 35006.
- Thommes, M., Kaneko, K., Neimark, A. V., Olivier, J. P., Rodriguez-Reinoso, F., Rouquerol, J., and Sing, K. S. W. (2015). Physisorption of gases, with special reference to the evaluation of surface area and pore size distribution (IUPAC Technical Report). *Pure and Applied Chemistry*, 87(9–10), 1051–1069.
- Tran, T. T. V., Kongparakul, S., Karnjanakom, S., Reubroycharoen, P., Guan, G., Chanlek, N., and Samart, C. (2019). Highly productive xylose dehydration using a sulfonic acid functionalized KIT-6 catalyst. *Fuel*, 236, 1156–1163.
- Ungureanu, A., Dragoi, B., Hulea, V., Cacciaguerra, T., Meloni, D., Solinas, V., and Dumitriu, E. (2012). Effect of aluminium incorporation by the “pH-adjusting” method on the structural, acidic and catalytic properties of mesoporous SBA-15. *Microporous and Mesoporous Materials*, 163, 51–64.
- van Grieken, R., Escola, J. M., Moreno, J., and Rodriguez, R. (2009). Direct synthesis of mesoporous M-SBA-15 (M = Al, Fe, B, Cr) and application to 1-hexene oligomerization. *Chemical Engineering Journal*, 155(1–2), 442–450.
- Vinu, A., Murugesan, V., Böhlmann, W., and Hartmann, M. (2004). An optimized procedure for the synthesis of AlSBA-15 with large pore diameter and high aluminum content. *Journal of Physical Chemistry B*, 108(31), 11496–11505.
- Wang, R., Liang, X., Shen, F., Qiu, M., Yang, J., and Qi, X. (2020). Mechanochemical synthesis of sulfonated palygorskite solid acid catalysts for selective catalytic conversion of xylose to furfural. *ACS Sustainable Chemistry and Engineering*, 8(2), 1163–1170.
- Weingarten, R., Tompsett, G. A., Conner, W. C., and Huber, G. W. (2011). Design of solid acid catalysts for aqueous-phase dehydration of carbohydrates: The role of Lewis and Brønsted acid sites. *Journal of Catalysis*, 279(1), 174–182.
- Wu, S., Han, Y., Zou, Y., Song, J., Zhao, L., and Di, Y. (2004). Synthesis of heteroatom

- substituted SBA-15 by the “pH-adjusting” method. *Chemistry of Materials*, 16(17), 486–492.
- Xing, S., Lv, P., Fu, J., Wang, J., Fan, P., Yang, L., and Yuan, Z. (2017). Direct synthesis and characterization of pore-broadened Al-SBA-15. *Microporous and Mesoporous Materials*, 239, 316–327.
- Xu, S., Pan, D., Wu, Y., Fan, J., Wu, N., Gao, L., Li, W., and Xiao, G. (2019). Catalytic conversion of xylose and xylan into furfural over Cr³⁺/P-SBA-15 catalyst derived from spent adsorbent. *Industrial and Engineering Chemistry Research*, 58(29), 13013–13020.
- Xu, S., Pan, D., Wu, Y., Song, X., Gao, L., Li, W., Das, L., and Xiao, G. (2018). Efficient production of furfural from xylose and wheat straw by bifunctional chromium phosphate catalyst in biphasic systems. *Fuel Processing Technology*, 175, 90–96.
- You, S. J., Kim, Y. T., and Park, E. D. (2014). Liquid-phase dehydration of D-xylose over silica-alumina catalysts with different alumina contents. *Reaction Kinetics, Mechanisms and Catalysis*, 111(2), 521–534.
- Yun, J. S., Bazardorj, S. E., and Ihm, S. K. (2009). Acidity control of Al-SBA-15 and its effect on the catalytic performance for steam reforming of dimethyl ether. *Journal of Chemical Engineering of Japan*, 42, 180–184.
- Zhao, D., Huo, Q., Feng, J., Chmelka, B. F., and Stucky, G. D. (1998). Nonionic triblock and star diblock copolymer and oligomeric surfactant syntheses of highly ordered, hydrothermally stable, mesoporous silica structures. *Journal of the American Chemical Society*, 120(24), 6024–6036.
- Zhao, D., Wan, Y., and Zhou, W. (2013). *Ordered Mesoporous Materials*. Weinheim, Germany : Wiley-VCH Verlag GmbH & Co.
- Zhu, J., Wang, T., Xu, X., Xiao, P., and Li, J. (2013). Pt nanoparticles supported on SBA-15 : Synthesis, characterization and applications in heterogeneous catalysis. *Applied Catalysis B: Environmental*, 130–131, 197–217.
- Zhu, Y., Kanamori, K., Brun, N., Péliisson, C., Moitra, N., Fajula, F., Hulea, V., Galarneau, A., Takeda, K., and Nakanishi, K. (2016). Monolithic acidic catalysts for the dehydration of xylose into furfural. *Catalysis Communications*, 87, 112–115.

CHAPTER VI

BIFUNCTIONAL METAL PHOSPHATE SUPPORTED ON Al-SBA-15 CATALYSTS FOR ONE-POT CONVERSION OF GLUCOSE TO 5-HYDROXYMETHYLFURFURAL IN A BIPHASIC SOLVENT SYSTEM

4.1 Abstract

The conversion of glucose into 5-hydroxymethylfurfural (5-HMF) using a combination of metal phosphates (Cr, Zr, Nb, Sr, and Sn) supported on mesoporous Al-SBA-15 catalysts with bifunctional Lewis-Brønsted acid sites was investigated. A biphasic solvent system consisting of NaCl-H₂O/*n*-butanol was employed for *in situ* product extraction. The metal phosphates were deposited on the Al-SBA-15 surface via a facile wet impregnation method. Characterization techniques such as NH₃-TPD and pyridine-DRIFT confirmed the presence of Lewis (L) and Brønsted (B) acid sites on the catalysts. Catalytic testing revealed that increasing the total acidity led to enhanced glucose conversions, while the yield of 5-HMF depended on the L/B ratio. Notably, the CrPO/Al-SBA-15 catalyst exhibited the highest performance, attributed to its highest acidity of 0.65 mmol/g and L/B ratio of 1.88. Furthermore, varying the PO/Cr ratios (2.0, 1.0, and 0.5) and studying their impact on the L/B ratio and structural properties using X-ray absorption spectroscopy (XAS) revealed that the CrPO/Al-SBA-15 catalyst with a PO/Cr molar ratio of 2 achieved the highest 5-HMF yield (52%) with a glucose conversion of 97% at 190 °C for 2 h. This alternative CrPO(2)/Al-SBA-15 could be considered a promising catalyst for glucose conversion into valuable chemicals in future biorefinery processes.

4.2 Introduction

The one-pot conversion of glucose to 5-hydroxymethylfurfural (5-HMF) is a crucial step in the sustainable utilization of renewable biomass (Shao, Ding, Dai, Long, and Hu, 2021). 5-HMF is a versatile platform molecule that can be further processed into various high-value chemicals and alternative fuels (Hou, Qi, Zhen, Qian, Nie, Bai, Zhang, Bai, and Ju, 2021; Kong, Li, Xu, and Fu, 2020; Shao et al., 2021; Xia, Xu, Hu, An, and Li, 2018; Xue, Ma, Li, and Mu, 2016). Among the different sugars, glucose stands out as a promising candidate for large-scale 5-HMF production due to its abundance in lignocellulosic biomass and relatively low cost compared to fructose (Hou et al., 2021). However, converting glucose into 5-HMF is more challenging compared to fructose due to the inherent stability of its cyclic structure, requiring additional reaction steps (Xia et al., 2018). As a result, further advancements are needed to overcome these limitations and develop effective technologies for the production of 5-HMF from glucose. In particular, glucose can be converted into 5-HMF within a two-step reaction, consisting of isomerization of glucose to fructose catalyzed by a Lewis acid catalyst and subsequent dehydration of fructose to 5-HMF facilitated by a Brønsted acid catalyst (Hu, Wu, Jiang, Wang, He, Song, Xu, Zhou, Zhao, and Xu, 2020; Yu and Tsang, 2017). Thus, the combined Lewis and Brønsted acid catalytic system is required because it is very crucial for the one-pot catalytic conversion of glucose to 5-HMF.

Several researchers have developed bifunctional acid catalysts with tunable Lewis and Brønsted acid sites for one-pot conversion of glucose to 5-HMF such as acidic resins, acidic zeolites, metal oxides and metal phosphates (Hu et al., 2020; Xue et al., 2016). While almost those heterogeneous catalysts were reported, metal phosphates (MPOs) have been claimed as alternative solid catalysts for glucose-to-5-HMF conversion due to their tunable Lewis and Brønsted acid sites and high thermal stability (Alam, De, Singh, Saha, and Abu-Omar, 2014; Zhang, Wei, Xiao, Li, Jin, Wei, and Wu, 2020). However, MPOs often exhibit limited surface areas, resulting in a lower number of active sites. To enhance their catalytic properties, the dispersion of metal phosphates on mesoporous materials such as SBA-15 (Samikannu et al., 2020; Zhu et al., 2017), KIT-6 (Najafi Sarpiri, Najafi Chermahini, Saraji, and Shahvar, 2021), and SiO₂ (Huang, Su, Long, Chen, and Yao, 2018) has been explored. However, those siliceous

materials have low acidity. Consequently, Al-containing mesoporous silica materials such as Al-MCM-41 and Al-SBA-15 are of interest as supports for the deposition of metal phosphates. These materials have uniform mesoporous structures and moderate acidity with Lewis and Brønsted acid sites which could effectively catalyze large molecules (Dragoi, Dumitriu, Guimon, and Auroux, 2009; Li, Zhang, Zhang, Yang, Wei, Feng, and Li, 2004; Rakngam, Osakoo, Wittayakun, Chanlek, Pengsawang, Sosa, Butburee, Faungnawakij, and Khemthong, 2021; Ungureanu, Dragoi, Hulea, Cacciaguerra, Meloni, Solinas, and Dumitriu, 2012). Among these materials, mesoporous Al-SBA-15 stands out due to its suitable acid properties and catalytic activity in the conversion of cellulosic sugars (Rakngam et al., 2021). The mesoporous structure of Al-SBA-15 provides high surface area and pore accessibility, facilitating the dispersion of metal phosphate species and promoting catalytic activity. Thus, Al-SBA-15 is chosen as the catalyst support in this work.

Another vital factor for the efficient conversion of glucose to 5-HMF is the nature of the solvent system. Typically, the yield of 5-HMF from glucose in an aqueous system is usually low due to the formation of by-products from side reactions such as rehydration and polymerization of intermediates and the decomposition of 5-HMF (Xue et al., 2016).

Utilizing a biphasic solvent system consisting of water and an organic solvent could prevent the occurrence of side reactions because the produced 5-HMF is separated into the organic solvent phase *in situ* (Saha and Abu-Omar, 2014; Yu and Tsang, 2017). Several biphasic solvent systems were employed for glucose conversion to 5-HMF, including NaCl-H₂O/THF (Rao, Souzanchi, Yuan, Ray, and Xu, 2017), H₂O/MIBK (Zhang, Wang, Li, Liu, Xia, Hu, Lu, and Wang, 2015), H₂O/THF (Xu, Yan, Bu, and Xia, 2016), ionic liquid [Bmim]Cl (Liu, Ba, Jin, and Zhang, 2015). There was a report on adding inorganic salts to a biphasic H₂O/*n*-butanol system to convert glucose (Nikolla, Román-Leshkov, Moliner, and Davis, 2011). It was observed that the 5-HMF selectivity was in the following order: NaCl > MgCl₂ > KBr > KCl. Adding NaCl leads to the highest partition coefficient, reflecting the extracting ability of organic solvents. 5-HMF formed in the aqueous phase of the NaCl-H₂O/*n*-butanol system is extracted by *n*-butanol, leading

to the highest 5-HMF selectivity. Thus, the biphasic NaCl-H₂O/*n*-butanol system is employed in this study.

The goal of this work is to compare the catalytic activity of phosphates of Cr, Zr, Nb, Sr, and Sn supported on Al-SBA-15 in glucose conversion to 5-HMF in the biphasic NaCl-H₂O/*n*-butanol solvent system. All catalysts were characterized by advanced techniques to gain insights into their physicochemical and acidic properties. The relationship between the acidic properties and catalytic performances is discussed. Moreover, the MPO/Al-SBA-15 catalyst with the best activity is optimized to determine the proper phosphate-to-metal (PO/M) molar ratio. Finally, the catalyst stability is studied regarding the leaching of active species and catalyst recyclability.

4.3 Experiment

4.3.1 Synthesis of MPO/Al-SBA-15

Mesoporous Al-SBA-15 with a Si/Al ratio of 20 was synthesized as a catalyst support using TEOS and NaAlO₂ as silica and aluminium precursors, respectively, through a hydrothermal method (refer to **section 3.3.1** for details).

Metal phosphates (MPO) of Cr, Zr, Nb, Sr, and Sn supported on Al-SBA-15 were prepared by a wet impregnation method (Yang et al., 2015). The metal loading was fixed at 10 wt., and an initial phosphate-to-metal mole ratio of 2 was used. Metal salts, including chromium (III) nitrate nonahydrate (Cr(NO₃)₃·9H₂O > 99%, Sigma-Aldrich), zirconyl chloride octahydrate (ZrOCl₂·8H₂O > 98%, ACROS organics), niobium (V) chloride (NbCl₅ ~99%, Sigma-Aldrich), strontium nitrate (Sr(NO₃)₂ ~99.99%, Sigma-Aldrich), tin (II) chloride dihydrate (SnCl₂·2H₂O ~98%, Sigma-Aldrich), were used as metal precursors, while ammonium dihydrogen phosphate (NH₄H₂PO₄·2H₂O ~99%, Merck) was used as a phosphates precursor. Prior to the synthesis, metal and phosphate precursors were dissolved in 2 mL of deionized (DI) water with stirring until a clear solution was obtained. Subsequently, the Al-SBA-15 support was added to the solution, and the mixture was stirred for 4 h. The impregnated samples were then dried in a vacuum oven at 80 °C for 12 h and calcined at 450 °C for 3 h with a heating rate of 5 °C/min. The calcined products were named MPO/Al-SBA-15, where M represents Cr, Zr, Nb, Sr, and Sn.

To further investigation, the best performance catalyst was studied for the effect of phosphate-to-metal mole ratios, prepared from the same procedure. For comparison purposes, CrPO(0.5)/Al-SBA-15 and CrPO(1)/Al-SBA-15 were prepared with phosphate-to-chromium ratios of 0.5 and 1, respectively. Additionally, Cr/Al-SBA-15 was prepared by adding only the chromium precursor (producing 10 wt.%) to Al-SBA-15, while PO/Al-SBA-15 was prepared by adding only the phosphate precursor (producing 10 wt.%) to Al-SBA-15.

4.3.2 Characterization of MPO/Al-SBA-15 samples

X-ray diffraction (XRD) patterns were investigated by a Bruker D8 advance diffractometer using Cu K α radiation ($\lambda = 1.5406 \text{ \AA}$) with nickel filtered at 40 kV and 40 mA in the 2θ range of $0.5 - 5^\circ$ and $5 - 60^\circ$ for low-angle and wide-angle scan, respectively, with an increment of 0.01° and the scan speed of 0.2 s/step.

N₂ adsorption-desorption isotherms of mesoporous materials were determined on a NOVA 2000e. Prior to measurement, the samples were outgassed at 300 °C for 3 h. Specific surface areas were calculated using the Brunauer-Emmett-Teller (BET) method at a relative pressure range of 0.05 – 0.30. Pore size distribution and pore volume were analyzed by the Barrett-Joyner-Halenda (BJH) method using the N₂ desorption isotherm.

Functional groups were identified by Fourier transform infrared (FTIR) spectroscopy using a Bruker Tensor 27 in transmission mode. A KBr technique was employed with a resolution of 4 cm^{-1} and a scan number of 128.

The total acidity of all catalysts was determined by temperature-programmed desorption of NH₃ (NH₃-TPD) using a Quantachrome ChemStar TPX instrument equipped with a thermal conductivity detector (TCD). Briefly, the sample was activated at 400 °C under a helium (He) flow rate of 30 mL/min for 1 h, then cooled down to 80 °C. After reaching the cooled down temperature, 5% NH₃ in He with a flow rate of 30 mL/min was applied for 1 h. After the adsorption process, each sample was flushed with He for 0.5 h to remove the excess NH₃. The desorption was carried out under He flow by ramping the temperature up to 550 °C with a heating rate of 10 °C/min.

The acid types of all catalysts were also further analyzed using an *in situ* diffuse reflectance infrared Fourier transform (DRIFT) spectroscopy of pyridine adsorption through a Thermo Scientific Nicolet iS50 FTIR spectrometer. Each sample was pretreated at 350 °C for 2 h under vacuum conditions to remove the adsorbed water molecules. Pyridine vapor was then introduced into the sample cell at 150 °C for 1 h. After that, the sample was degassed at 150 °C for 30 min to remove gas-phase pyridine molecules. FTIR spectra were collected in the range of 400 – 4000 cm^{-1} with a resolution of 4 cm^{-1} . KBr powder was used as a reference.

The elemental analysis of Si, Al, O, Cr, and P in the best catalyst was determined using SEM-EDS analysis (SU8230, Hitachi) with a voltage of 5 kV. Transmission electron microscopy (TEM) was performed on a JEM-2100 JEOL microscope operated at an accelerating voltage of 200 kV. The oxidation states and forms of catalysts were analyzed by X-ray absorption near edge structure (XANES) at Beamline 5.2 of the Synchrotron Light Research Institute (SLRI, Public Organization). The XANES spectra of Cr K-edge and P K-edge were collected at room temperature in transmission and fluorescence modes, respectively. Chemical states of surface species of Cr 1s and P 2p were identified by X-ray photoelectron spectroscopy (XPS) using ULVAC-PHI PHI5000 VersaProbe II with Al K α radiation.

4.3.3 Catalytic testing on glucose conversion to 5-HMF

Each catalytic test was carried out in a 100 mL stainless-steel batch reactor equipped with a 75-mL Teflon liner using 0.1 g of catalyst, 0.3 g of glucose, and 30 mL of the solvent containing NaCl-saturated water (9 mL) and *n*-butanol (21 mL). The reactor was purged and pressured with N₂ to 15 bar and heated under a continuous magnetic stirring of 300 rpm. The final product solution was collected and extracted to separate aqueous and organic phases using a separatory funnel. The liquid products in both phases were filtered with a 0.22 μm syringe nylon filter before analyzing by high-performance liquid chromatography (HPLC) on a Shimadzu LC-20A series with a Bio-rad Aminex HPX-87H column, following similar conditions as described in section 3.3.3. The catalytic performance, the glucose conversion, fructose and 5-HMF yields,

and 5-HMF selectivity were calculated according to the following equations (4.1) – (4.4):

$$\text{Glucose conversion (\%)} = \left(\frac{\text{mole of initial glucose} - \text{mole of final glucose}}{\text{mole of initial glucose}} \right) \times 100 \quad (4.1)$$

$$\text{Fructose yield (\%)} = \left(\frac{\text{mole of produced fructose}}{\text{mole of initial glucose}} \right) \times 100 \quad (4.2)$$

$$\text{5-HMF yield (\%)} = \left(\frac{\text{mole of produced 5-HMF}}{\text{mole of initial glucose}} \right) \times 100 \quad (4.3)$$

$$\text{5-HMF selectivity (\%)} = \left(\frac{\text{mole of produced 5-HMF}}{\text{mole of reacted glucose}} \right) \times 100 \quad (4.4)$$

The best catalyst (CrPO) was further investigated to understand the effect of phosphate-to-metal molar ratios, including CrPO(0.5)/Al-SBA-15 and CrPO(1)/Al-SBA-15 catalysts. Additionally, Cr/Al-SBA-15 and PO/Al-SBA-15 were studied for comparison. The leaching of chromium into the reaction solution was quantified by an inductively coupled plasma optical emission spectrometer (ICP-OES, Perkinelmer, AVIO200).

4.4 Results and discussion

4.4.1 Influence of various metal phosphates supported on Al-SBA-15

4.4.1.1 Characterization of MPO/Al-SBA-15 (M = Cr, Zr, Nb, Sr, and Sn)

Low-angle XRD patterns of MPO/Al-SBA-15 samples are compared with the parent Al-SBA-15 in **Figure 4.1A**. The patterns of all MPO/Al-SBA-15 samples exhibit three well-resolved peaks indexed as (100), (110), and (200) reflections, indicating the well-ordered mesostructures of *P6mm* hexagonal symmetry of Al-SBA-15 materials (Wu, Han, Zou, Song, Zhao, and Di, 2004). This observation could confirm that the structure of Al-SBA-15 remains after steps of impregnating metal phosphates. Considering the (100) peak intensity of MPO/Al-SBA-15 samples, it was observed that this peak is lower than that of the parent Al-SBA-15 implying some partial filling of Al-

SBA-15 pores by metal phosphate particles. This assumption is in line with the work reported by Zhang et al., 2010. They explained that the peak intensities decrease after grafting zirconium phosphate onto SBA-15 due to the filling of mesopores. The wide-angle XRD patterns of all samples in **Figure 4.1B** exhibit a broad peak at $2\theta \sim 23.0^\circ$, corresponding to an amorphous phase of the Al-SBA-15 catalyst support (Bhange, Bhange, Pradhan, and Ramaswamy, 2011). However, SrPO/Al-SBA-15 was an exception; it shows diffraction peaks attributing to SrHPO₄ phase (Gashti, Stir, and Hulliger, 2016). Noticeably, the characteristic peaks of other metal phosphates were not observed in the XRD patterns, implying that these metal phosphates are present either in amorphous forms or with crystalline sizes smaller than 5 nm, which cannot be detected by XRD (Samikannu et al., 2020).

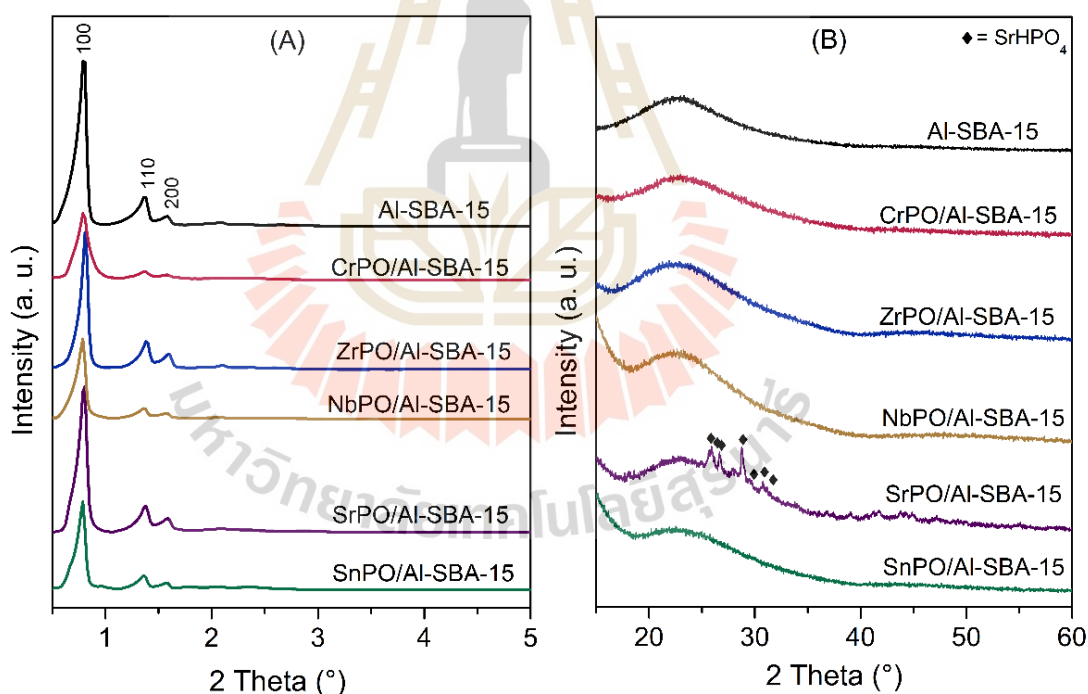


Figure 4.1 Low-angle (A) and wide-angle (B) XRD patterns of Al-SBA-15 and all MPO/Al-SBA-15 samples with different metal types (M = Cr, Zn, Nb, Sr, and Sn).

Figure 4.2 presents the N₂ adsorption-desorption isotherms and pore size distributions of all the samples. The specific surface areas and pore volumes of

all samples are summarized in **Table 4.1**. In **Figure 4.2A**, the isotherms of both Al-SBA-15 and MPO/Al-SBA-15 samples are classified as type IV according to the IUPAC classification (Thommes, Kaneko, Neimark, Olivier, Rodriguez-Reinoso, Rouquerol, and Sing, 2015). This type of adsorption behavior is characteristic of mesoporous materials, involving the adsorption of N_2 to form a monolayer on the mesoporous walls, followed by multilayer formation and condensation within the mesopores (Thommes et al., 2015). The presence of an H1-type hysteresis loop at a high relative pressure ($P/P_0 = 0.65-0.85$) is observed for Al-SBA-15 and all MPO/Al-SBA-15 samples, indicating a narrow range of cylindrical mesopores (Thommes et al., 2015). The adsorbed volumes, the specific surface areas, and pore volumes of MPO/Al-SBA-15 samples were smaller than Al-SBA-15. This can be attributed to the agglomeration of metal phosphate species on the surface of Al-SBA-15 and pore-blocking effects (Zhu et al., 2017a; Zhu, Song, Dai, and Song, 2017b), correlating with the decrease in the mesoporous structure observed in the XRD analysis.

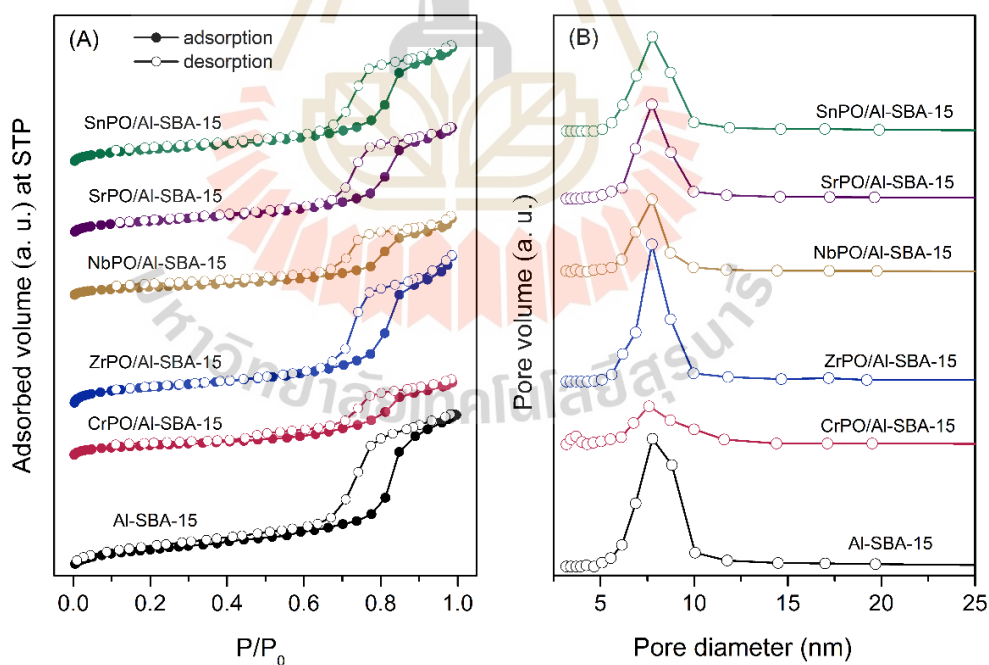


Figure 4.2 N_2 adsorption-desorption isotherms (A) and pore size distributions (B) of Al-SBA-15 and MPO/Al-SBA-15 with different metal types (M = Cr, Zn, Nb, Sr, and Sn).

The element compositions and surface chemical state of the MPO/Al-SBA-15 samples were investigated by X-ray photoelectron spectroscopy (XPS) and the XPS spectra of metal and phosphate species are shown in **Figure 4.3**. The Cr 2p XPS spectra of CrPO/Al-SBA-15 in **Figure 4A** show two peaks at 578.1 and 580.8 eV, corresponding to Cr³⁺ 2p_{3/2} and Cr⁶⁺ 2p_{3/2}, respectively. These two peaks exhibit higher binding energy (B.E.) than those of Cr³⁺ 2p_{3/2} and Cr⁶⁺ 2p_{3/2} in chromium oxide due to the difficult emission of electrons in this sample. The P 2p XPS spectra of CrPO/Al-SBA-15 (**Figure 4.3B**) exhibit peaks at 133.9 and 134.8 eV, corresponding to P 2p_{3/2} and P 2p_{1/2} of phosphate species.

For the ZrPO/Al-SBA-15 sample (in **Figure 4.3C**), the Zr 3d XPS spectrum displays two peaks at 183.5 and 185.9 eV, corresponding to Zr 3d_{5/2} and Zr 3d_{3/2}, respectively. This result is consistent with the literature (Saravanan, Park, Jeon, and Bae, 2018) who investigated mesoporous zirconium phosphates and observed the characteristic of Zr⁴⁺ species. The binding energy of the P 2p XPS spectra in ZrPO/Al-SBA-15 (**Figure 4.3D**) are observed at 133.9 and 135.1 eV, corresponding to P 2p_{3/2} and P 2p_{1/2} of metal phosphate species.

In the case of NbPO/Al-SBA-15 (**Figure 4.3E**), the two prominent peaks at 208.0 eV and 210.8 eV are assigned to Nb 3d_{5/2} and Nb 3d_{3/2}, respectively (Samikannu et al., 2020). This observation is consistent with the NbPO/SBA-15 samples reported by Samikannu et al. (2020) who observed the formation of the Si-O-Nb linkages (Si-O-NbOPO₄). The binding energy of the P 2p XPS spectra in NbPO/Al-SBA-15 (**Figure 4.3F**) are observed at 134.3 and 135.5 eV, corresponding to P 2p_{3/2} and P 2p_{1/2} of metal phosphate species.

The Sr 3d XPS spectrum of SrPO/Al-SBA-15 (**Figure 4.3G**) shows two peaks at 134.1 and 135.7 eV, corresponding to Sr 3d_{5/2} and Sr 3d_{3/2}, respectively. The binding energy of Sr 3d_{5/2} in this sample is higher than that in SrO (132.9 eV), implying the difficult emission of electrons from Sr atoms. From **Figure 4.3H**, the binding energy of the P 2p XPS spectra in SrPO/Al-SBA-15 are observed at 134.0 and 135.7 eV corresponding to P 2p_{3/2} and P 2p_{1/2} of metal phosphate species.

For SnPO/Al-SBA-15, the Sn 3d XPS spectrum (**Figure 4.3I**) displays two main peaks at 487.9 eV and 496.5 eV, corresponding to Sn 3d_{5/2} and Sn 3d_{3/2},

respectively. This is in accordance with the binding energies reported in the literature for SnPO with tetra-coordinated Sn^{4+} species (Hou, Zhen, Liu, Chen, Huang, Zhang, Li, and Ju, 2018; Wang, Liang, Huang, Li, and Chen, 2015). The binding energy of the P 2p XPS spectra in SnPO/Al-SBA-15 (**Figure 4.3J**) are observed at 134.1 and 135.0 eV, corresponding to P $2p_{3/2}$ and P $2p_{1/2}$ of metal phosphate species.



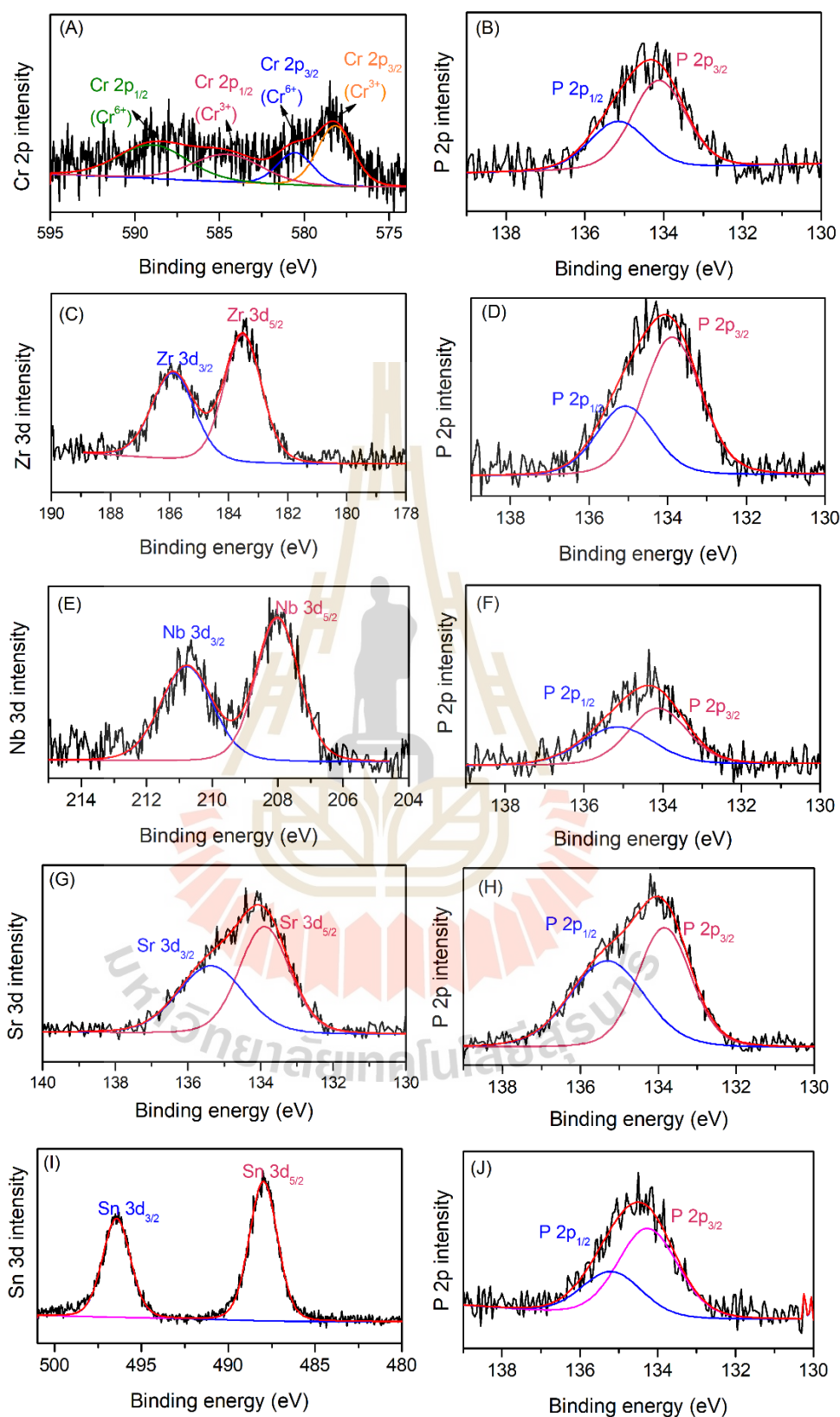


Figure 4.3 XPS spectra of CrPO/Al-SBA-15 (A-B), ZrPO/Al-SBA-15 (C-D), NbPO/Al-SBA-15 (E-F), SrPO/Al-SBA-15 (G-H) and SnPO/Al-SBA-15 (I-G) samples.

Since the conversion of glucose to 5-HMF on heterogeneous catalysts requires acid sites (Hou et al., 2018; Song, Yue, Zhu, Wen, Chen, Liu, Ma, and Wang, 2021), an investigation of the surface acidity is essential for understanding their catalytic activity. Therefore, the surface acidity of the parent Al-SBA-15 and MPO/Al-SBA-15 samples was determined by NH₃-TPD. The obtained NH₃-TPD profiles of all samples are presented in **Figure 4.4A**. Their total acidities are listed in **Table 4.1**. The NH₃-TPD profile of the parent Al-SBA-15 shows broad desorption in the temperatures range between 100 to 450 °C which originates from the incorporation of aluminium (Al) species (Rakngam et al., 2021). According to the literature (Krishna and Selvam, 2017), the desorption around 200 – 300 °C is attributed to weak Lewis acid sites of extra-framework Al species, confirmed by Al MAS NMR spectra. In the case of MPO/Al-SBA-15 samples, the total acidities are significantly higher than that of the parent Al-SBA-15. This observation is consistent with the previous reports (Samikannu et al., 2020; Najafi Sarpiri et al., 2021). The total acid amounts of the MPO/Al-SBA-15 samples were in the following order: ZrPO/Al-SBA-15 < NbPO/Al-SBA-15 < SrPO/Al-SBA-15 < SnPO/Al-SBA-15 < CrPO/Al-SBA-15. Besides the total acidity from the NH₃-TPD technique, all MPO/Al-SBA-15 samples were further analyzed by pyridine adsorption to distinguish the nature and type of acid sites.

The results from DRIFT spectra of pyridine adsorption of the Al-SBA-15 and MPO/Al-SBA-15 samples are shown in **Figure 4.3B**. The spectrum of each sample shows four peaks centered at 1446, 1455, 1491, and 1546 cm⁻¹, attributing to hydrogen bonding between pyridine and hydroxyl groups (H), pyridine adsorbed on Lewis acid sites (L), pyridine adsorbed on Brønsted and Lewis acid sites (B+L), and pyridine adsorbed on Brønsted acid sites (B), respectively (Li et al., 2004; Rakngam et al., 2021; Rezayan, Wang, Nie, Lu, Wang, Zhang, and Xu, 2022; Serrano, García, Vicente, Linares, Procházková, and Čejka, 2011; Wang, Rezayan, Si, Zhang, Nie, Lu, Wang, and Xu, 2021). The intensities of the H peaks from NbPO/Al-SBA-15 and ZrPO/Al-SBA-15 are considerably higher than those from other samples, implying the larger amounts of surface hydroxyl species (Serrano et al., 2011; Wang et al., 2021). The L/B ratios for all investigated samples are summarized in **Table 4.1**. The relative L/B peak area ratios

were in the following order: SnPO/Al-SBA-15 > CrPO/Al-SBA-15 > Al-SBA-15 > NbPO/Al-SBA-15 > ZrPO/Al-SBA-15 > SrPO/Al-SBA-15.

From the pyridine adsorption profiles, it can be concluded that the surface of all MPO/Al-SBA-15 samples possesses both Lewis and Brønsted acid sites. The metal cation site (M^+) could function as Lewis acid, while the P-OH site could act as Brønsted acid (Ordonsky, Sushkevich, Schouten, Van Der Schaaf, and Nijhuis, 2013). Notably, this evidence suggests the potential of these materials as solid catalysts for catalytic conversion of glucose to 5-HMF.

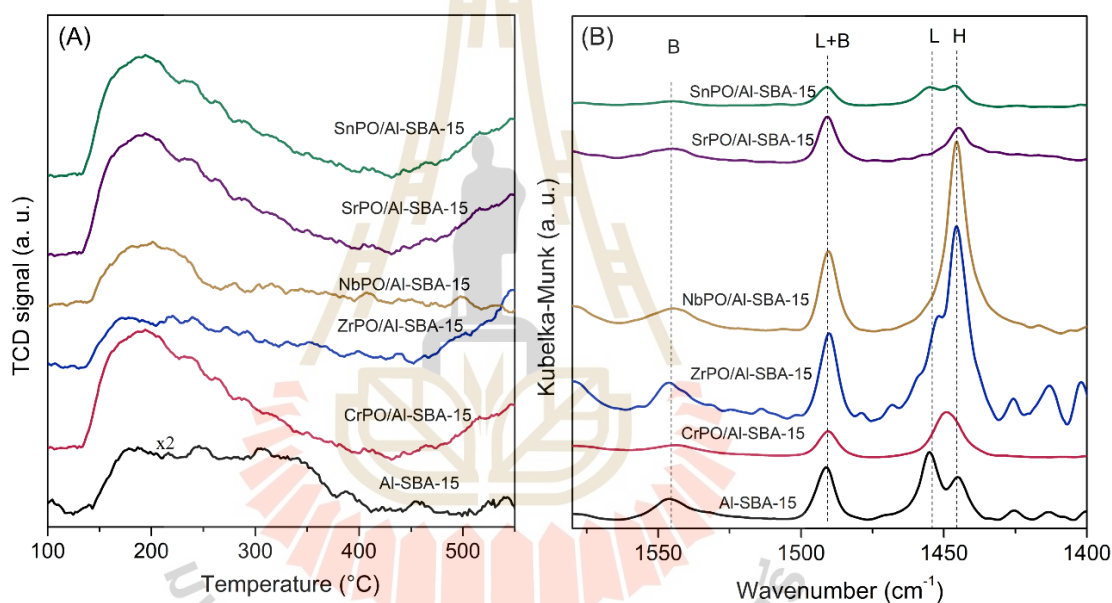


Figure 4.4 NH₃-TPD profiles (A) and pyridine-DRIFT spectra (B) of Al-SBA-15 and MPO/Al-SBA-15 samples (M = Cr, Zn, Nb, Sr, and Sn).

Table 4.1 Acidity and textural properties of Al-SBA-15 and MPO/Al-SBA-15.

Catalyst	Total acidity (mmol/g) ^a	L/B ^b	Textural properties	
			Surface area (m ² /g) ^c	Pore volume (cm ³ /g) ^d
Al-SBA-15	0.22	1.59	520	1.28
CrPO/Al-SBA-15	0.65	1.88	259	0.57
ZrPO/Al-SBA-15	0.40	0.76	402	1.13
NbPO/Al-SBA-15	0.42	1.31	230	0.75
SrPO/Al-SBA-15	0.53	0.61	302	0.80
SnPO /Al-SBA-15	0.59	1.97	317	0.89

^aDetermined by NH₃-TPD analysis. ^bCalculated by the relative peak area ratio of Lewis/Brønsted acid sites (L/B) from pyridine-DRIFT profiles. ^cAnalyzed by the BET method. ^dCalculated by the BJH method.

4.4.1.2 Catalytic screening of MPO/Al-SBA-15 for conversion of glucose to 5-HMF

In the initial screening, the reaction for the conversion of glucose to 5-HMF was tested at 150 °C for 4 h using a mesoporous Al-SBA-15 in two different solvents: monophasic water and biphasic NaCl-H₂O/*n*-butanol. The results are in **Figure 4.5**. In the monophasic water solvent, the yield of 5-HMF was low (approximately 8%) due to undesired side reactions to the formation of humins through rehydration of 5-HMF, and polymerization of 5-HMF and glucose (Xue et al., 2016). In the case of the biphasic NaCl-H₂O/*n*-butanol solvent, the glucose conversion was improved to 43% with the 5-HMF yield of 18%. This improvement can be attributed to the suppression of side reactions by *in situ* extraction of 5-HMF product into the organic layer (Songtawee, Rungtaweevoranit, Klaysom, and Faungnawakij, 2021; Yu and Tsang, 2017; Zhang et al., 2020). Moreover, the reaction without a catalyst provided glucose conversion of 30% with a low 5-HMF yield (8%). This phenomenon results from the acid-base properties of H₃O⁺ and OH⁻ ions, generated by the self-ionization of water

solvent at high temperatures (Akiya and Savage, 2002). Based on these findings, the biphasic NaCl-H₂O/*n*-butanol solvent system was selected as the reaction media for further study.

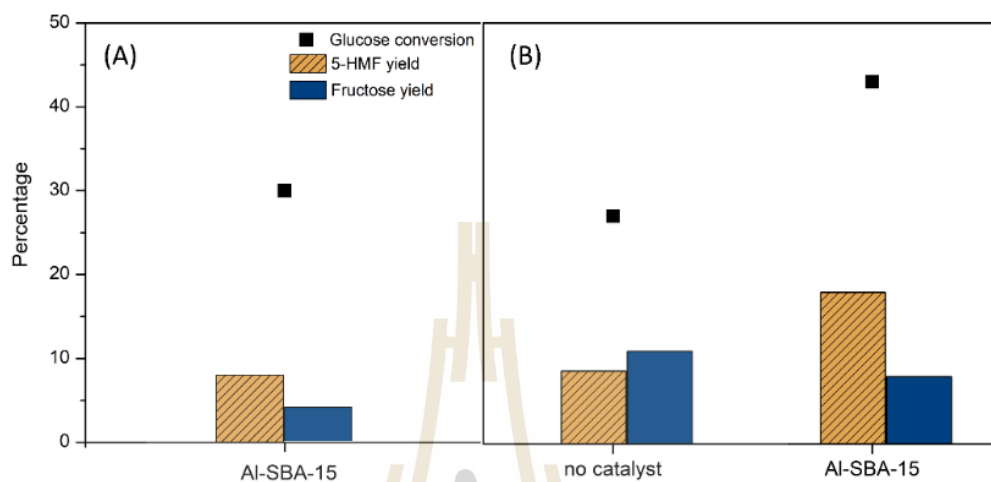
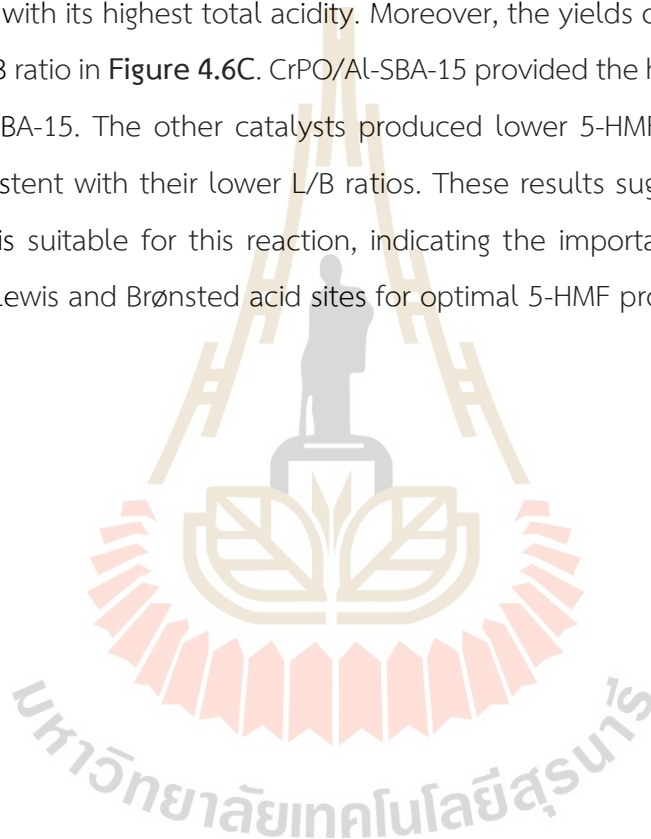


Figure 4.5 Effect of monophasic (A) and biphasic (B) solvent on glucose conversion to 5-HMF over a mesoporous Al-SBA-15. Reaction condition: glucose 0.3 g in 30 mL of biphasic NaCl-H₂O/*n*-butanol solvent, catalyst = 0.1 g, temperature = 150 °C, reaction time = 4 h.

Figure 4.6A compares the catalytic performance of all MPO/Al-SBA-15 catalysts and the parent Al-SBA-15 in glucose conversion to 5-HMF in a biphasic NaCl-H₂O/*n*-butanol system at 150 °C for 4 h. It is known from the literature (Hu et al., 2020; Yu and Tsang, 2017) that the reaction has two steps: glucose isomerization to fructose catalyzed by bases or Lewis acids and fructose dehydration to 5-HMF by Brønsted acid sites. The parent Al-SBA-15 catalyst gave a glucose conversion and 5-HMF of 43% and a yield of 18%. This performance is due to the presence of dual Lewis and Brønsted acid sites confirmed by pyridine adsorption. The framework Al species act as Lewis acid sites, while the bridging hydroxyl groups act as Brønsted acid sites (Rakngam et al., 2021). Hence, Al-SBA-15 is both a support and a catalyst to produce 5-HMF, agreeing with the literature (Lucas, Kokate, Nagpure, and Chilukuri, 2013).

After depositing the metal phosphates on Al-SBA-15, the glucose conversion increased to 52% on CrPO/Al-SBA-15 but decreased to ~30-35% on other

samples (**Figure 4.6A**). The trend of the glucose conversion based on the type of the metal phosphates follows this order: CrPO/Al-SBA-15 > SnPO/Al-SBA-15 > SrPO/Al-SBA-15 > NbPO/Al-SBA-15 > ZrPO/Al-SBA-15. This trend aligns with the order of the total acidity listed in **Table 4.1**, indicating that higher acidity results in higher conversion of glucose under identical employed reaction conditions. The glucose conversion is plotted versus the total acidity in **Figure 4.6B**. The plot indicates that total acidity is the key parameter for the reaction. The highest conversion achieved with CrPO/Al-SBA-15 correlates with its highest total acidity. Moreover, the yields of 5-HMF were plotted versus the L/B ratio in **Figure 4.6C**. CrPO/Al-SBA-15 provided the highest yield, followed by SnPO/Al-SBA-15. The other catalysts produced lower 5-HMF yields than bare Al-SBA-15, consistent with their lower L/B ratios. These results suggest that an L/B ratio of around 2 is suitable for this reaction, indicating the importance of balancing the presence of Lewis and Brønsted acid sites for optimal 5-HMF production.



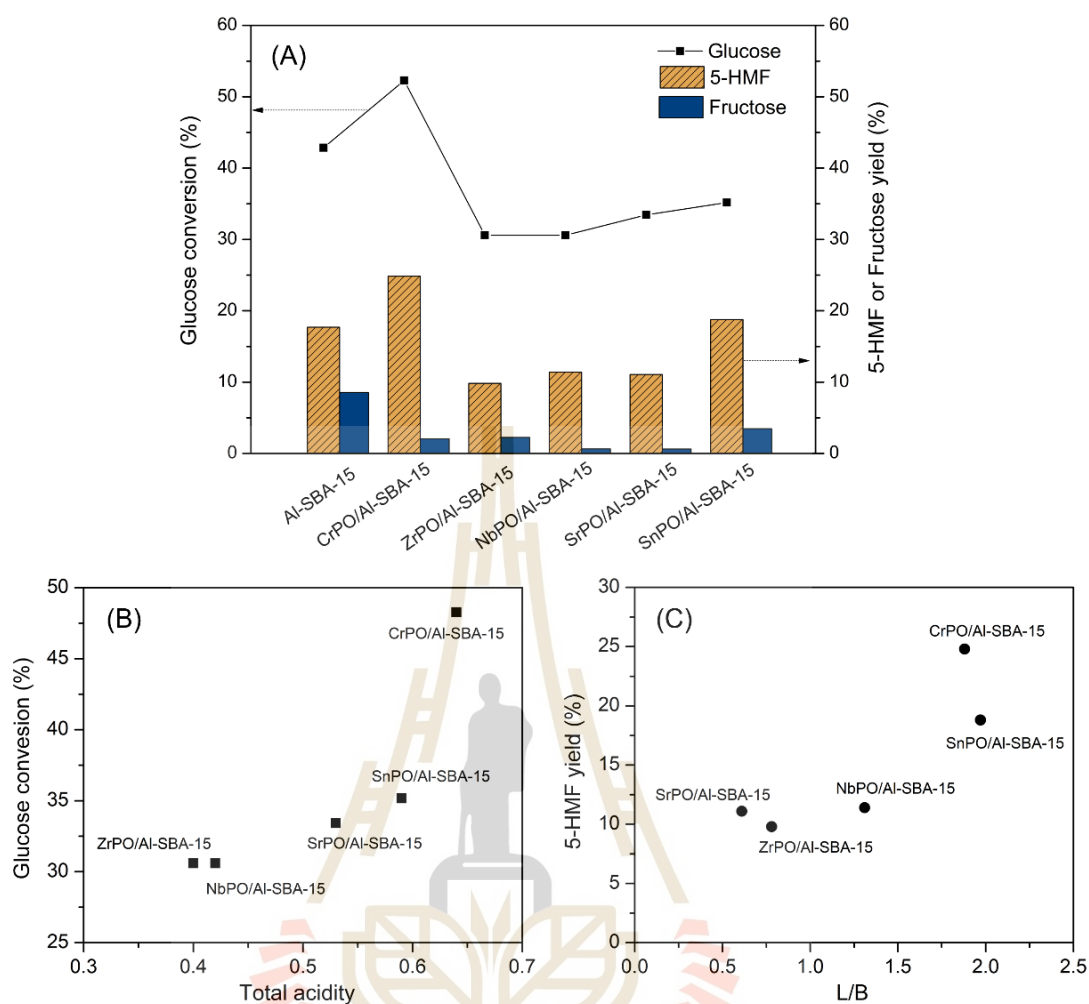


Figure 4.6 (A) Catalytic screening of MPO/Al-SBA-15 on conversion of glucose to 5-HMF. (B) Effect of total acid amount on glucose conversion. (C) Effect of Lewis to Brønsted acid ratio (L/B) on 5-HMF yield. Reaction condition: glucose 0.3 g in 30 mL of biphasic NaCl-H₂O/*n*-butanol solvent, catalyst = 0.1 g, temperature = 150 °C, reaction time = 4 h.

4.4.2 Influence of PO/Cr ratios supported on Al-SBA-15 on the catalytic performance of glucose conversion to 5-HMF

4.4.2.1 Physicochemical and acid properties of the catalysts

The XRD patterns of CrPO(*x*)/Al-SBA-15, where *x* is phosphate-to-chromium ratios (PO/Cr) of 0.5, 1.0 and 2.0, are displayed in **Figure 4.7**. The patterns of Cr/Al-SBA-15 and PO/Al-SBA-15 are also included for comparison. The low-angle XRD patterns of each sample (**Figure 4.7A**) shows the characteristic structure of mesoporous Al-SBA-15 materials (Rakngam et al., 2021), indicating that the structure of

Al-SBA-15 is preserved even after incorporating chromium phosphate species. The peak intensities decrease with the larger loading. In the wide-angle XRD patterns (**Figure 4.7B**), all the samples display a broad peak characteristic of the amorphous nature of mesoporous Al-SBA-15 material. No distinct peaks corresponding to chromium phosphate species are observed in any of the PO/Cr samples, suggesting that the catalysts exist either in an amorphous form or as small crystalline particles. On the other hand, the Cr/Al-SBA-15 sample exhibits the characteristic peaks of the Cr_2O_3 phases (Afzal, Atiq, Saleem, Ramay, Naseem, and Siddiqi, 2016).

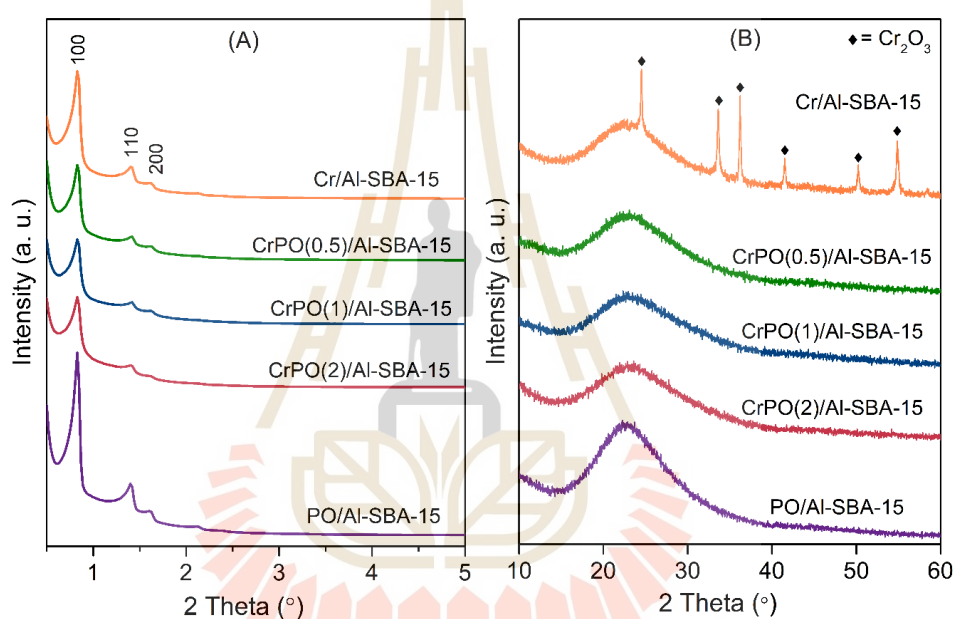


Figure 4.7 Low-angle (A) and wide-angle (B) XRD patterns of PO/Al-SBA-15, Cr/Al-SBA-15, and CrPO(x)/Al-SBA-15 with different PO/Cr molar ratios.

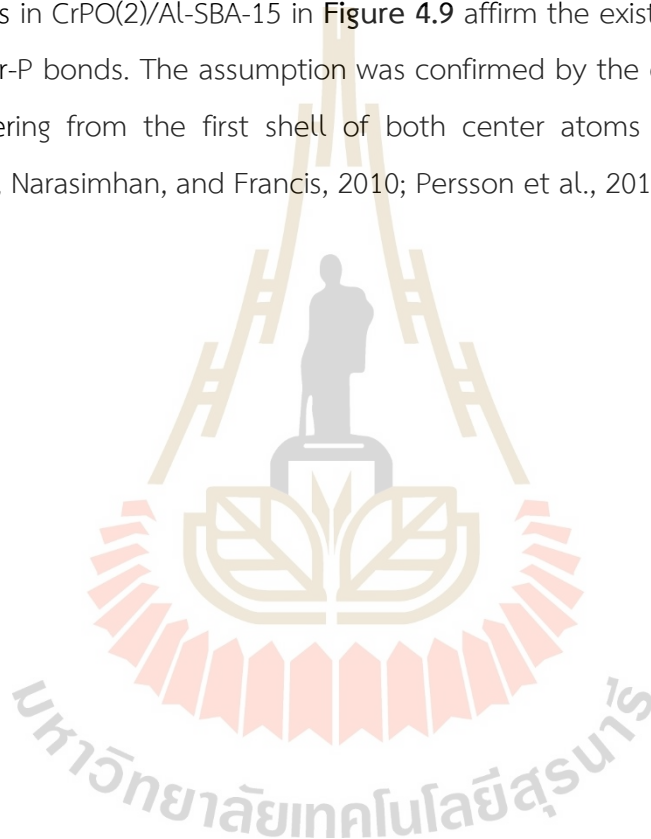
The existence of chromium phosphate species, oxidation states and local environment of all catalysts after adding chromium and phosphorous series are further confirmed by XANES. Compared with the standard materials, the XANES spectra in Cr K-edge and P K-edge region, are illustrated in **Figure 4.8A** and **4.8B**, respectively. Pre-edge peak similar to CrO_3 are observed on some samples with different intensity in the following order: $\text{CrPO}(0.5)/\text{Al-SBA-15} > \text{Cr/Al-SBA-15} > \text{CrPO}(1)/\text{Al-SBA-15}$. In contrast, the pre-edge of $\text{CrPO}(2)/\text{Al-SBA-15}$ has two peaks with low intensity, similar to the combined feature of CrPO_4 and Cr_2O_3 . In the edge region, $\text{CrPO}(2)/\text{Al-SBA-15}$ and

CrPO(1)/Al-SBA-15 have edge energy close to Cr(III) in CrPO₄ and Cr₂O₃. Whereas CrPO(0.5)/Al-SBA-15 has edge energy similar to Cr(VI) in CrO₃. As the results, low chromium content of CrPO(2)/Al-SBA-15 catalysts is fit to Cr(III) species. An increase in chromium content of CrPO(1)/Al-SBA-15 and CrPO(0.5)/Al-SBA-15 results increasing in Cr(VI) component on those catalysts by presenting of the pre-edge XANES spectra. However, the pre-edge intensity of the catalysts is lower than that of CrO₃ standard implying a mixed component of Cr(VI) and Cr(III) in those catalysts.

The information from XANES spectra suggests that CrPO(2)/Al-SBA-15 contains Cr(III) in the form of CrPO₄ and Cr₂O₃. CrPO(1)/Al-SBA-15 contains Cr(III) in the form of CrPO₄ and Cr₂O₃ and Cr(VI) in the form of CrO₃. CrPO(1)/Al-SBA-15 mainly contains Cr(VI) in the form of CrO₃. The slight differences in pre-edge intensity and edge energy of the catalysts from the standards might be from the interaction with the support. The pre-edge caused by electron transition from 1s → 3d orbital of metal is an allowed in tetrahedral coordination but dipole-forbidden in octahedral coordination (Osakoo, Khemthong, Roessner, Kidkhunthod, Chanlek, Prayoonpokarach, and Wittayakun, 2020). The pre-edge intensity of the catalysts decreased with the higher PO/Cr ratio. These results indicated that the octahedral coordination arrangement is predominant when the PO/Cr ratio is 2.0. This finding is in good agreement with the work reported by Liu et al. (Liu, He, Chao, Xie, and Ruchenstein, 2012) that the oxidation state and local structure of chromium phosphates with the ratio of PO/Cr > 1.8 prepared by the solid-state reaction is dominantly Cr (III) in octahedral coordination surrounded by phosphates.

Furthermore, the P K-edge XANES spectra of all catalysts are displayed in **Figure 4.8B**. The XANES spectra of all samples were distinct from those of phosphorous standards, suggesting the presence of different phosphorous species. Therefore, the feature and white line position at 2147.20 eV of all samples were similar to phosphate species (PO₄)³⁻ as provided in the literature (Persson, Klysubun, and Lundberg, 2019). Interestingly, a small shoulder at a pre-edge region was observed in all Cr-added catalysts. This shoulder is the characteristic of the electronic transitions from P 1s → O 2p → M 4p (Khare, Hesterberg, Beauchemin, and Wang, 2004). The pre-edge shoulders deduced from CrPO(x)/Al-SBA-15 samples slightly shift to lower energy

in comparison to the PO/Al-SBA-15 standard. Thus, an incorporation of the CrPO_4 structure on all $\text{CrPO}(x)/\text{Al-SBA-15}$ catalysts are suggested. It was noticeable that the pre-edge intensity (seen in the zoom-in scale of **Figure 4.8B**) is proportional to the PO content, implying a more significant amount of Cr(III) phosphate. It was noticeable that the pre-edge intensity is proportional to the PO/Cr ratio in $\text{CrPO}(x)/\text{Al-SBA-15}$ structures. Thus, an increase of Cr amount increases the Cr-incorporation in CrPO_4 form), consistent with the evidence obtained from Cr K-edge XANES. In addition, EXAFS of Cr and P K-edges in $\text{CrPO}(2)/\text{Al-SBA-15}$ in **Figure 4.9** affirm the existence of Cr-O and P-O rather than Cr-P bonds. The assumption was confirmed by the characteristic distance of backscattering from the first shell of both center atoms (Nancharaiah, Dodge, Venugopalan, Narasimhan, and Francis, 2010; Persson et al., 2019).



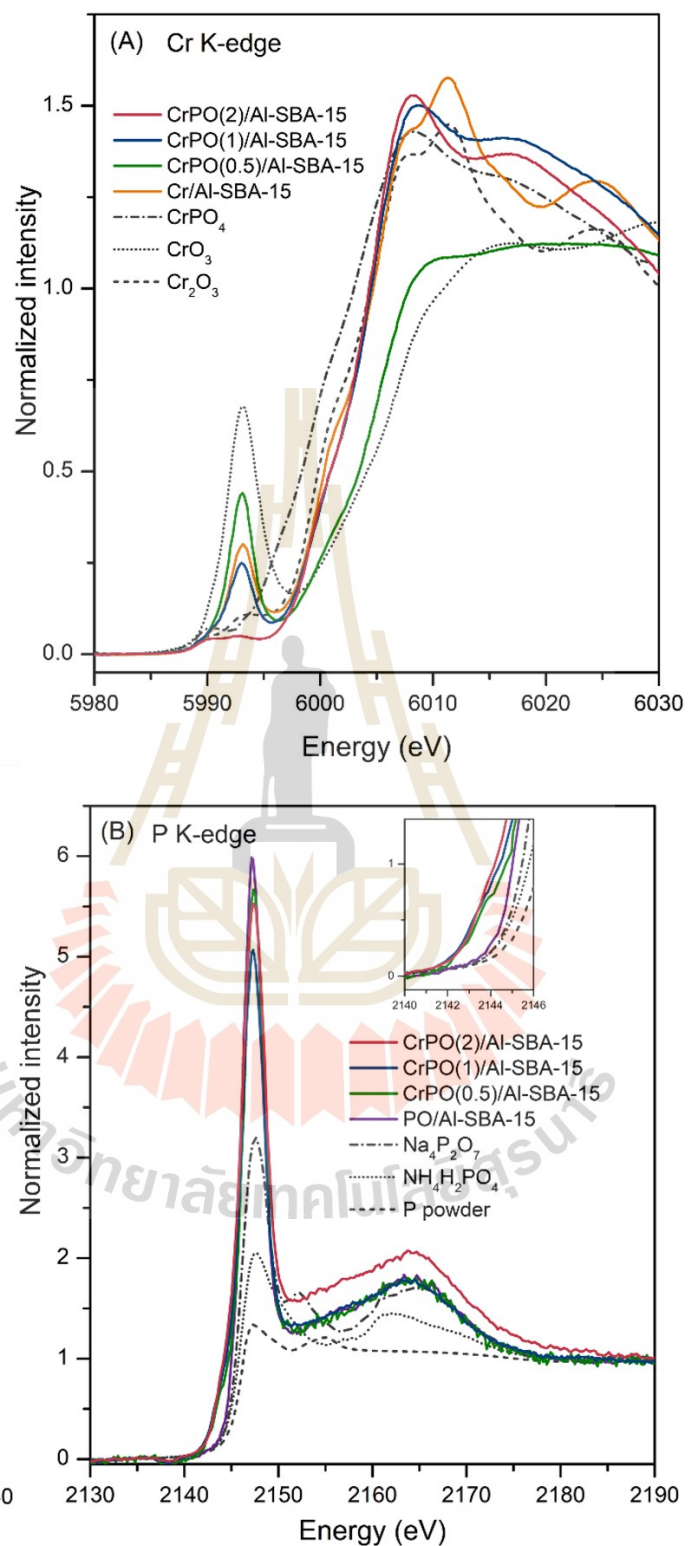


Figure 4.8 (A) Cr K-edge XANES spectra of Cr/Al-SBA-15, CrPO(x)/Al-SBA-15 with different PO/Cr ratios, CrPO₄, CrO₃, and Cr₂O₃. (B) P K-edge XANES spectra of PO/Al-SBA-15, CrPO/Al-SBA-15 with different PO/Cr ratios, Na₄P₂O₇, NH₄H₂PO₄, P powder.

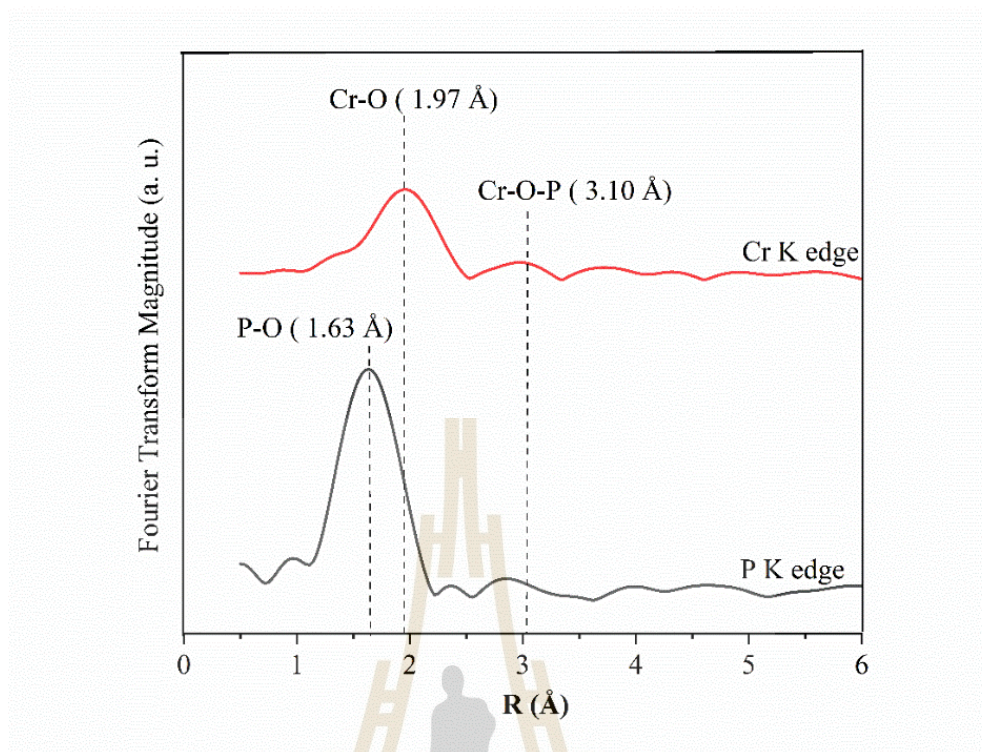


Figure 4.9 The k^2 -weighted magnitude of the Fourier Transform for Cr K edge and P K edge in CrPO(2)/Al-SBA-15.

Concurrently, the XPS spectra of P 2p in CrPO(2)/Al-SBA-15 and PO/Al-SBA-15 provide crucial information on surface species, as shown in **Figure 4.10**. Both catalysts present two critical peaks ranging from 132 to 136 eV, corresponding to doublets of P 2p_{3/2} and 2p_{1/2} in phosphate species (Majjane, Chahine, Et-Tabirou, Echchahed, Do, and Breen, 2014). The peaks around 134.5 and 133.9 eV were attributed to the characteristic peak of P-OH species (Rodríguez-Aguado, Infantes-Molina, Ballesteros-Plata, Cecilia, Barroso-Martín, and Rodríguez-Castellón, 2017). It was remarkable that the peak position of P 2p in CrPO(2)/Al-SBA-15 shifted to lower binding energy when compared with PO/Al-SBA-15 sample. This phenomenon could be caused by the increase of the electronic state density around P, resulting from the formation of P—O—Cr bonds (Majjane et al., 2014). These results are in good agreement with the XANES result. Overall, XANES, EXAFS and XPS results convince us that the PO content influences the quantity of Cr (III) phosphate formation. The most suitable PO/Cr ratio is 2.0, providing the greatest content of Cr (III) phosphate.

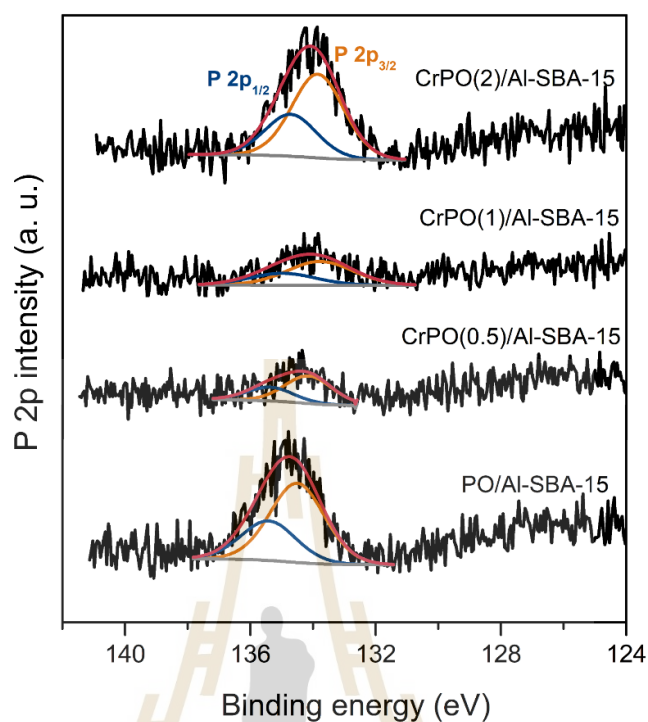


Figure 4.10 XPS spectra of P 2p for PO/Al-SBA-15 and CrPO(x)/Al-SBA-15 with PO/Cr ratio of 0.5, 1 and 2.

Regarding the functional groups, the FTIR spectra of Cr/Al-SBA-15, PO/Al-SBA-15, and all CrPO/Al-SBA-15 samples were compared to that of the parent Al-SBA-15 in **Figure 4.11**. All samples exhibit four main bands at 1089, 952, 804, and 465 cm^{-1} corresponding to Si-O-T stretching (ν), Si-OH stretching, T-O stretching (T = Si or Al), and O-T-O bending (δ) modes, respectively (Betiha, Hassan, Al-Sabagh, Khder, and Ahmed, 2012; Xing, Lv, Fu, Wang, Fan, Yang, and Yuan, 2017). Interestingly, the adsorption band at 972 cm^{-1} corresponding to P-OH stretching was observed in the phosphate-containing samples (Zu, Gao, Lian, Cai, Li, Zhong, Hao, Zhang, Gong, Liu, Wang, and Cui, 2018). In the case of CrPO/Al-SBA-15 samples, the additional peak at 904 cm^{-1} assigned to the Cr-O vibration of Cr(VI) was observed (Weckhuysen, Wachs, and Schoonheydt, 1996). In contrast, the two sharp peaks at 563 and 624 cm^{-1} corresponding to Cr-O stretching vibration modes of the crystalline Cr_2O_3 (Makhlouf, Bakr, Al-Attar, and Moustafa, 2013) were observed in the spectrum of Cr/Al-SBA-15.

These results are consistent with the XRD and XANES results, confirming the existence of chromium and phosphate groups on the surface of Al-SBA-15.

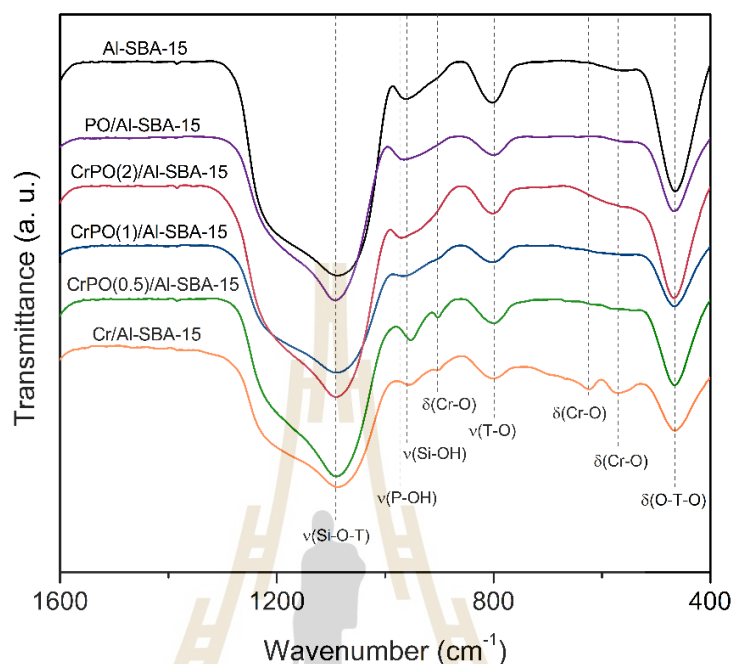


Figure 4.11 FTIR spectra of Al-SBA-15, PO/Al-SBA-15, Cr/Al-SBA-15, and CrPO(x)/Al-SBA-15 with different PO/Cr molar ratios.

N_2 sorption full isotherms of the modified samples are shown in **Figure 4.12**. The type IV isotherms with H1 hysteresis loops are still observed in all investigated samples, indicating the characteristic of mesoporous Al-SBA-15 materials. This observation agrees with the XRD results, confirming the presence of mesoporous Al-SBA-15 in the modified samples. The BET surface area, pore diameter, and pore volume of all samples are summarized in **Table 4.2**. The modification of Al-SBA-15 with Cr, PO, and CrPO species led to smaller surface areas, suggesting that the deposited species partially covered the surface of Al-SBA-15. The total surface areas of the CrPO(x)/Al-SBA-15 decrease with an increase PO/Cr ratio. With a low PO/Cr ratio of CrPO(0.5)/Al-SBA-15, a separated chromium oxide species is dominated and partial covering on the surfaces corresponded to a presence of CrO_3 content in Cr K-edge XANES analysis. Thus, the surfaces of CrPO(x)/Al-SBA-15 are lower than Cr/Al-SBA-15 and PO/Al-SBA-15 standards. An increase in PO/Cr ratio increase the $CrPO_4$ covered

species on the catalysts led to decreasing in surface area and reducing in pore volume compared with CrPO(0.5)/Al-SBA-15.

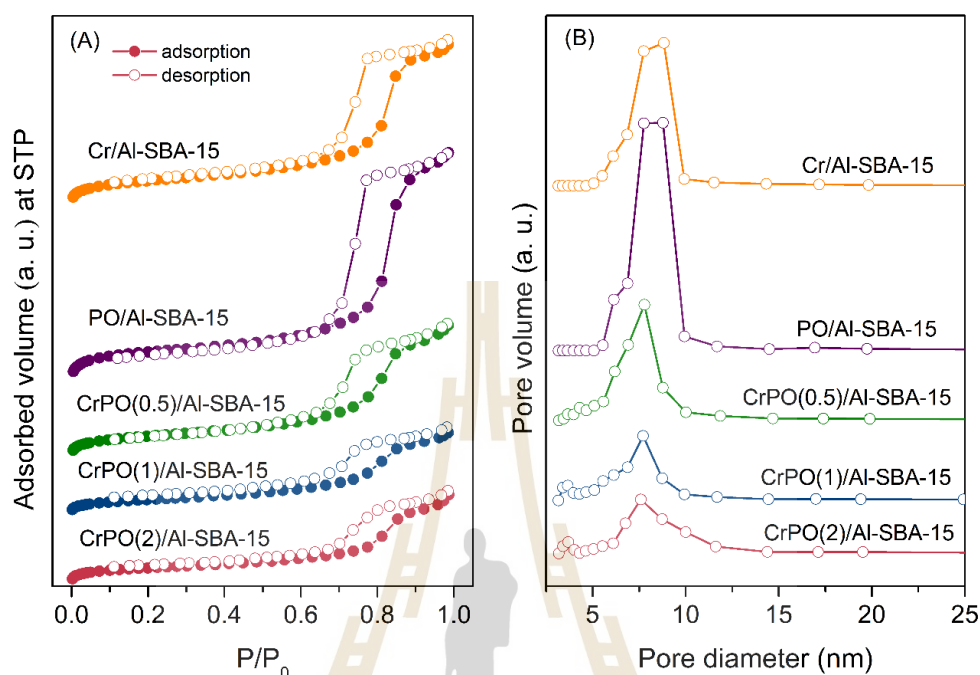


Figure 4.12 N_2 adsorption-desorption isotherms (A) and pore size distributions (B) of PO/Al-SBA-15, Cr/Al-SBA-15, and all CrPO/Al-SBA-15 with different PO/Cr molar ratios.

Table 4.2. Acidity and textural properties of Cr/Al-SBA-15, PO/Al-SBA-15, and all CrPO/Al-SBA-15 with different PO/Cr molar ratios.

Sample	Acidity (mmol/g) ^a	L/B ^b	Textural properties	
			Surface area (m ² /g) ^c	Pore volume (cm ³ /g) ^d
Cr/Al-SBA-15	0.61	N.A.	377	0.96
PO/Al-SBA-15	0.67	N.A.	417	1.45
CrPO(0.5)/Al-SBA-15	0.64	3.96	315	0.78
CrPO(1)/Al-SBA-15	0.60	3.39	198	0.47
CrPO(2)/Al-SBA-15	0.65	1.88	259	0.57

^aDetermined by NH₃-TPD analysis. ^bCalculated by the relative peak area ratio of Lewis/Brønsted acid sites (L/B) from pyridine adsorption. ^cCalculated by the BET method. ^dCalculated by the BJH method. N.A. = not analyzed.

Considering the acid properties, NH₃-TPD profiles of Cr/Al-SBA-15, PO/Al-SBA-15, and CrPO(x)/Al-SBA-15 samples with different PO/Cr molar ratios are presented in **Figure 4.13**. Cr/Al-SBA-15 exhibits a broad center peak at 191 °C, while PO/Al-SBA-15 shows a peak at 166 °C. In the case of all the CrPO(x)/Al-SBA-15 samples, the NH₃-TPD profiles are different, suggesting the presence of acid sites with different acid strengths. The calculated amounts of acidity are listed in **Table 4.2**. The total amount of acid of the investigated samples was in the following order: PO/Al-SBA-15 > CrPO(2)/Al-SBA-15 > CrPO(0.5)/Al-SBA-15 > Cr/Al-SBA-15 > CrPO(1)/Al-SBA-15

The acid types of the CrPO(x)/Al-SBA-15 samples with different PO/Cr molar ratios are distinguished by DRIFT spectroscopy of pyridine adsorption. Their profiles are shown in **Figure 4.13B**. It was found that the DRIFT profiles of all samples present the characteristic peaks of Lewis acid sites (L) and Brønsted acid sites (B) at 1455 and 1546 cm⁻¹, respectively. The calculated L/B ratios for all samples are listed in **Table 4.2**. The relative ratios of L/B obtained from peak area decreased in the following order: CrPO(0.5)/Al-SBA-15 > CrPO(1)/Al-SBA-15 > CrPO(2)/Al-SBA-15. It was noticeable that the decrease in the PO/Cr mole ratios for the CrPO(x)/Al-SBA-15 samples could increase the relative ratios of L/B acid sites, probably due to the less of Brønsted acid sites from phosphate groups (Rao et al., 2017). Noticeably, the peak position attributed to the Brønsted acid site shifted to a lower wavenumber with increased PO content. This result could imply the presence of different acid strengths due to the different interactions between P-OH and the lone pair electrons of N in pyridine. The stronger interactions generate the stronger Brønsted acid due to the decrease in the bond order of aromatic pyridine (Lima, Campos, Paiva, Linares, Dias, and Dias, 2021).

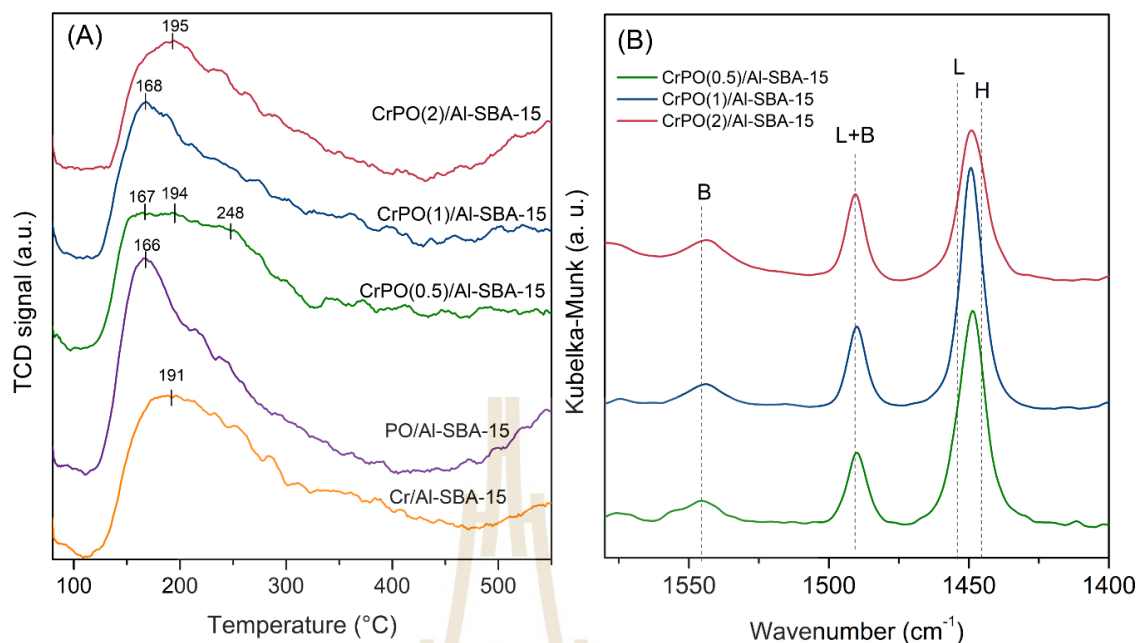


Figure 4.13 (A) NH₃-TPD profiles of PO/Al-SBA-15, Cr/Al-SBA-15, and CrPO/Al-SBA-15 with different PO/Cr molar ratios. (B) Pyridine-DRIFT spectra of PO/Al-SBA-15, Cr/Al-SBA-15, an CrPO/Al-SBA-15 with different PO/Cr molar ratios.

4.4.2.2 Catalytic activity on glucose conversion to 5-HMF

The catalytic performances of Cr/Al-SBA-15, PO/Al-SBA-15, and CrPO(x)/Al-SBA-15 with different PO/Cr molar ratios (PO/Cr = 0.5, 1, and 2) for glucose conversion to 5-HMF are presented in **Figure 4.14**. The highest glucose conversion of 98% was achieved from Cr/Al-SBA-15, while the lowest (71%) was obtained when PO/Al-SBA-15 was used. In the case of CrPO/Al-SBA-15 catalysts, the glucose conversions were 95%, 97%, and 87% on the samples with the PO/Cr molar ratios of 0.5, 1, and 2, respectively. The 5-HMF yields from the reaction system with Cr/Al-SBA-15 and PO/Al-SBA-15 were comparable and they were lower than those with CrPO/Al-SBA-15. The higher yields of 5-HMF were clearly observed when CrPO(x)/Al-SBA-15 was employed, indicating that the combination of Cr and PO species with the PO/Cr nominal ratios of 0.5, 1, and 2 can enhance the yields of 5-HMF under the employed reaction conditions. The 5-HMF yield increased with an increase in the PO/Cr molar ratio. The highest yield of 51% was achieved when CrPO(2)/Al-SBA-15 was employed. Consequently, the CrPO(2)/Al-SBA-15 was further studied.

The superior activity of CrPO(x)/Al-SBA-15 could be attributed to the synergistic effects of Cr and PO species. Cr(III) ions in octahedral structure (Lewis acid sites) promote the isomerization of glucose to fructose and the surface hydroxyl groups of phosphates (Brønsted acid sites) accelerate the dehydration of fructose to 5-HMF (Saravanan et al., 2018). Moreover, the Brønsted acid peak of CrPO(2)/Al-SBA-15 had a lower wavenumber than other samples (see **Figure 4.13B**), suggesting a stronger site, leading to a higher 5-HMF yield. The hypothesis is possible because the stronger Brønsted acid could accelerate the dehydration of fructose intermediate to 5-HMF (Lima et al., 2021). This observation agrees well with the presence of P-O-Cr covalent bonds in Cr(III) phosphate property, which is dominant in CrPO(2)/Al-SBA-15 suggested by XANES of P K-edge. This explanation is consistent with Ramis et al. (Ramis, Busca, Lorenzelli, Ginestra, Galli, and Massucci, 1988) that the Brønsted acid strength of the surface P-OH groups increases with increasing covalency of the (PO)-M bond.

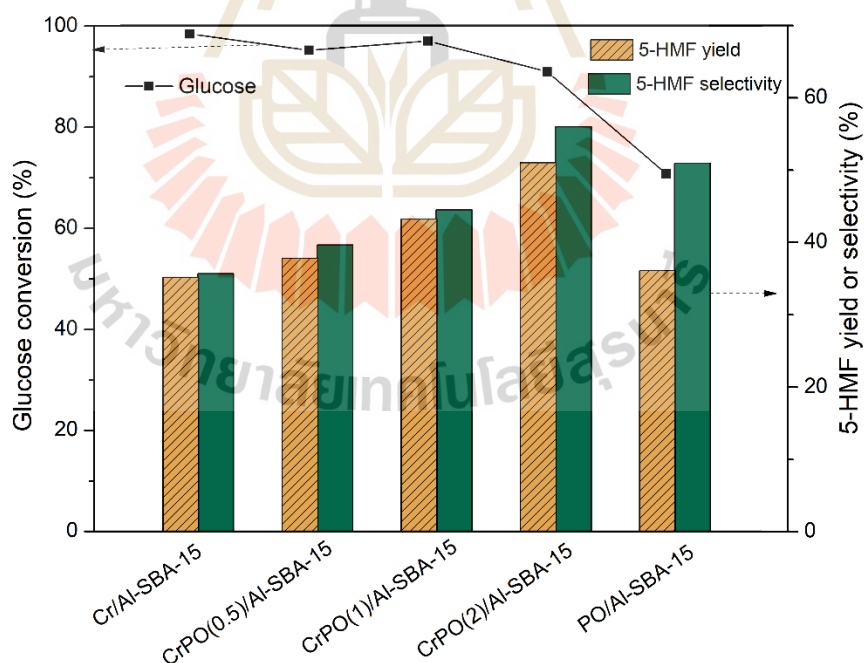


Figure 4.14 Catalytic screening on conversion of glucose to 5-HMF. Reaction conditions: glucose 0.3 g in 30 mL of biphasic NaCl-H₂O/*n*-butanol solvent, catalyst = 0.1 g, temperature = 170 °C, reaction time = 4 h.

4.4.2.3 Effect of reaction temperature, time, and glucose concentration

The effect of reaction temperature on the catalytic activity of CrPO(2)/Al-SBA-15 was investigated. The results are presented in **Figure 4.15A**. The glucose conversion increased from 14 to 98% with an increase in the reaction temperature from 130 to 190 °C for the reaction of 4 h, indicating that the rate of glucose conversion is enhanced by elevating the operational temperature. In terms of 5-HMF yield, it was negligible at 130 °C. Upon an increase in the reaction temperature to 170 °C, the 5-HMF yield increased and reached the maximum value of 51%. The further increase to 190 °C resulted in a slight decrease in the 5-HMF yield. This phenomena could be attributed to the undesired side reactions such as rehydration, polymerization, and formation of humins which are more favorable at such temperatures (Rezayan et al., 2022).

The effect of reaction time on the catalytic activity for glucose conversion to 5-HMF of CrPO(2)/Al-SBA-15 at 170 and 190 °C was also studied. The results are shown in **Figure 4.15B**. The higher 5-HMF yield, 52% was obtained at 190 °C in 2 h. The yield improvement by the higher temperature and shorter reaction time was possibly due to the fewer formation of by-products.

The influence of glucose concentration was also investigated with the concentrations of 3, 5, and 10 wt.% over the CrPO(2)/Al-SBA-15 catalyst at 170 °C for 4 h. As shown in **Figure 4.16**, the glucose conversion increased from 83% to 91% with the increased glucose concentration from 3 to 5 wt.%. A slight decrease in the conversion of glucose was observed when glucose concentration was further increased up to 10 wt.%. A slight contrast to the glucose conversion was seen in the 5-HMF yield. Upon an increase in the glucose concentration from 3 to 10 wt.%, the 5-HMF yield went down from 51% to approximately 42%. Such a decrease could be partly associated with the insufficient acid active sites on the surface of CrPO(2)/Al-SBA-15 for the higher glucose concentration. The reaction with an initial higher glucose concentration generates a higher amount of 5-HMF product.

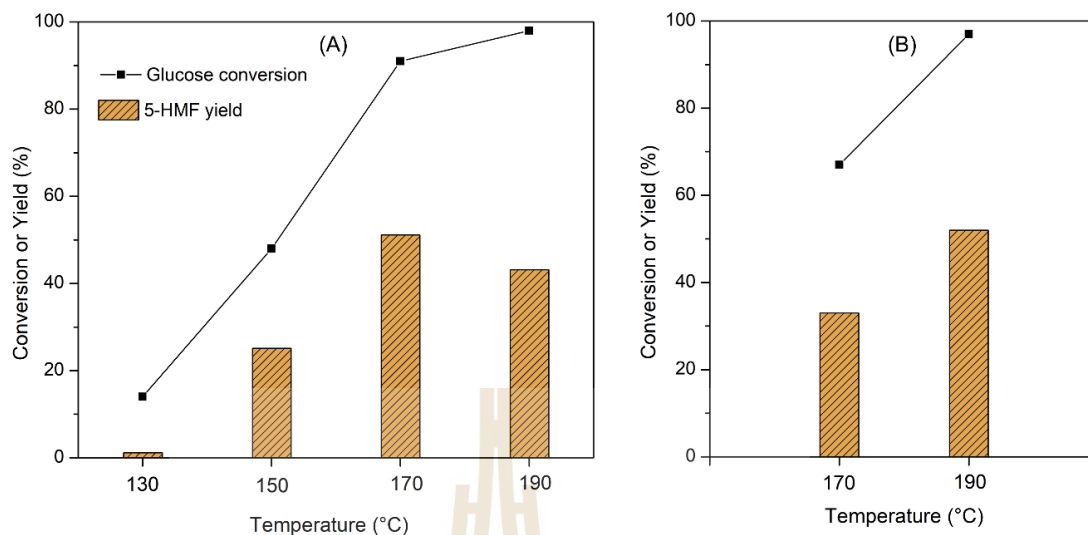


Figure 4.15 Effect of reaction temperatures and times. Reaction conditions: glucose 0.3 g in 30 mL of biphasic NaCl-H₂O/*n*-butanol solvent, CrPO(2)/Al-SBA-15 catalyst = 0.1 g, reaction time of 4 h (A) and 2 h (B).

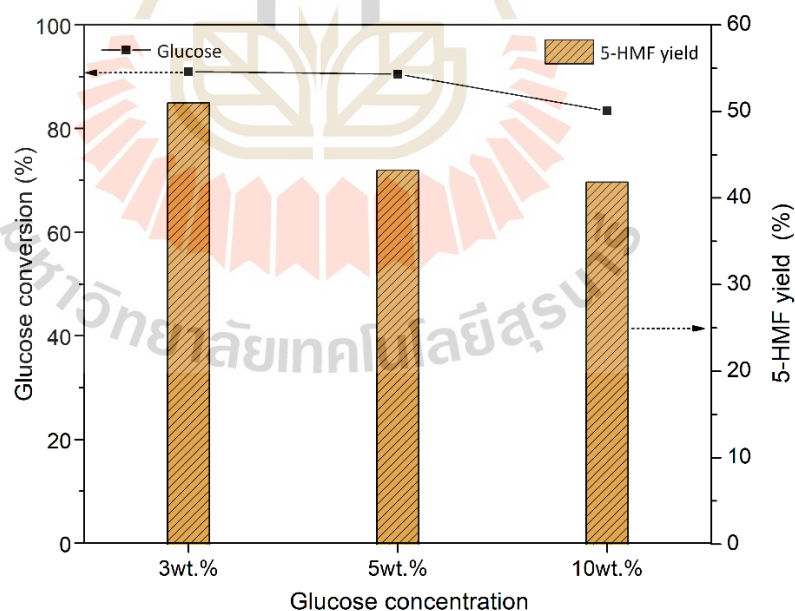


Figure 4.16 Effect of glucose concentration on the conversion of glucose to 5-HMF. Reaction conditions: using a constant CrPO(2)/Al-SBA-15 catalyst loading = 0.1 g, temperature = 170 °C, and reaction time = 4 h.

4.4.2.4 Catalyst reusability of CrPO(2)/Al-SBA-15

Reusability is important for heterogeneous catalysts in industrial applications. The CrPO(2)/Al-SBA-15 catalyst was reused for three consecutive runs under the optimum reaction condition. The spent catalyst was recovered by filtration, washing with DI water and ethanol, and drying at 100 °C for the next run. The CrPO(2)/Al-SBA-15 maintained good catalytic performance for glucose conversion with a slightly decreased 5-HMF yield (4%) after three cycles (Figure 4.17), indicating satisfied reusability. This result could imply that CrPO(2)/Al-SBA-15 catalyst has strong interactions between chromium phosphate species and Al-SBA-15. This assumption agreed well with the chromium leaching of less than 0.01 ppm after the first cycle determined by ICP-OES. The results confirmed that CrPO(2)/Al-SBA-15 was a stable catalyst.

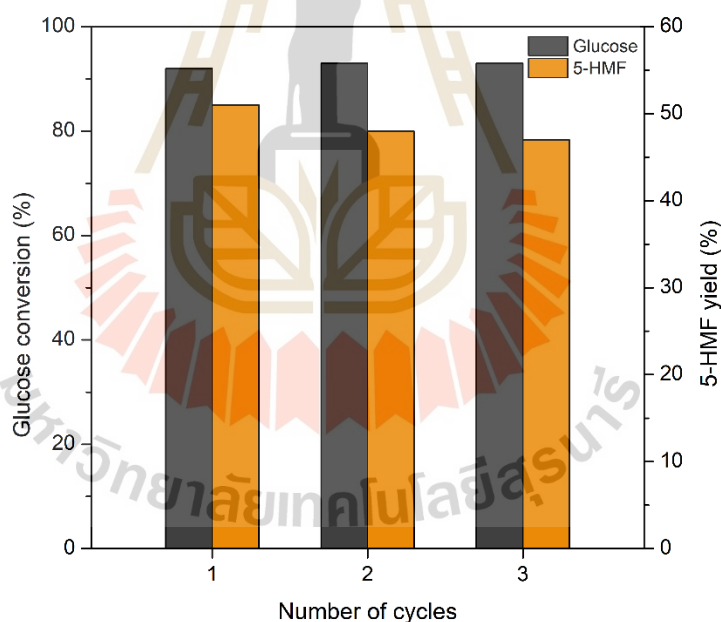
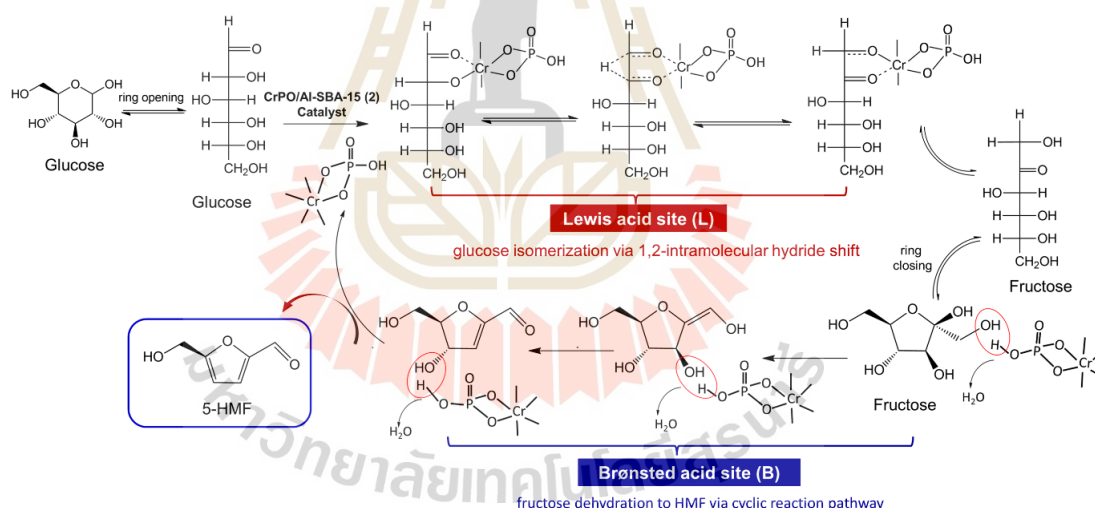


Figure 4.17 Reusability of CrPO(2)/Al-SBA-15 catalyst. Reaction conditions: catalyst 0.1 g, glucose 0.3 g in 30 mL of NaCl-H₂O/*n*-butanol at 170 °C for 4 h.

4.4.3 Proposed catalytic reaction pathway in glucose conversion over Cr(III)PO₄/Al-SBA-15

The proposed reaction pathway of glucose conversion to 5-HMF over CrPO(2)/Al-SBA-15 catalyst is illustrated in **Scheme 4.1**. These proposed reaction mechanisms are based on the results obtained from XANES, FTIR, and pyridine-DRIFT. In this case, the CrPO(2)/Al-SBA-15 catalyst possesses both Lewis (Cr(III)) from CrPO and Brønsted acid sites from P-OH.

Initially, a glucose molecule undergoes ring opening to form acyclic glucose which is subsequently isomerized to an open-chain fructose over the Cr(III) Lewis acid site through the 1,2-intramolecular hydride shift mechanism (Saravanan et al., 2018). Then, the open-chain fructose undergoes ring closing to form a cyclic fructose which is catalytically dehydrated to 5-HMF on the P-OH Brønsted acid sites (Saravanan et al., 2018).



Scheme 4.1 Proposed reaction pathway for glucose conversion to HMF over the bifunctional CrPO(2)/Al-SBA-15 acid catalyst.

To investigate the catalyst stability, the spent CrPO/Al-SBA-15 was characterized by TEM and low-angle XRD. The TEM images of both fresh and spent CrPO/Al-SBA-15 catalysts are compared in **Figure 4.18**. The images revealed similar hexagonal arrays. Moreover, the XRD pattern of the spent CrPO/Al-SBA-15 (**Figure 4.19**)

still shows three characteristic peaks of hexagonal mesoporous structure. These results indicated that the catalyst has good thermal stability under the reaction condition.

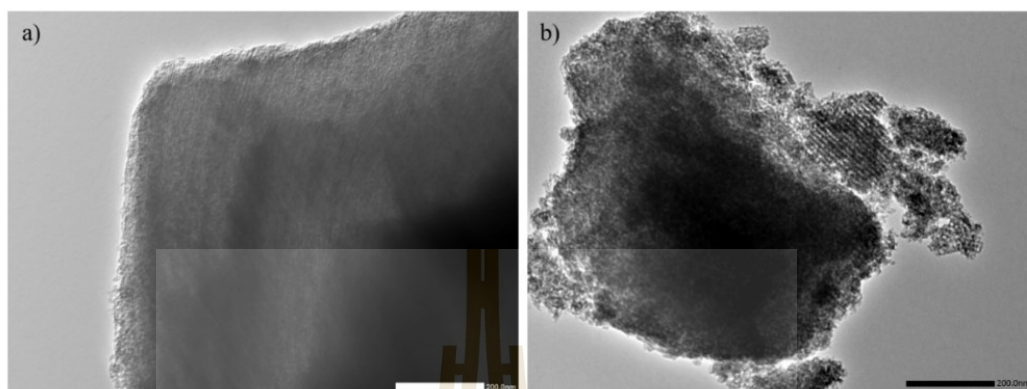


Figure 4.18 TEM images of (a) fresh and (b) spent CrPO(2)/Al-SBA-15 catalysts.

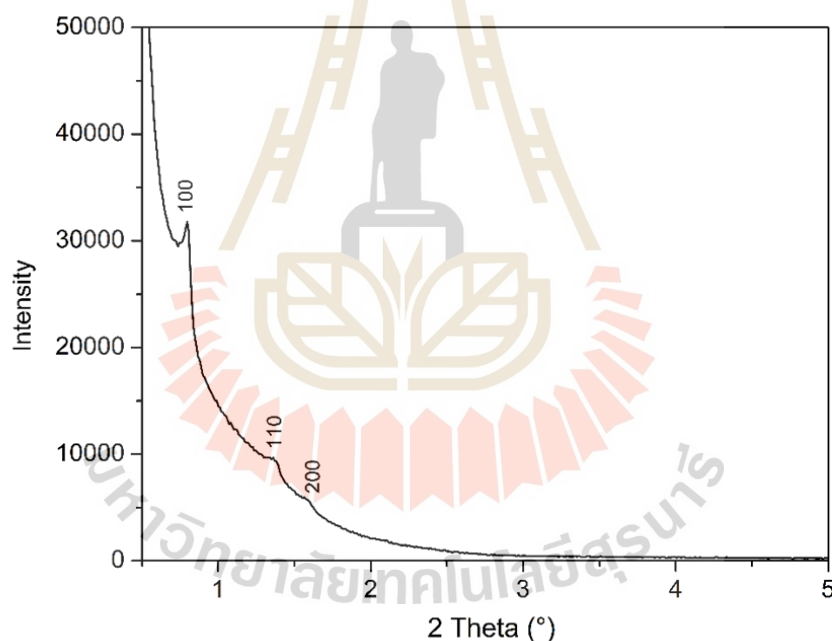


Figure 4.19 XRD pattern of spent CrPO(2)/Al-SBA-15 catalyst.

Table 4.3 compares the catalytic performance for glucose conversion to 5-HMF from CrPO(2)/Al-SBA-15 in this work and those from Cr-based catalysts in the literature [26,27,60,61]. Despite the different catalyst supports, reaction conditions and solvent systems, the conversion and yield from this work were relatively high and comparable to those in the literature. Interestingly, the catalyst in the present work

has the highest glucose/catalyst weight ratio, indicating that less catalyst amount is required. This is beneficial in terms of the economic aspect. Besides, using a biphasic NaCl-H₂O/*n*-butanol system is a more environment-friendly solvent and cost-effective separation. These combined properties prove that CrPO(2)/Al-SBA-15 is a promising catalyst in glucose conversion to 5-HMF.

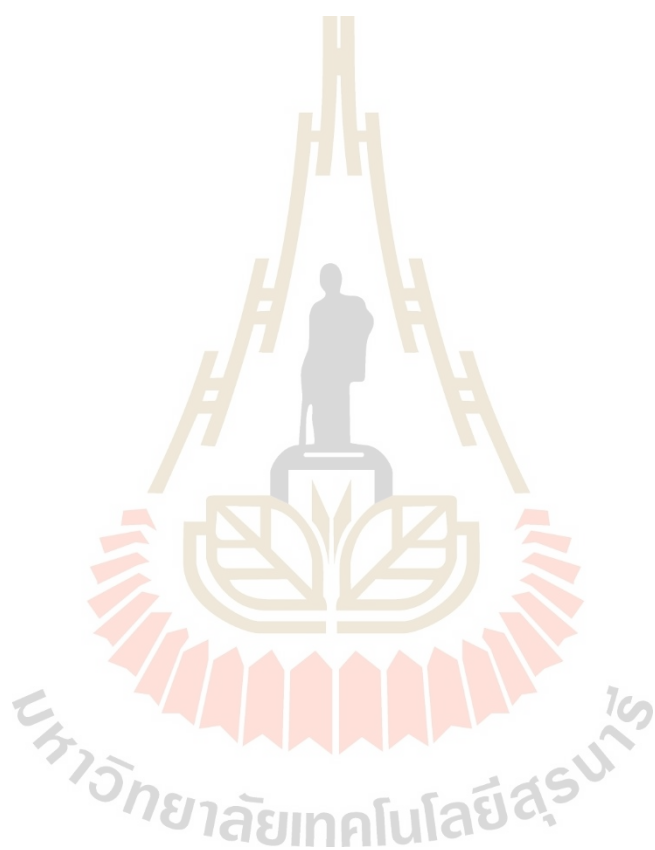


Table 4.3 Comparison of catalytic performance for the production of 5-HMF from glucose.

Catalyst	Reaction condition			Glucose/ catalyst weight ratio	Glucose conversion (%)	5-HMF yield (%)	Reference
	Solvent	Temp. (°C)	Time (h)				
Cr-ZrPO	[Bmim]Cl	120	12	1.8	95	43	(Liu et al., 2015)
Cr/USY zeolite	[Bmim]Cl	130	1	1	N. A.	54	(Sezgin, Esen Keçeci, Akmaz, and Koc, 2019)
Cr/ZSM-5 zeolite	[Bmim]Cl	130	1	1	N. A.	11	
Cr/ β zeolite	[Bmim]Cl	130	1	1	N. A.	59	
CrPO	H ₂ O/THF	140	0.5	0.8	99	63	(Xu et al., 2016)
Cr/ β zeolite	NaCl-H ₂ O/THF	150	1.5	0.5	87	72	(Xu, Pan, Hu, Wu, Wang, Chen, Yuan, Gao, and Xiao, 2019)
CrPO(2)/Al-SBA-15	NaCl-H ₂ O/ <i>n</i> - butanol	170	4	3	91	51	

N.A. = not analyzed.

4.5 Conclusions

This work compares the properties of phosphates of Cr, Zr, Nb, Sr, and Sn supported on mesoporous Al-SBA-15 and the performances as catalysts for 5-HMF production from glucose. The acid properties of these catalysts influence the conversion of glucose to 5-HMF in a biphasic NaCl-H₂O/*n*-butanol solvent system. The different metal phosphates significantly affect the acid properties and ratio of Lewis and Brønsted acids (L/B). The glucose conversion and 5-HMF yield correlate well with the total acidity and L/B acids ratio rather than surface area. From the catalytic performance, chromium phosphate with the PO/Cr ratio of 2 is considered the best catalyst for glucose conversion to 5-HMF, consistent with the greatest total acidity and suitable L/B ratio. The combined results from XANES, EXAFS, and XPS proved that the chromium (III) phosphate with octahedral structure is a dominant species in CrPO(2)/Al-SBA-15 catalyst. This alternative solid acid catalyst could be considered as a promising bifunctional Lewis-Brønsted material for the transformation of glucose to high-value-added chemicals in future biorefinery processes.

4.6 References

- Afzal, A., Atiq, S., Saleem, M., Ramay, S. M., Naseem, S., and Siddiqi, S. A. (2016). Structural and magnetic phase transition of sol-gel-synthesized Cr_2O_3 and MnCr_2O_4 nanoparticles. *Journal of Sol-Gel Science and Technology*, *80*(1), 96–102.
- Akiya, N., and Savage, P. E. (2002). Roles of water for chemical reactions in high-temperature water. *Chemical Reviews*, *102*(8), 2725–2750.
- Alam, M. I., De, S., Singh, B., Saha, B., and Abu-Omar, M. M. (2014). Titanium hydrogenphosphate: An efficient dual acidic catalyst for 5-hydroxymethylfurfural (HMF) production. *Applied Catalysis A: General*, *486*, 42–48.
- Betiha, M. A., Hassan, H. M. A., Al-Sabagh, A. M., Khder, A. E. R. S., and Ahmed, E. A. (2012). Direct synthesis and the morphological control of highly ordered mesoporous ALSBA-15 using urea-tetrachloroaluminate as a novel aluminum source. *Journal of Materials Chemistry*, *22*(34), 17551–17559.
- Bhange, P., Bhange, D. S., Pradhan, S., and Ramaswamy, V. (2011). Direct synthesis of well-ordered mesoporous Al-SBA-15 and its correlation with the catalytic activity. *Applied Catalysis A: General*, *400*(1–2), 176–184.
- Dragoi, B., Dumitriu, E., Guimon, C., and Auroux, A. (2009). Acidic and adsorptive properties of SBA-15 modified by aluminum incorporation. *Microporous and Mesoporous Materials*, *121*(1–3), 7–17.
- Gashti, M. P., Stir, M., and Hulliger, J. (2016). Growth of strontium hydrogen phosphate/gelatin composites: a biomimetic approach. *New Journal of Chemistry*, *40*(6), 5495–5500.
- Hou, Q., Qi, X., Zhen, M., Qian, H., Nie, Y., Bai, C., Zhang, S., Bai, X., and Ju, M. (2021). Biorefinery roadmap based on catalytic production and upgrading 5-hydroxymethylfurfural. *Green Chemistry*, *23*(1), 119–231.
- Hou, Q., Zhen, M., Liu, L., Chen, Y., Huang, F., Zhang, S., Li, W., and Ju, M. (2018). Tin phosphate as a heterogeneous catalyst for efficient dehydration of glucose into 5-hydroxymethylfurfural in ionic liquid. *Applied Catalysis B: Environmental*, *224*, 183–193.
- Hu, L., Wu, Z., Jiang, Y., Wang, X., He, A., Song, J., Xu, J., Zhou, S., Zhao, Y., and Xu, J. (2020). Recent advances in catalytic and autocatalytic production of biomass-

- derived 5-hydroxymethylfurfural. *Renewable and Sustainable Energy Reviews*, *134*, 110317.
- Huang, F., Su, Y., Long, Z., Chen, G., and Yao, Y. (2018). Enhanced formation of 5 - hydroxymethylfurfural from glucose using a silica-supported phosphate and iron phosphate heterogeneous catalyst. *Industrial & Engineering Chemistry Research*, *57*, 10198–10205.
- Khare, N., Hesterberg, D., Beauchemin, S., and Wang, S.-L. (2004). XANES determination of adsorbed phosphate distribution between ferrihydrite and boehmite in mixtures. *Soil Science Society of America Journal*, *68*(2), 460–469.
- Kong, Q. S., Li, X. L., Xu, H. J., and Fu, Y. (2020). Conversion of 5-hydroxymethylfurfural to chemicals: A review of catalytic routes and product applications. *Fuel Processing Technology*, *209*, 106528.
- Krishna, N. V., and Selvam, P. (2017). Acid-mediated synthesis of ordered mesoporous aluminosilicates: The challenge and the promise. *Chemistry - A European Journal*, *23*(7), 1604–1612.
- Li, Y., Zhang, W., Zhang, L., Yang, Q., Wei, Z., Feng, Z., and Li, C. (2004). Direct synthesis of Al-SBA-15 mesoporous materials via hydrolysis-controlled approach. *The Journal of Physical Chemistry B*, *108*(28), 9739–9744.
- Lima, J. P. V., Campos, P. T. A., Paiva, M. F., Linares, J. J., Dias, S. C. L., and Dias, J. A. (2021). Dehydration of fructose to 5-hydroxymethylfurfural: Effects of acidity and porosity of different catalysts in the conversion, selectivity, and yield. *Chemistry*, *3*(4), 1189–1202.
- Liu, B., Ba, C., Jin, M., and Zhang, Z. (2015). Effective conversion of carbohydrates into biofuel precursor 5-hydroxymethylfurfural (HMF) over Cr-incorporated mesoporous zirconium phosphate. *Industrial Crops and Products*, *76*, 781–786.
- Liu, Q., He, H., Chao, Z. S., Xie, J., and Ruchenstein, E. (2012). Synthesis of mesoporous chromium phosphates via solid-state reaction at low temperature. *New Journal of Chemistry*, *36*(1), 139–147.
- Lucas, N., Kokate, G., Nagpure, A., and Chilukuri, S. (2013). Dehydration of fructose to 5-hydroxymethyl furfural over ordered AlSBA-15 catalysts. *Microporous and Mesoporous Materials*, *181*, 38–46.

- Majjane, A., Chahine, A., Et-Tabirou, M., Echchahed, B., Do, T. O., and Breen, P. M. (2014). X-ray photoelectron spectroscopy (XPS) and FTIR studies of vanadium barium phosphate glasses. *Materials Chemistry and Physics*, *143*(2), 779–787.
- Makhlouf, S. A., Bakr, Z. H., Al-Attar, H., and Moustafa, M. S. (2013). Structural, morphological and electrical properties of Cr₂O₃ nanoparticles. *Materials Science and Engineering B: Solid-State Materials for Advanced Technology*, *178*(6), 337–343.
- Najafi Sarpiri, J., Najafi Chermahini, A., Saraji, M., and Shahvar, A. (2021). Dehydration of carbohydrates into 5-hydroxymethylfurfural over vanadyl pyrophosphate catalysts. *Renewable Energy*, *164*, 11–22.
- Nancharaiah, Y. V., Dodge, C., Venugopalan, V. P., Narasimhan, S. V., and Francis, A. J. (2010). Immobilization of Cr(VI) and its reduction to Cr(III) phosphate by granular biofilms comprising a mixture of microbes. *Applied and Environmental Microbiology*, *76*(8), 2433–2438.
- Nikolla, E., Román-Leshkov, Y., Moliner, M., and Davis, M. E. (2011). “One-pot” synthesis of 5-(hydroxymethyl)furfural from carbohydrates using tin-beta zeolite. *ACS Catalysis*, *1*(4), 408–410.
- Ordonsky, V. V., Sushkevich, V. L., Schouten, J. C., Van Der Schaaf, J., and Nijhuis, T. A. (2013). Glucose dehydration to 5-hydroxymethylfurfural over phosphate catalysts. *Journal of Catalysis*, *300*, 37–46.
- Osakoo, N., Khemthong, P., Roessner, F., Kidkhunthod, P., Chanlek, N., Prayoonpokarach, S., and Wittayakun, J. (2020). Development and characterization of silica supported cobalt oxides for ethanol oxidation using different preparation methods. *Radiation Physics and Chemistry*, *171*, 108718.
- Persson, I., Klysubun, W., and Lundberg, D. (2019). A K-edge P XANES study of phosphorus compounds in solution. *Journal of Molecular Structure*, *1179*, 608–611.
- Rakngam, I., Osakoo, N., Wittayakun, J., Chanlek, N., Pongsawang, A., Sosa, N., Butburee, T., Faungnawakij, K., and Khemthong, P. (2021). Properties of mesoporous Al-SBA-15 from one-pot hydrothermal synthesis with different aluminium precursors and catalytic performances in xylose conversion to furfural. *Microporous and*

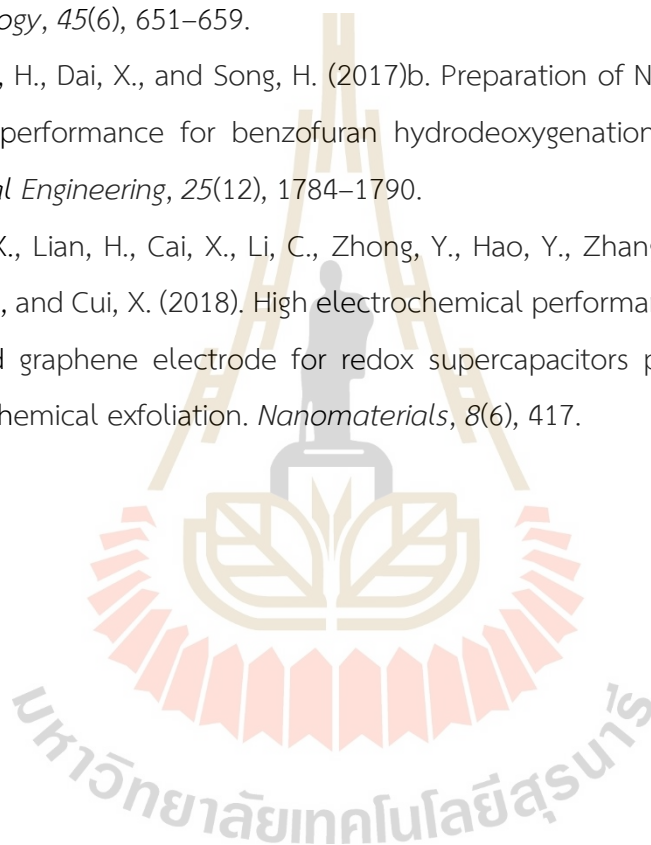
Mesoporous Materials, 317, 110999.

- Ramis, G., Busca, G., Lorenzelli, V., Ginestra, A. La, Galli, P., and Massucci, M. A. (1988). Surface acidity of the layered pyrophosphates of quadrivalent Ti, Zr, Ge, and Sn and their activity in some acid-catalysed reactions. *Dalton Transactions*, (4), 881–886.
- Rao, K. T. V., Souzanchi, S., Yuan, Z., Ray, M. B., and Xu, C. (2017). Simple and green route for preparation of tin phosphate catalysts by solid-state grinding for dehydration of glucose to 5-hydroxymethylfurfural (HMF). *RSC Advances*, 7(76), 48501–48511.
- Rezayan, A., Wang, K., Nie, R., Lu, T., Wang, J., Zhang, Y., and Xu, C. C. (2022). Synthesis of bifunctional tin-based silica-carbon catalysts, Sn/KIT-1/C, with tunable acid sites for the catalytic transformation of glucose into 5-hydroxymethylfurfural. *Chemical Engineering Journal*, 429, 132261.
- Rodríguez-Aguado, E., Infantes-Molina, A., Ballesteros-Plata, D., Cecilia, J. A., Barroso-Martin, I., and Rodríguez-Castellón, E. (2017). Ni and Fe mixed phosphides catalysts for O-removal of a bio-oil model molecule from lignocellulosic biomass. *Molecular Catalysis*, 437, 130–139.
- Saha, B., and Abu-Omar, M. M. (2014). Advances in 5-hydroxymethylfurfural production from biomass in biphasic solvents. *Green Chemistry*, 16(1), 24–38.
- Samikannu, A., Konwar, L. J., Rajendran, K., Lee, C. C., Shchukarev, A., Virtanen, P., and Mikkola, J. P. (2020). Highly dispersed NbOPO₄/SBA-15 as a versatile acid catalyst upon production of renewable jet-fuel from bio-based furanics via hydroxyalkylation-alkylation (HAA) and hydrodeoxygenation (HDO) reactions. *Applied Catalysis B: Environmental*, 272, 118987.
- Saravanan, K., Park, K. S., Jeon, S., and Bae, J. W. (2018). Aqueous phase synthesis of 5-hydroxymethylfurfural from glucose over large pore mesoporous zirconium phosphates: Effect of calcination temperature. *ACS Omega*, 3(1), 808–820.
- Serrano, D. P., García, R. A., Vicente, G., Linares, M., Procházková, D., and Čejka, J. (2011). Acidic and catalytic properties of hierarchical zeolites and hybrid ordered mesoporous materials assembled from MFI protozeolitic units. *Journal of Catalysis*, 279(2), 366–380.

- Sezgin, E., Esen Keçeci, M., Akmaz, S., and Koc, S. N. (2019). Heterogeneous Cr-zeolites (USY and Beta) for the conversion of glucose and cellulose to 5-hydroxymethylfurfural (HMF). *Cellulose*, 26(17), 9035–9043.
- Shao, Y., Ding, Y., Dai, J., Long, Y., and Hu, Z.-T. (2021). Synthesis of 5-hydroxymethylfurfural from dehydration of biomass-derived glucose and fructose using supported metal catalysts. *Green Synthesis and Catalysis*, 2, 187–197.
- Song, X., Yue, J., Zhu, Y., Wen, C., Chen, L., Liu, Q., Ma, L., and Wang, C. (2021). Efficient conversion of glucose to 5-hydroxymethylfurfural over a Sn-modified SAPO-34 zeolite catalyst. *Industrial & Engineering Chemistry Research*, 60(16), 5838–5851.
- Songtawee, S., Rungtaweavoranit, B., Klaysom, C., and Faungnawakij, K. (2021). Tuning Brønsted and Lewis acidity on phosphated titanium dioxides for efficient conversion of glucose to 5-hydroxymethylfurfural. *RSC Advances*, 11(47), 29196–29206.
- Thommes, M., Kaneko, K., Neimark, A. V., Olivier, J. P., Rodriguez-Reinoso, F., Rouquerol, J., and Sing, K. S. W. (2015). Physisorption of gases, with special reference to the evaluation of surface area and pore size distribution (IUPAC Technical Report). *Pure and Applied Chemistry*, 87(9–10), 1051–1069.
- Ungureanu, A., Dragoi, B., Hulea, V., Cacciaguerra, T., Meloni, D., Solinas, V., and Dumitriu, E. (2012). Effect of aluminium incorporation by the “pH-adjusting” method on the structural, acidic and catalytic properties of mesoporous SBA-15. *Microporous and Mesoporous Materials*, 163, 51–64.
- Wang, K., Rezayan, A., Si, L., Zhang, Y., Nie, R., Lu, T., Wang, J., and Xu, C. (2021). Highly efficient 5 - hydroxymethylfurfural production from glucose over bifunctional SnOx/C catalyst. *ACS Sustainable Chemistry & Engineering*, 9(34), 11351–11360.
- Wang, X., Liang, F., Huang, C., Li, Y., and Chen, B. (2015). Highly active tin(IV) phosphate phase transfer catalysts for the production of lactic acid from triose sugars. *Catalysis Science and Technology*, 5(9), 4410–4421.
- Weckhuysen, B. M., Wachs, I. E., and Schoonheydt, R. A. (1996). Surface chemistry and spectroscopy of chromium in inorganic oxides. *Chemical Reviews*, 96(8), 3327–3349.
- Wu, S., Han, Y., Zou, Y., Song, J., Zhao, L., and Di, Y. (2004). Synthesis of heteroatom

- substituted SBA-15 by the “pH-adjusting” method. *Chemistry of Materials*, 16(17), 486–492.
- Xia, H., Xu, S., Hu, H., An, J., and Li, C. (2018). Efficient conversion of 5-hydroxymethylfurfural to high-value chemicals by chemo- and bio-catalysis. *RSC Advances*, 8(54), 30875–30886.
- Xing, S., Lv, P., Fu, J., Wang, J., Fan, P., Yang, L., and Yuan, Z. (2017). Direct synthesis and characterization of pore-broadened Al-SBA-15. *Microporous and Mesoporous Materials*, 239, 316–327.
- Xu, S., Pan, D., Hu, F., Wu, Y., Wang, H., Chen, Y., Yuan, H., Gao, L., and Xiao, G. (2019). Highly efficient Cr/ β zeolite catalyst for conversion of carbohydrates into 5-hydroxymethylfurfural: Characterization and performance. *Fuel Processing Technology*, 190, 38–46.
- Xu, S., Yan, X., Bu, Q., and Xia, H. (2016). Highly efficient conversion of carbohydrates into 5-hydroxymethylfurfural using the bi-functional CrPO₄ catalyst. *RSC Advances*, 6(10), 8048–8052.
- Xue, Z., Ma, M. G., Li, Z., and Mu, T. (2016). Advances in the conversion of glucose and cellulose to 5-hydroxymethylfurfural over heterogeneous catalysts. *RSC Advances*, 6(101), 98874–98892.
- Yang, Y., Ochoa-Hernández, C., de la Peña O’Shea, V. A., Pizarro, P., Coronado, J. M., and Serrano, D. P. (2015). Transition metal phosphide nanoparticles supported on SBA-15 as highly selective hydrodeoxygenation catalysts for the production of advanced biofuels. *Journal of Nanoscience and Nanotechnology*, 15(9), 6642–6650.
- Yu, I. K. M., and Tsang, D. C. W. (2017). Conversion of biomass to hydroxymethylfurfural: A review of catalytic systems and underlying mechanisms. *Bioresource Technology*, 238, 716–732.
- Zhang, J., Ma, Z., Jiao, J., Yin, H., Yan, W., Hagaman, E. W., Yu, J., and Dai, S. (2010). Surface functionalization of mesoporous silica SBA-15 by liquid-phase grafting of zirconium phosphate. *Microporous and Mesoporous Materials*, 129(1–2), 200–209.
- Zhang, T., Wei, H., Xiao, H., Li, W., Jin, Y., Wei, W., and Wu, S. (2020). Advance in constructing acid catalyst-solvent combinations for efficient transformation of

- glucose into 5-Hydroxymethylfurfural. *Molecular Catalysis*, 498, 111254.
- Zhang, Y., Wang, J., Li, X., Liu, X., Xia, Y., Hu, B., Lu, G., and Wang, Y. (2015). Direct conversion of biomass-derived carbohydrates to 5-hydroxymethylfurfural over water-tolerant niobium-based catalysts. *Fuel*, 139, 301–307.
- Zhu, L., Wang, J., Zhao, P., Song, F., Sun, X., Wang, L., Cui, H., and Yi, W. (2017)a. Preparation of the Nb-P/SBA-15 catalyst and its performance in the dehydration of fructose to 5-hydroxymethylfurfural. *Journal of Fuel Chemistry and Technology*, 45(6), 651–659.
- Zhu, T., Song, H., Dai, X., and Song, H. (2017)b. Preparation of Ni₂P/Al-SBA-15 catalyst and its performance for benzofuran hydrodeoxygenation. *Chinese Journal of Chemical Engineering*, 25(12), 1784–1790.
- Zu, L., Gao, X., Lian, H., Cai, X., Li, C., Zhong, Y., Hao, Y., Zhang, Y., Gong, Z., Liu, Y., Wang, X., and Cui, X. (2018). High electrochemical performance phosphorus-oxide modified graphene electrode for redox supercapacitors prepared by one-step electrochemical exfoliation. *Nanomaterials*, 8(6), 417.

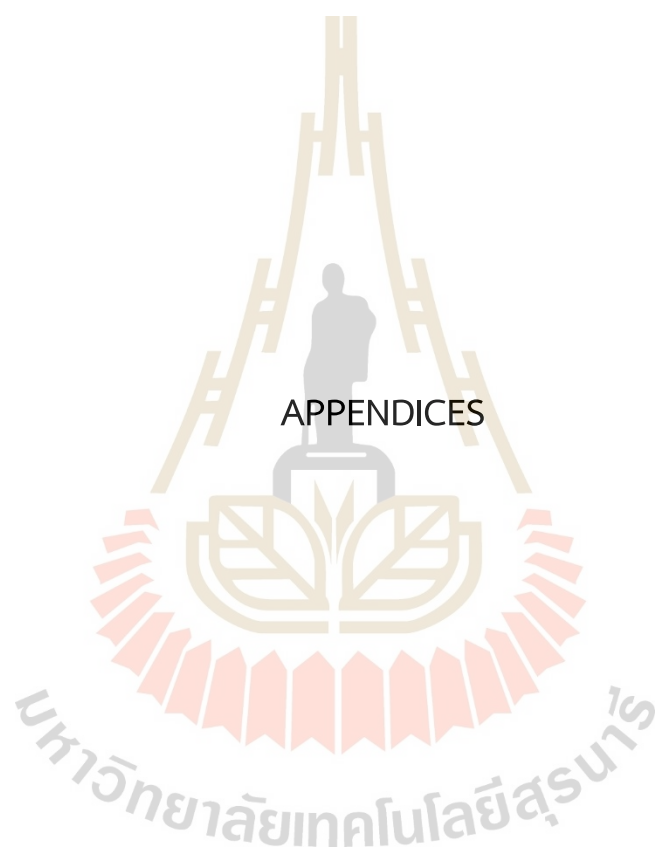


CHAPTER V

CONCLUSIONS

Aluminium incorporated siliceous SBA-15 (Al-SBA-15) samples from three different aluminium sources including, sodium aluminate (SA), aluminium sulphate (AS), and aluminium isopropoxide (AI) were successfully synthesized by a one-step hydrothermal with pH adjusting method. The source of aluminium plays a crucial role in determining the structural properties, surface acidities, and morphologies of the resulting Al-SBA-15 catalysts. In the catalytic conversion of xylose to furfural, the xylose conversions increased with the total acidity of the catalysts. On the other hand, furfural yields depended on the ratios of Lewis-to-Bronsted acids (L/B). Additionally, an increase in Al in octahedral coordination (Al_{oct}) led to the formation of lactic acid as a by-product. According to the highest furfural selectivity and good thermal stability, Al-SBA-15 (SA) was the best catalyst for producing furfural from xylose.

Al-SBA-15 was modified by depositing phosphates of Cr, Zr, Nb, Sr, and Sn by a facile wet-impregnation method. The MPO/Al-SBA-15 catalysts were employed to convert glucose to 5-HMF in a biphasic H_2O/n -butanol solvent. The different types of metal phosphates significantly impacted the acid properties and ratio of L/B. The glucose conversion and 5-HMF yield correlated well with the total acidity and the ratio of L/B acids, rather than the catalyst surface area. From the catalytic performance, CrPO/Al-SBA-15 was the suitable catalyst for the glucose conversion to 5-HMF, resulting from the highest acidity and suitable L/B ratio. Furthermore, the effect of different PO/Cr molar ratios (2.0, 1.0, and 0.5) on the catalytic properties and activity was also investigated. The highest yield of 5-HMF was obtained from the CrPO(2)/Al-SBA-15 catalyst, which predominantly contained chromium (III) phosphate species with an octahedral structure.



APPENDIX A

ADDITIONAL CHARACTERIZATION RESULTS FOR Al-SBA-15 WITH
VARIOUS ALUMINIUM SOURCES AND CALIBRATION CURVES FOR
XYLOSE CONVERSION

A.1 TGA profiles of Al-SBA-15 with various Al sources

The thermograms are shown in Figure A.1. The weight loss of the bare SBA-15 consisted of two steps. A weight loss at around 100 °C corresponded to the loss of moisture or physically adsorbed water (Dai, Zhao, Fang, Liu, Dong, and Jiang, 2017). The further loss at the higher temperature was from the desorption of chemisorbed water and dehydroxylation of the silanol groups (Tayebie et al., 2015). TGA profiles of SA, AS, and AI exhibited weight loss of 20.19, 22.15, and 22.47%, respectively.

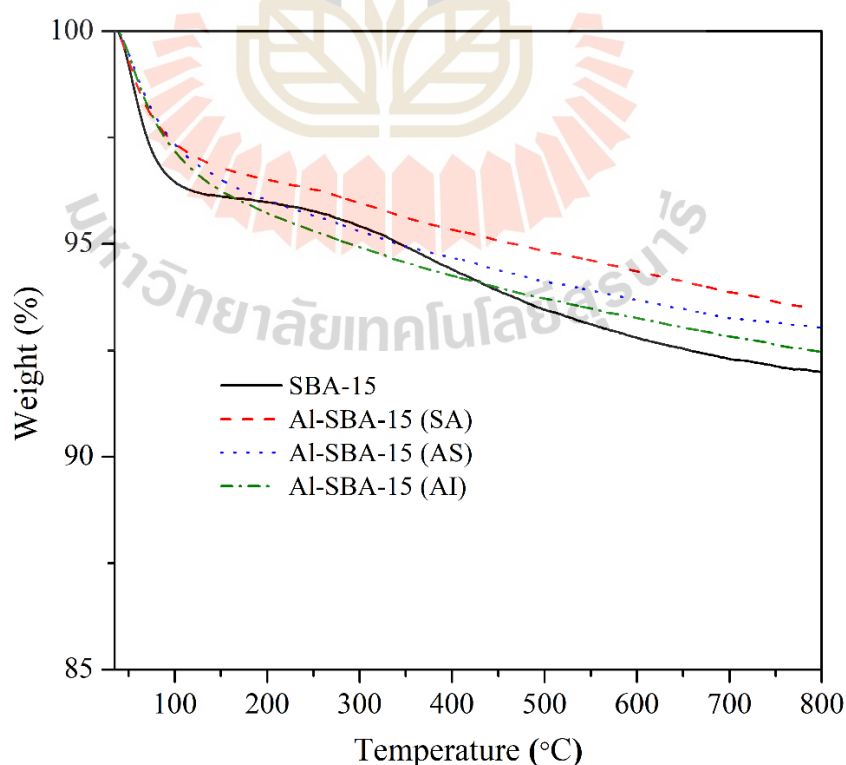


Figure A.1 TGA profiles of SBA-15 and Al-SBA-15 samples with various Al sources.

A.2 Distribution of pore diameter and wall thickness by TEM

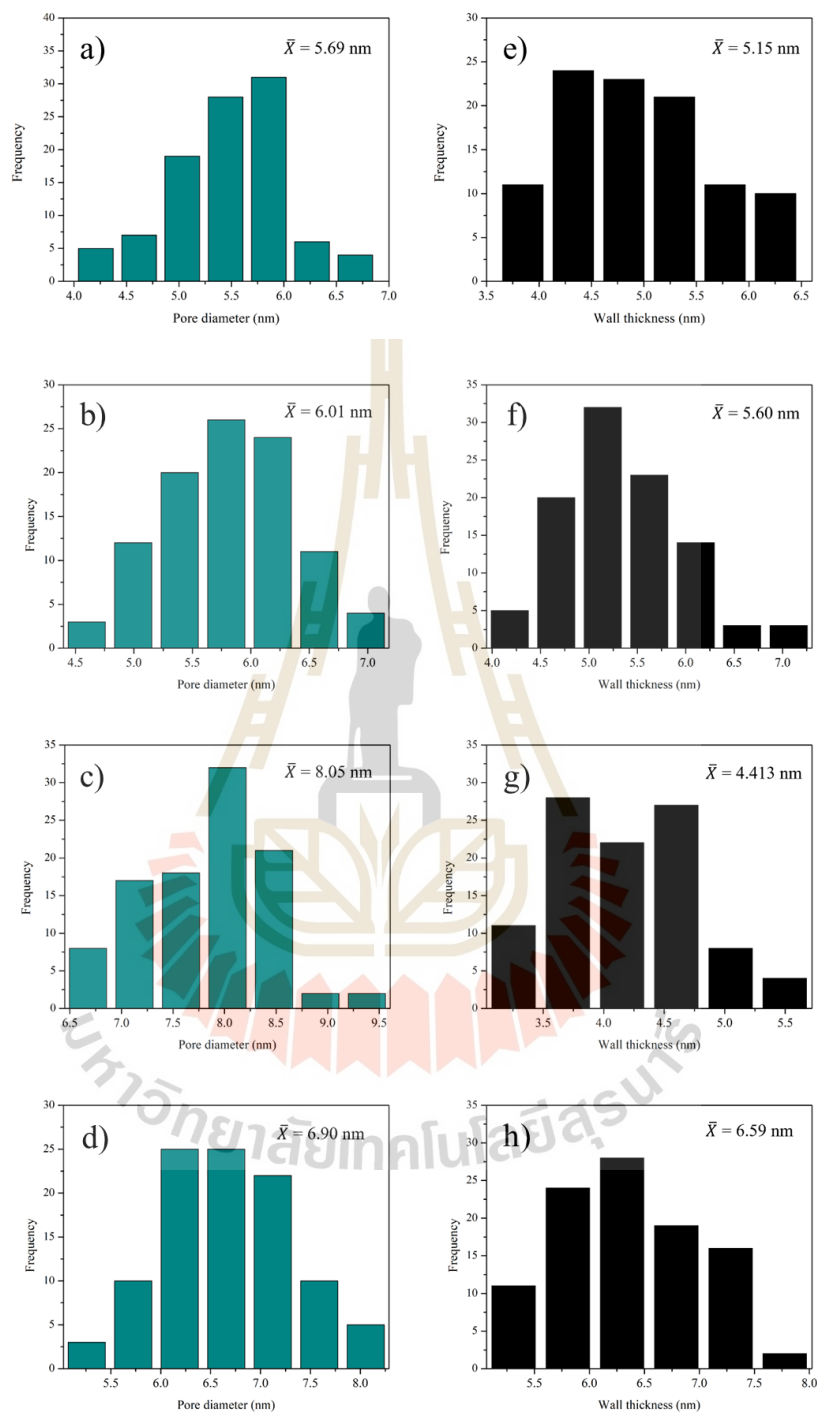


Figure A.2 Pore diameter distribution of a) SBA-15, b) Al-SBA-15 (SA), c) Al-SBA-15 (AS) and d) Al-SBA-15 (AI) and wall thickness distribution of e) SBA-15, f) Al-SBA-15 (SA), g) Al-SBA-15 (AS) and h) Al-SBA-15 (AI).

A.3 Calibration curve of xylose conversion

The calibration curve was composed from the mixed standard solution by the following procedure. The stock solution of xylose with the concentration of 50 mg/mL was prepared by dissolving 1.2502 g of xylose in DI water 25 mL. Then it was diluted with the DI water to concentrations of 0.05, 0.5, 2, 10 and 25 mg/mL.

The stock solution of furfural with the concentration of 20 mg/mL was prepared by dissolving 0.5000 g of xylose in DI water 25 mL. Then it was diluted with the DI water to concentrations of 0.1, 0.5, 2, 5 and 10 mg/mL.

The stock solution of lactic acid with the concentration of 50 mg/mL was prepared by dissolving 1.2504 g of lactic acid in DI water 25 mL. Then it was diluted with the DI water to concentrations of 0.05, 0.5, 2, 5 and 25 mg/mL.

The stock solution of formic acid with the concentration of 50 mg/mL was prepared by dissolving 1.2501 g of formic acid in DI water 25 mL. Then it was diluted with the DI water to concentrations of 0.05, 0.5, 2, 5 and 25 mg/mL.

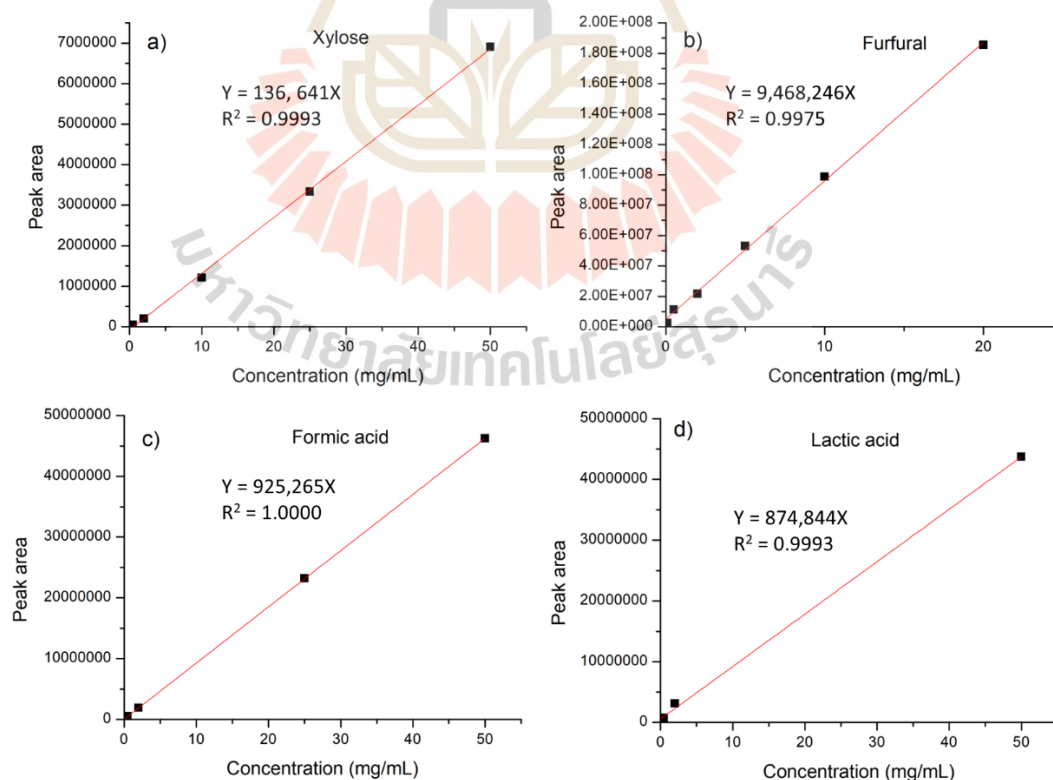
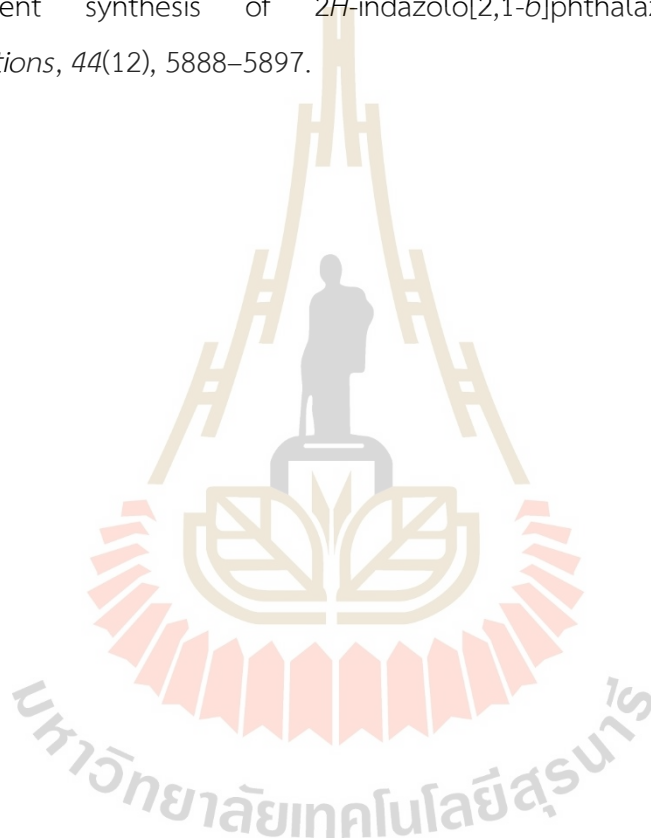


Figure A.3 Calibration curves of a) xylose, b) furfural, c) lactic acid, and d) formic acid.

A.4 References

Dai, L., Zhao, Q., Fang, M., Liu, R., Dong, M., and Jiang, T. (2017). Catalytic activity comparison of Zr-SBA-15 immobilized by a Brønsted-Lewis acidic ionic liquid in different esterifications. *RSC Advances*, 7(51), 32427–32435.

Tayebee, R., Amini, M. M., Pouyamanesh, S., and Aliakbari, A. (2015). A new inorganic-organic hybrid material Al-SBA-15-TPI/H₆P₂W₁₈O₆₂ catalyzed one-pot, three-component synthesis of 2*H*-indazolo[2,1-*b*]phthalazine-triones. *Dalton Transactions*, 44(12), 5888–5897.



APPENDIX B
ADDITIONAL CHARACTERIZATION RESULTS FOR MPO/Al-SBA-15
WITH VARIOUS METAL TYPES AND CALIBRATION CURVES FOR
GLUCOSE CONVERSION

B.1 SEM-EDS and TEM of the best CrPO(2)/Al-SBA-15 catalyst

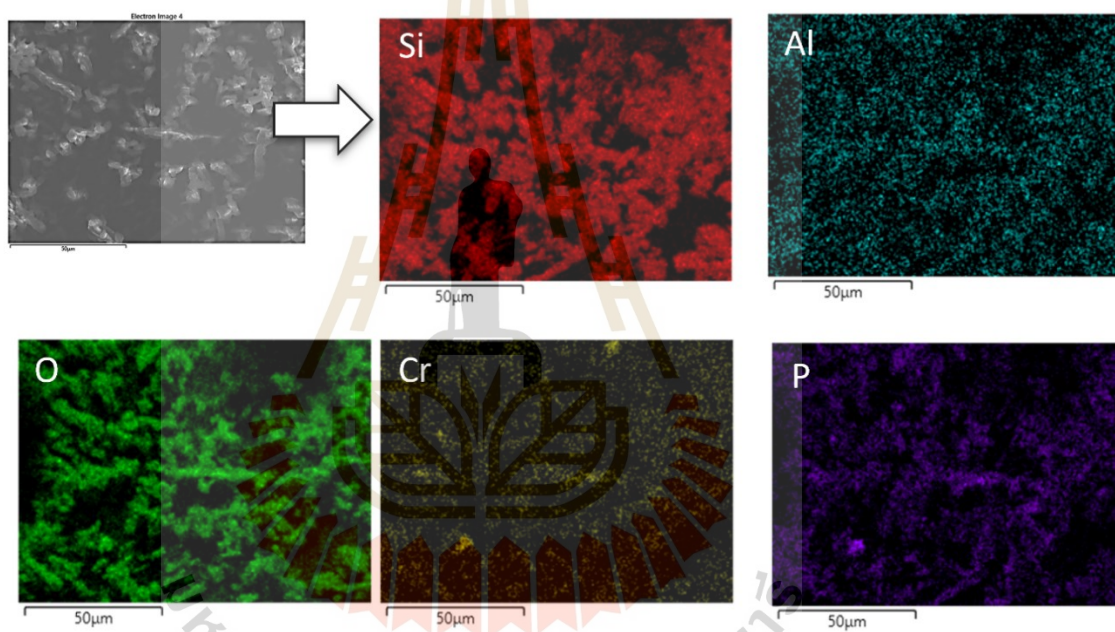


Figure B.1 SEM-EDS microelement mapping of CrPO(2)/Al-SBA-15 catalyst.

B.2 XRD of spent MPO/Al-SBA-15 catalysts

To investigate the stability of MPO/Al-SBA-15 catalysts after the reaction testing at 150 °C for 4 hours, the spent catalysts were washed, dried, and characterized by low-angle XRD. In **Figure B.2**, the XRD patterns of spent Al-SBA-15, CrPO/Al-SBA-15, SrPO/Al-SBA-15, and SnPO/Al-SBA-15 catalysts still showed the same characteristic peaks similar to the fresh catalysts. On the other hand, the patterns of spent ZrPO/Al-SBA-15 and NbPO/Al-SBA-15 catalysts showed weak diffraction at the low-angle region, indicating that the collapses of the hexagonal mesoporous structures.

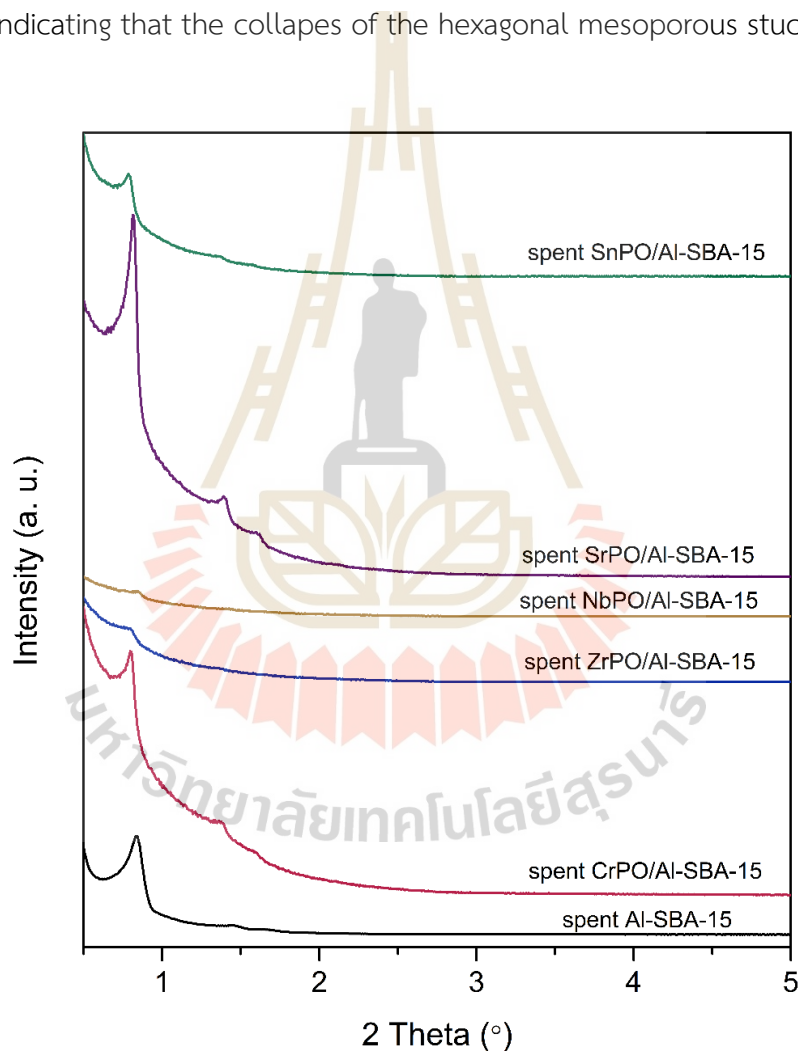


Figure B.2 XRD patterns of spent MPO/Al-SBA-15 catalysts.

B.3 Calibration curve of glucose conversion

The calibration curve was composed of the mixed standard solution by the following procedure. The stock solution of glucose with the concentration of 50 mg/mL was prepared by dissolving 1.2501 g of glucose in DI water 25 mL. Then it was diluted with the DI water to concentrations of 0.05, 0.5, 2, 25, and 50 mg/mL.

The stock solution of fructose with the concentration of 40 mg/mL was prepared by dissolving 1.005 g of fructose in DI water 25 mL. Then it was diluted with the DI water to concentrations of 2.5, 5.5, 12, 20, and 40 mg/mL.

The stock solution of 5-HMF with the concentration of 20 mg/mL was prepared by dissolving 0.5004 g of 5-HMF in DI water 25 mL. Then it was diluted with the DI water to concentrations of 0.05, 0.5, 2, and 10 mg/mL.

The stock solution of 5-HMF with the concentration of 20 mg/mL was prepared by dissolving 0.5006 g of 5-HMF in *n*-butanol 25 mL. Then it was diluted with the DI water to concentrations of 0.1, 0.5, 2, 5 and 10 mg/mL.

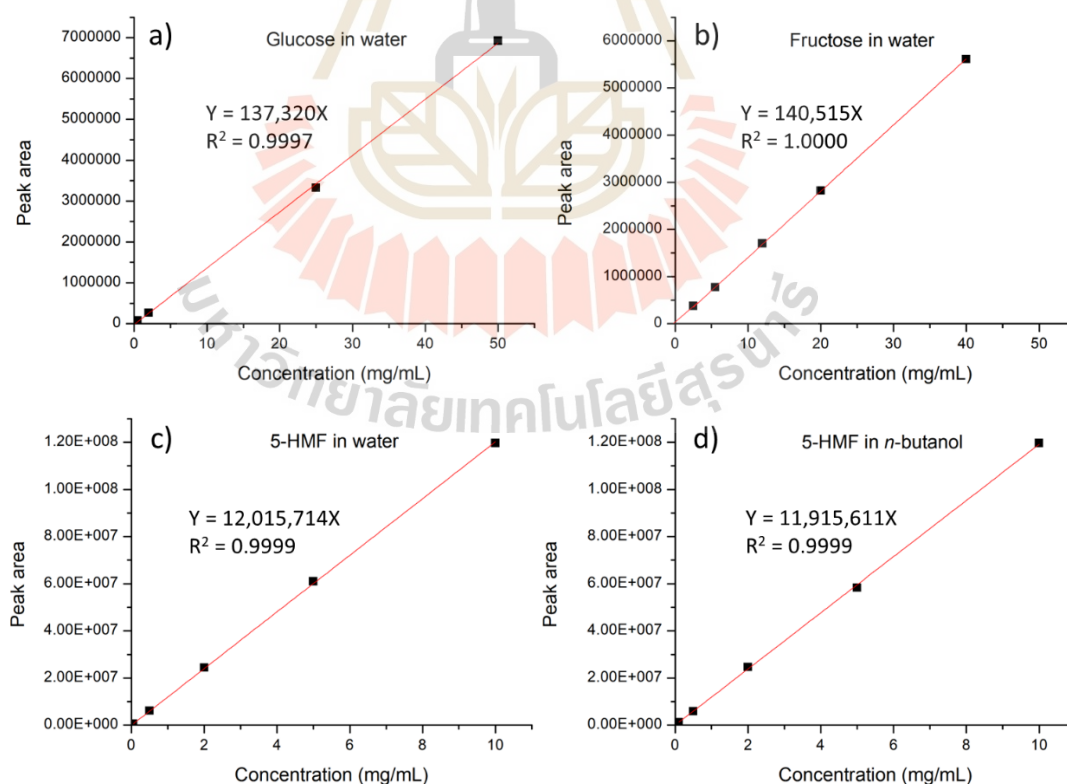


Figure B.3 Calibration curve of a) glucose in water, b) fructose in water, c) 5-HMF in water, and d) 5-HMF in *n*-butanol.

B.4 Computational results

The DFT calculations revealed that the three dehydration steps occur spontaneously for converting sugar to 5-HMF over CrPO, with negative Gibbs free energy values as shown in **Figure 4.18**. Moreover, the relative ΔG value for the CrPO catalytic system was found to be lower than that of the non-catalytic system, by 9-17 kcal/mol. This suggests that the reaction is thermodynamically favorable in the presence of CrPO as a catalyst. Among the dehydration steps in the CrPO catalytic system, the 3rd dehydration step (C \rightarrow D) was found to be the most thermodynamically favorable. The chromium atom served as Lewis acid sites, promoting the binding of sugar and stabilizing intermediates during the dehydration reaction as presented the reaction pathway in **Figure 4.19**. This observation is similar the work by Orasa et al. (In-noi, Daorattanachai, Rungnim, Prasitnok, Rungtaweevoranit, Faungnawakij, and Khemthong, 2021) that the metal atom in metal phosphates acts as Lewis acid sites and enhances the reaction process.

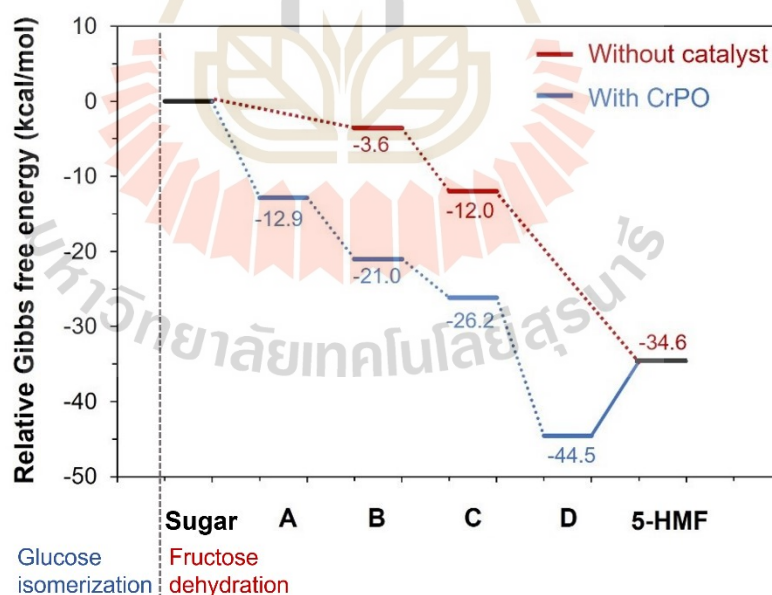


Figure B.4 Relative Gibbs free energy (kcal/mol) of various intermediates involved in C6 sugar dehydration to 5-HMF with and without CrPO catalyst.

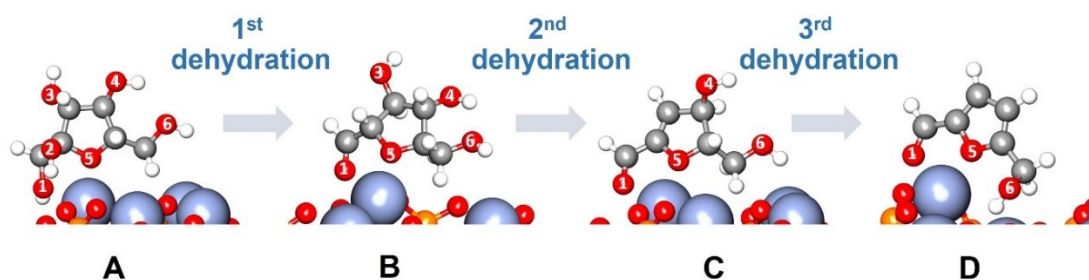


Figure B.5 Optimized structures along the reaction pathway of sugar dehydration over CrPO catalyst.

B.5 References

In-noi, O., Daorattanachai, P., Rungnim, C., Prasitnok, K., Rungtaweevoranit, B., Faungnawakij, K., and Khemthong, P. (2021). Insight into fructose dehydration over Lewis acid α - $\text{Cu}_2\text{P}_2\text{O}_7$ catalyst. *ChemNanoMat*, 7(3), 292–298.

CURRICULUM VITAE

ISSARAPORN RAKNGAM

Place of Birth Surin, Thailand

Education

- 2012-2016 B.Sc. in Chemistry (Second Class Honors)
Suranaree University of Technology, Nakhon Ratchasima, Thailand
- 2016-2023 Ph.D. candidate in Chemistry
Suranaree University of Technology, Nakhon Ratchasima, Thailand

Scholarship

- 2016-2023 Royal Golden Jubilee Ph.D. Programme from the Thailand
Science Research and Innovation (TSRI)

Publication

Rakngam, I., Osakoo, N., Wittayakun, J., Chanlek, N., Pongsawang, A., Sosa, N., Butburee, T., Faungnawakij, K., and Khemthong, P. (2021). Properties of mesoporous Al-SBA-15 from one-pot hydrothermal synthesis with different aluminium precursors and catalytic performances in xylose conversion to furfural. *Microporous and Mesoporous Materials*, 317, 110999.